The role of the oxygen sensors PHD2 and PHD3 in the response of macrophages to ischemia-induced inflammation

Doctoral Thesis

In partial fulfillment of the requirements for the degree

“Doctor rerum naturalium (Dr. rer. nat.)”

in the Molecular Medicine Study Program

at the Georg-August University Göttingen

submitted by

Angelika Beneke

born in Bremen, Germany

Göttingen, September 2016

Members of the thesis committee

Prof. Dr. Dörthe M. Katschinski (Supervisor)
Institute of Cardiovascular Physiology
Humboldtallee 23
University Medical Center Göttingen
0551-39 5896
doerthe.katschinski@med.uni-goettingen.de

Prof. Dr. Thomas Meyer (Co-supervisor)
Clinic for Psychosomatic Medicine and Psychotherapy
Waldweg 33
University Medical Center Göttingen
0551-39-4881
thomas.meyer@med.uni-goettingen.de

Prof. Dr. Holger Reichardt (Co-supervisor)
Institute for Cellular and Molecular Immunology
Humboldtallee 34
University Medical Center Göttingen
0551-39 33365
hreichardt@med.uni-goettingen.de

Date of the defense: 24 October 2016

Affidavit

I hereby declare that my doctoral thesis entitled “The role of the oxygen sensors PHD2 and PHD3 in the response of macrophages to ischemia-induced inflammation” has been written independently with no other sources and aids than quoted.

_____

Angelika Beneke

Göttingen, 5 September 2016

List of publications

PHD2 is a regulator for glycolytic reprogramming in macrophages.
Guentsch A, Beneke A, Swain L, Farhat K, Nagarajan S, Wielockx B, Dudek J, Rehling P, Zieseniss A, Jatho A, Chong M, Santos C, Shah A, Katschinski DM. *Mol Cell Biol*. in revision.

Ferritin-Mediated Iron Sequestration Stabilizes Hypoxia-Inducible Factor-1α upon LPS Activation in the Presence of Ample Oxygen.
Siegert I, Schödel J, Nairz M, Schatz V, Dettmer K, Dick C, Kalucka J, Franke K, Ehrenschwender M, Schley G, Beneke A, Sutter J, Moll M, Hellerbrand C, Wielockx B, Katschinski DM, Lang R, Galy B, Hentze MW, Koivunen P, Oefner PJ, Bogdan C, Weiss G, Willam C, Jantsch J. *Cell Rep.* 13:2048-2055.

Prolyl-4-hydroxylase domain 3 (PHD3) is a critical terminator for cell survival of macrophages under stress conditions.
Swain L, Wottawa M, Hillemann A, Beneke A, Odagiri H, Terada K, Endo M, Oike Y, Farhat K, Katschinski DM. *J Leukoc Biol.* 96:365-375.

Table of contents

List of tables

List of figures

Abbreviations

12-HHT	12-hydroxyheptadecatrenoic acid
2-OG	2-oxoglutarate
A	Ampere
AAR	Area at risk
AHR	Aryl hydrocarbon receptor
AON	Area of necrosis
APC	Antigen-presenting cell
APC	Allophycocyanin
ARNT	Aryl hydrocarbon repector nuclear translocator
ASC	Apoptosis-associated speck-like protein containing a CARD
Asn	Asparagine
ATF-4	Activating transcription factor 4
ATP	Adenosine triphosphate
Bcl-XL	B cell lymphoma-extra large
bHLH	Basic-helix-loop-helix
BLT2	Leukotriene B4 receptor 2
BMDM	Bone marrow-derived macrophage
Bnip3	BCL2/adenovirus E1B 19 kDa protein-interacting protein 3
bp	Base pair
BSA	Bovine serum albumin
CCL2	C-C chemokine ligand 2
CD	Cluster of differentiation
cDNA	Complementary DNA
CO_2	Carbon dioxide
c-P4H	Collagen-Prolyl-4-hydroxylase
CXCL	C-X-C motif ligand
Cy7	Cyanine7
Cyp2s1	Cytochrome P450 family 2 subfamily S member 1
d	Diastole
DAMP	Damage-associated molecular membrane pattern
DCA	Dichloroacetate
DMEM	Dulbecco´s modified eagle medium
DMOG	Dimethyloxaloylglycine
DNA	Deoxyribonucleic acid
DNase	Deoxyribonuclease
dNTP	Deoxyribonucleotide triphosphate

ECL	Enhanced chemiluminescence
EDTA	Ethylenediaminetetraacetic acid
EF	Ejection fraction
EP	Prostaglandin E receptor
EPO	Erythropoietin
ER	Endoplasmatic reticulum
FAS	Fractional area shortening
FCS	Fetal calf serum
Fe(II)	Bivalent iron
FIH	Factor inhibiting HIF
FITC	Fluorescein isothiocyanate
FMO	Fluorescence minus one
FSC	Forward scatter
fw	Forward (primer)
g	gram(s)
(x)g	Gravitational force
G-CSF	Granulocyte colony-stimulating factor
GLUT	Glucose transporter
GM	Gastrocnemicus muscle
GM-CSF	Granulocyte macrophage colony-stimulating factor
GR	Glucocorticoid receptor
HBSS	Hank´s balanced salt solution
HEPES	4-(2-hydroxyethyl)-1-piperazineethanesulfonic acid
HIF	Hypoxia-inducible factor
HMGB1	High-mobility group box 1
HRE	Hypoxia-responsive element
HRP	Horseradish peroxidase
hrs	Hours
HSP	Heat shock protein
H_2O	water
IFN-ɣ	Interferon-ɣ
IgG	Immunoglobulin G
IL	Interleukin
iNOS	Inducible NO synthase
IPAS	Inhibitory PAS domain protein
kb	Kilo base pairs
l	Liter

LAD	Left anterior descending artery
LPS	Lipopolysaccharide
LysM	Lysozyme M
M	Molar
MCP-1	Monocyte chemoattractant protein-1
M-CSF	Macrophage colony-stimulating factor
MHC	Major histocompatibility complex
MI	Myocardial infarction
min	Minute(s)
mRNA	Messenger RNA
NaCl	Sodium chloride
NF-κB	Nuclear factor kappa-light-chain-enhancer of activated B cells
NES	Nuclear export sequence
NLRP3	NOD-, LRR-, and pyrin domain containing 3
NLS	Nuclear localization sequence
NO	Nitric oxide
ODDD	Oxygen-dependent degradation domain
PAD	Peripheral artery disease
PAMP	Pathogen-associated molecular membrane pattern
PAS	Per-ARNT-Sim
PBS	Phosphate-buffered saline
PCR	Polymerase chain reaction
PDH	Pyruvate dehydrogenase
PDK-1	Pyruvate dehydrogenase lipoamide kinase isoenzyme-1
PE	Phycoerythrin
Pfk-1	Phosphofructokinase-1
PG	Prostaglandin
PHD	Prolyl-4-hydroxylase domain enzyme
Phlda3	Pleckstrin homology like domain family a member 3
PKM1/2	Pyruvate kinase isoenzyme M1/2
pO_2	Partial oxygen pressure
Pro	Proline
P/S	Penicillin streptomycin
pVHL	von-Hippel Lindau tumor suppressor protein
P4H	Prolyl-4-hydroxylase
qRT-PCR	Quantitative realtime polymerase chain reaction
RAGE	Receptor for advanced glycation endproducts

Rbm4	RNA binding motif protein 4
rev	Reverse (primer)
RIN	RNA integrity number
RNA	Ribonucleic acid
ROI	Region of interest
ROS	Reactive oxygen species
rpm	Rounds per minute
rRNA	Ribosomal RNA
SDS	Sodium dodecyl sulfate
s	Systole
sec	Second(s)
SEM	Standard error of the mean
SNAP	S-nitroso-N-acetyl penicillamine
SSC-A	Sideward scatter area
SSC-W	Sideward scatter width
STAT	Signal transducer and activator of transcription
TCA	Tricarboxylic acid
TEMED	Tetramethylethylenediamine
TGF-β	Transforming growth factor-β
TLR	Toll-like receptor
TNF-α	Tumor necrosis factor-α
TNF-R	Tumor necrosis factor receptor
TR	Texas red
TTC	2,3,5-triphenyltetrazolium chloride
U	Unit
V	Volt
VEGF	Vascular endothelial growth factor
WT	Wild type

Abstract

Ischemic diseases, caused by the occlusion of a supplying blood vessel, result in a severe lack of oxygen and nutrients within the tissue. The ischemic insult triggers an inflammatory response of the innate immune system. Myeloid cells such as neutrophils and macrophages are recruited to the tissue to clear up debris and necrotic cells. In ischemia, adaptation to low oxygen levels is essential to cell survival. Prolyl-4-hydroxylase domain enzymes (PHD) 1, 2 and 3 regulate the protein-stability of the α-subunit of hypoxia-inducible factor (HIF), which makes them the oxygen-sensors of the cells. In myeloid cells, PHD3 is a potent regulator of apoptosis in neutrophils and macrophages. PHD2 on the other hand affects macrophage metabolism and migration. The aim of this thesis was to further characterize the functions of PHD2 and 3 for macrophages in the context of ischemic diseases.

I studied the role of PHD3 in myeloid cells upon induction of hind limb ischemia in a myeloid-specific PHD3$^{-/-}$ mouse. After hind limb ischemia surgery, the infiltration of myeloid cells into the hind limb muscle as well as their clearance was analyzed via flow cytometry. The inflammatory response of PHD3$^{-/-}$ macrophages was blunted 4 and 5 days after surgery compared to wild type. Furthermore, the PHD3$^{-/-}$ macrophage population showed an increased surface expression of the anti-inflammatory marker CD206 4 and 5 days after surgery, indicating a faster initiation of wound healing compared to wild type. Despite the blunted macrophage response, perfusion recovery and angiogenesis were unaltered between PHD3$^{-/-}$ and wild type mice. However, the development of fibrosis was decreased in PHD3$^{-/-}$ mice 4 weeks after surgery, which could have been caused by the attenuated macrophage response. Neither a change in apoptosis nor in migratory behavior was observed in PHD3$^{-/-}$ macrophages which could serve as a possible explanation for the decreased inflammatory response of PHD3$^{-/-}$ macrophages. RNA sequencing of macrophages sorted from the hind limb 5 days after surgery revealed 10 differentially regulated genes. Cyp2s1, an epoxygenase which metabolizes Prostaglandin (PG) G2 and H2 to 12-hydroxyheptadecatrenoic acid (12-HHT), was significantly downregulated in PHD3$^{-/-}$ macrophages. This downregulation could be mimicked in bone marrow-derived macrophages (BMDM) when cultivated in starvation medium in hypoxia (1% O_2). Under these conditions, BMDM also displayed a significantly higher secretion of PGE2, which might be explained by the downregulation of Cyp2s1. PGG2 and PGH2 are substrates for 12-HHT and PGE2 synthesis likewise. Lower Cyp2s1 expression could therefore leave more substrates for PGE2 synthesis. PGE2 can induce anti-inflammatory behavior in

macrophages and therefore presents a putative explanation for the attenuated macrophage response in PHD3$^{-/-}$ mice.

To study the role of PHD2 in macrophages in an ischemia model, I analyzed the effect of myocardial infarction in myeloid-specific PHD2$^{-/-}$ mice. Macrophage but not neutrophil invasion and clearance in the ischemic heart muscle were altered between wild type and PHD2$^{-/-}$ mice. Macrophage infiltration into the ischemic heart was delayed in PHD2$^{-/-}$ macrophages, which was linked to a worse heart function measured by echocardiography. In line with this, previous *in vitro* studies, conducted by another member of the Institute of Cardiovascular Physiology, found a migration defect in PHD2$^{-/-}$ BMDM as well as a lower phagocytotic capacity, which might account for the *in vivo* findings. These findings demonstrate non-redundant roles for PHD-isoforms PHD2 and PHD3 in myeloid cells. Myeloid-specific PHD2-deficiency presents a disadvantage in the resolution of ischemia-induced inflammation while myeloid PHD3-deficiency leads to a faster resolution of inflammation with positive effects on wound-healing.

1. Introduction

1.1 Ischemic diseases

Ischemic diseases present a serious and frequent health threat to modern society. Pathologic ischemia is most commonly caused by the occlusion of blood vessels which hinders the supply of oxygen and nutrients to the tissue of an organ or a whole extremity. Vessels can be either permanently or transiently closed. Both the acute lack of blood supply, as well as the reperfusion of the tissue, can cause severe damage, which leads to an inflammatory reaction by the innate immune system. In the long term, the loss of functional tissue by ischemia causes organ remodeling, which ultimately results in organ failure (reviewed by (Cohn et al., 2000)). Prominent examples for ischemic diseases are myocardial infarction (MI) or peripheral artery disease (PAD), both of them having a high prevalence worldwide.

1.1.1 Myocardial infarction

Myocardial infarction is a major cause of death worldwide. It is characterized by the ischemia-induced necrosis of heart tissue, which is caused by the occlusion of at least one coronary artery. Arteries occlude most commonly due to atherosclerotic plaques, but also due to vasospasms or endothelial dysfunction in less frequent cases (reviewed by (Thygesen et al., 2012)).

Following the initial ischemic insult the myocardium undergoes several stages before a scar is formed. Within 2-4 hours after the ischemic event cells become necrotic. This is followed by an inflammatory reaction of the innate immune system and ultimately by the formation of a scar within 5-6 weeks after MI (reviewed by (Thygesen et al., 2012)). The resulting scar does not possess contractility, which impairs the heart muscle function. In turn, this leads to the remodeling of the heart. Cardiac remodeling takes the form of wall dilatation, hypertrophy or fibrosis and can ultimately lead to cardiac failure (reviewed by (Cohn et al., 2000)). The initial phases of tissue necrosis and the inflammatory response in the infarcted heart are important factors which influence the subsequent phase of cardiac remodeling and therefore the clinical outcome for each patient. A persistent inflammatory reaction, for example characterized by elevated serum monocyte chemoattractant protein (MCP)-1, correlates with reduced survival of the patients (de Lemos et al., 2007). However, the inflammatory reaction is also vital for the removal of cell debris. This is why therapeutic intervention should be well thought-out and specific and has so far not been successfully introduced into the therapy of MI patients.

Current therapy aims at the fast restoration of the blood flow via locally administered fibrinolytica in combination with anticoagulants and antiplatelet therapy. On the long term, patients are treated with anti-hypertension and anti-thrombotic drugs, combined with a lifestyle intervention including cessation of smoking, weight control and more physical activity (reviewed by (Steg et al., 2012)).

1.1.2 Peripheral artery disease (PAD)

PAD has a high prevalence, affecting around 5% of 45-49 years-old worldwide. This number drastically increases with the age of the patients to around 20% in over 80-years old (Fowkes et al., 2013). PAD is characterized by the complete or partial occlusion of the superficial femoral artery. In less common cases the iliac, common femoral or tibiopereonal artery in the leg can be occluded by an atherosclerotic plaque. The occlusion of an artery leads to an ischemic state of the surrounding muscle tissue. This results in muscle fiber apoptosis and other morphological alterations of the muscle, including atrophy and muscle fiber denervation. These phenomena are linked to increased levels of inflammatory mediators such as tumor necrosis factor (TNF)-α and interleukin (IL)-6 (Brevetti et al., 2010).

The course of PAD can range from asymptomatic to chronic limb ischemia, the latter being connected to ischemic pain, ulceration of the extremity and leading to limb amputation in 12% of the cases (reviewed by (Peach et al., 2012)). Clinical treatment focuses on treating symptoms and is only partially able to ameliorate the state of the patient. Examples include patients being advised to do more exercise or patients being pharmacologically treated with anti-platelet and vasodilatative therapeutics like cilostazol. In severe cases, surgical bypasses and stents are a frequent treatment method (reviewed by (Berger and Hiatt, 2012)).

More recently, gene therapies have been tested, which introduce pro-angiogenic genes via adenoviral or plasmid liposome transfer into the muscle tissue. Among the genes with promising clinical trial results are for example vascular endothelial growth factor (VEGF) and also hypoxia-inducible factor (HIF) (reviewed by (Berger and Hiatt, 2012)).

1.2 Mechanisms that trigger sterile inflammation

An inflammatory reaction, which is not induced by infectious pathogens such as bacteria or viruses, is called sterile inflammation. There are various triggers for a sterile inflammation such as irritant particles like asbestos or toxins, trauma, ischemia or ischemia reperfusion. These triggers cause cell death by necrosis. Necrotic cells are characterized by a permeable cell membrane and an uncontrolled release of cytoplasmic and organelle-associated molecules. Some intracellular molecules are under normal conditions not accessible to the innate immune system. Their sudden release presents a danger signal which attracts

leukocytes to the site. When for example healthy cell cytoplasm is injected into mice, components of this cytoplasm induce a sterile inflammation (Eigenbrod et al., 2008).

Many intracellular components have been shown to act as inflammatory trigger. They have been termed pro-inflammatory damage-associated molecular membrane patterns (DAMPs). Among these DAMPs are for example the nuclear protein high-mobility group box 1 (HMGB1), endogenous DNA, adenosine triphosphate (ATP) or mitochondrial compounds (Bours et al., 2006; Imaeda et al., 2009; Scaffidi et al., 2002; Zhang et al., 2010). In addition to that, cells can store inflammatory cytokines like IL-1α or IL-33 as active precursors inside the cell (Eigenbrod et al., 2008; Moussion et al., 2008). Upon uncontrolled membrane breakdown, these cytokines get released and can induce an inflammatory reaction. Extracellular proteins like hyaluronan act as DAMP when they are cleaved by intracellular proteases released by necrotic cells (Jiang et al., 2005).

The pathways by which immune cells detect DAMPs and their respective contribution to the *in vivo* situation are not completely understood. Several proteins, such as HMGB1 and heat shock proteins (HSPs), are recognized by Toll-like receptors (TLRs) 2 and 4 (Quintana and Cohen, 2005; Vabulas et al., 2001; Yu et al., 2006). These receptors also play a major role in the recognition of pathogen-associated molecular membrane patterns (PAMPs) of viral or bacterial origin. TLR9 has been shown to not only recognize viral and bacterial DNA, but also endogenous DNA. TLR9 especially recognizes DNA from apoptotic cells or from mitochondria (Imaeda et al., 2009; Zhang et al., 2010). Other receptors, like the receptor for advanced glycation endproducts (RAGE) which recognizes S100 proteins, are unique to DAMP recognition (Hofmann et al., 1999).

In addition, the NOD-, LRR-, and pyrin domain containing 3 (NLRP3) inflammasome can be activated by ATP or uric acid in order to stimulate secretion of active IL-1β (Kono et al., 2010; Mariathasan et al., 2006; Martinon et al., 2006). Upon activation, NLRP3 gets linked to pro-caspase-1 via the adaptor protein apoptosis-associated speck-like protein containing a CARD (ASC). This process induces a self-cleavage of pro-caspase-1 into caspase-1, which can cleave inactive pro-IL-1β to IL-1β (reviewed by (Chen and Nunez, 2010). IL-1β is then released and induces neutrophil infiltration via its receptor IL-1R.

Several other pathways and DAMPs have been implicated in the mediation of sterile inflammation. All of these pathways eventually lead to activation of tissue-resident macrophages and other tissue cells and recruitment of neutrophils and monocytes to the inflamed site.

1.3 Cellular responses in sterile inflammation

1.3.1 Macrophages

Macrophages, first described by Elie Metchnikoff at the end of the 19th century, are very versatile cells (reviewed by (Gordon, 2007)). Under resting conditions, tissue macrophages act as sentinels. They home into different tissues, detect potential harm and attract other immune cells to the site to initiate an immunological response. In addition to that, they mediate organ homeostasis by phagocytosis of apoptotic cells. Together with dendritic cells, they are responsible for mediating peripheral tolerance in the lymph nodes. Along with B-cells, dendritic cells and thymus epithelial cells they form the group of professional antigen-presenting cells (APCs). Both intracellular and extracellular particles are being processed by professional APCs and presented on the cell surface via the proteins major histocompatibility complex (MHC) I and II to T-cells and B-cells (reviewed by (Roche and Furuta, 2015)). This allows for a close collaboration of the innate and adaptive immune system. Tissue macrophages develop already during embryogenesis. Several tissue-specific macrophage subtypes have evolved including for example Kupffer cells in the liver, microglia in the brain and osteoclasts in the bone (reviewed by (Epelman et al., 2014)).

Macrophages detect danger signals, for example by TLRs as well as by phagocytosis of particles. This detection is mediated via complement, Fc and scavenger receptors (reviewed by (Gordon, 2007)). Upon detection of a danger signal, macrophages become activated and start to secrete cytokines and chemokines to fight pathogens and attract other immune cells. The diversity of potentially dangerous factors makes it necessary for the macrophage to have an equally diverse way to respond. Upon bacterial infection for example, macrophages can adopt a pro-inflammatory phenotype. This phenotype is effective at killing bacteria by increased nitric oxide (NO) and reactive oxygen species (ROS) production, as well as by secretion of pro-inflammatory cytokines like TNF-α, IL-1β and IL-6. In the environment of a tumor or during the resolution of inflammation, macrophages adopt a more anti-inflammatory phenotype. This phenotype is linked to increased secretion of IL-10 and increased phagocytosis of dead cells. Anti-inflammatory macrophages secrete pro-angiogenic factors like VEGF. They also produce transforming growth factor (TGF)-β, which stimulates the production of extracellular matrix (reviewed by (Murray and Wynn, 2011)).

In cell culture, these pro- and anti-inflammatory phenotypes can be mimicked by administering specific cytokines. Interferon (IFN)-ɣ and lipopolysaccharide (LPS) induce naïve macrophages to polarize towards the classically activated (M1) pro-inflammatory macrophage type. LPS and IFN-ɣ mediate this activation via signal transducer and activator of transcription (STAT)1 and nuclear factor kappa-light-chain-enhancer of activated B cells (NF-κB) signaling. Addition of the cytokines IL-4 and IL-13 induces an alternatively activated

(M2) anti-inflammatory state via STAT6 (reviewed by (Sica and Mantovani, 2012)). Various subtypes of M2-macrophages can be distinguished based on the different stimuli that induce them (Murray et al., 2014) or by their surface markers and secreted cytokines (reviewed by (Roszer, 2015)).

1.3.2 Monocytes

Monocytes are myeloid cells derived from the bone marrow that make up 5-10% of the nucleated cells in the blood stream. Two types of circulating monocytes can be distinguished: pro-inflammatory "classical" monocytes and patrolling monocytes. The patrolling monocytes migrate along the inside walls of vessels, where they most likely control the integrity of the endothelial layer. Inflammatory monocytes can be recruited to a site of inflammation, where they differentiate into pro-inflammatory macrophages or dendritic cells (reviewed by (Shi and Pamer, 2011)). In steady state however, their contribution to replenishing macrophage and dendritic cells in the tissue is limited (reviewed by (Ginhoux and Jung, 2014)).

1.3.3 Neutrophils

Neutrophils were first described as phagocytotic "microphages" by Elie Metchnikoff (reviewed by (Cavaillon, 2011)). Neutrophils are armed with many different antibacterial defense mechanisms. Like macrophages, they can generate NO and ROS to fight extracellular pathogens. They also store a wide range of proteolytic enzymes, like cathepsin G, and antimicrobial peptides, such as defensins (reviewed by (Geering et al., 2013)). These defense mechanisms are rather unspecific and can also cause much damage to healthy tissue when they get released. This is why neutrophil lifespan and localization are tightly controlled.

Neutrophils are differentiated in the bone marrow from myeloid progenitors. Their differentiation is regulated by the granulocyte colony-stimulating factor (G-CSF) (reviewed by (Demetri and Griffin, 1991)). In resting conditions, mature neutrophils are released into the blood stream where they have a restricted lifespan of 1 to 5 days (Pillay et al., 2010). As they are a potential threat to tissue cells, neutrophils do not migrate into healthy tissues. At the end of their short lifespan, senescent neutrophils are removed in spleen, liver and in the bone marrow (reviewed by (Furze and Rankin, 2008)). A pool of mature neutrophils is kept in the bone marrow and is constantly replenished. This allows for a very fast response during the initiation of inflammation.

1.3.4 Neutrophil, monocyte and macrophage interplay in sterile inflammation

A sterile inflammation such as ischemia-induced injury is initiated when DAMPs get recognized by tissue macrophages. Via binding to receptors such as IL-1R, TLRs and RAGE, macrophages get activated and secrete inflammatory mediators like chemokine (C-X-C motif) ligand 1 (CXCL1), IL-8 and TNFα (reviewed by (Chen and Nunez, 2010)). IL-8 and

CXCL1 gradients in the blood attract neutrophils which migrate into the tissue (reviewed by (Silva, 2010). Neutrophils are rapidly recruited from the blood and from the bone marrow. They arrive in the injured tissue within hours, which makes them the first wave of inflammatory cells migrating to the place of injury.

Activated endothelial cells and macrophages secrete chemokines like C-C chemokine ligand (CCL) 2, which attracts monocytes and mediates adhesion and migration of pro-inflammatory "classical" monocytes into the tissue. In addition, neutrophils release granules while they extravasate through the endothelial layer into the tissue. These granules contain for example cathepsin G and azurodicin, which are potent monocyte attractants. The invading monocytes differentiate into pro-inflammatory macrophages and dendritic cells upon migration into the tissue and, together with neutrophils and activated tissue macrophages, mediate the early phase of inflammation (reviewed by (Soehnlein and Lindbom, 2010)). In addition to the monocyte-derived macrophages, there is evidence that tissue macrophages can also proliferate locally upon induction of inflammation (Robbins et al., 2013).

The interaction of the different immune cells with each other and with their environment is vital for the time course of inflammation. The restricted lifespan of neutrophils is prolonged by macrophage-derived pro-inflammatory cytokines such as TNF-α, IL-1β, G-CSF and granulocyte macrophage colony-stimulating factor (GM-CSF). Additionally, hypoxia, which is a common condition in inflamed loci, increases neutrophil lifespan and regulates the inflammatory response of macrophages (Cramer et al., 2003; Walmsley et al., 2005). To ultimately limit neutrophil recruitment to the tissue, macrophages secrete prostaglandins (PG) E2 and D2. PGE2 and PGD2 stimulate the synthesis of anti-inflammatory mediators such as lipoxins which inhibit neutrophil infiltration while promoting monocyte migration.

The resolution of inflammation is initiated by the phagocytosis of apoptotic neutrophils by macrophages. Apoptotic neutrophils release anti-inflammatory mediators such as Annexin A1. Also, they upregulate "find me" signals like sphingosine-1-phosphate to attract macrophages which phagocytose the dying neutrophils (reviewed by (Ravichandran, 2010)). The phagocytosis of dead cells, also called efferocytosis, primes macrophages to a more anti-inflammatory (M2) phenotype.

In the following restoration of tissue homeostasis, macrophages secrete VEGF to enhance angiogenesis as well as immunosuppressive factors like IL-10. In addition, macrophages produce TGF-β which activates fibroblasts and enhances their secretion of extracellular matrix components. Fibrotic tissue forms a scar to replace the functional tissue which has been lost due to the original trigger of injury and to the ensuing inflammatory reaction (reviewed by (Lech and Anders, 2013).

1.4 Hypoxia

Molecular oxygen is needed for aerobic metabolism, which provides the foundation for the life of most complex organisms. The human body takes up oxygen from the air via the alveolae in the lung. Oxygen then gets distributed via the blood stream and reaches the different tissues via diffusion. Physiological partial oxygen pressures (pO_2) within the cells can vary depending on the organ and typically lie between 25-65 mm Hg (Vaupel et al., 1989). Hypoxia occurs when the pO_2 drops below the physiological level of the respective tissue, causing an imbalance between oxygen supply and consumption within the cells.

Both physiological and pathological conditions can trigger hypoxia. Being at high altitudes for example, where the pO_2 is lower than at sea level, presents a physiological trigger for hypoxia. During parts of embryogenesis, hypoxia is vital for the correct formation of organs and blood vessels, with differentiation of progenitor cells being in part mediated by oxygen levels (reviewed by (Simon and Keith, 2008)). In pathological settings, hypoxia occurs most frequently by insufficient blood flow to a tissue, which results in ischemic diseases such as MI. Hypoxia can also occur in inflamed lesions by the massive infiltration of oxygen-consuming immune cells or when a tumor outgrows its blood supply.

Hypoxia, especially in pathologic conditions, can present a major challenge for the cells in a tissue as they highly depend on it to mobilize energy: many cells metabolize nutrients predominantly via the oxygen-dependent oxidative phosphorylation. This reaction generates ATP, which is needed for every energy-consuming reaction happening in a cell. When oxygen is no longer available at sufficient levels, cells either undergo cell death or they adapt to hypoxia. Adaptation to hypoxia includes short term effects, like the shift of metabolism towards anaerobic glycolysis, as well as long term adaptation via induction of erythropoiesis and angiogenesis. Most of these adaptations are regulated by the transcriptional regulation of the respective enzymes or growth factors. The hypoxia-inducible factors (HIFs), a transcription factor family, present the key mechanism to this hypoxic adaptation.

1.4.1 Hypoxia-inducible factors

HIFs were first described as proteins binding to the enhancer of the *EPO* gene in a hypoxia-inducible manner (Semenza and Wang, 1992). HIFs comprise a small family of heterodimeric transcription factors, which are composed of a hypoxia-regulated HIFα subunit and HIF-1β which is present at constant levels (Wang et al., 1995; Wang and Semenza, 1995). HIF-1β had already been described as aryl hydrocarbon receptor nuclear translocator (ARNT) before, a protein which can interact with aryl hydrocarbon receptor (AHR) in order to function as a receptor for dioxins and polycyclic aromatic hydrocarbons (Hoffman et al., 1991). Both HIFα and HIF-1β are basic-helix-loop-helix (bHLH) proteins containing Per-ARNT-Sim (PAS) domains at their N-terminus, which are important for their interaction (Figure 1).

The group of HIFα proteins that can interact with HIF-1β are comprised of HIF-1α, HIF-2α and HIF-3α. HIF-1α and HIF-2α show a similar protein structure, with bHLH and PAS domains at the N-terminus. They also include an oxygen-dependent degradation (ODD) domain, as well as two transactivation domains (N-TAD and C-TAD) for transcriptional activity (Figure 1) (Jiang et al., 1997; Pugh et al., 1997). HIF-1α and HIF-2α have a common, but not completely overlapping, set of target genes indicating their synergistic function.

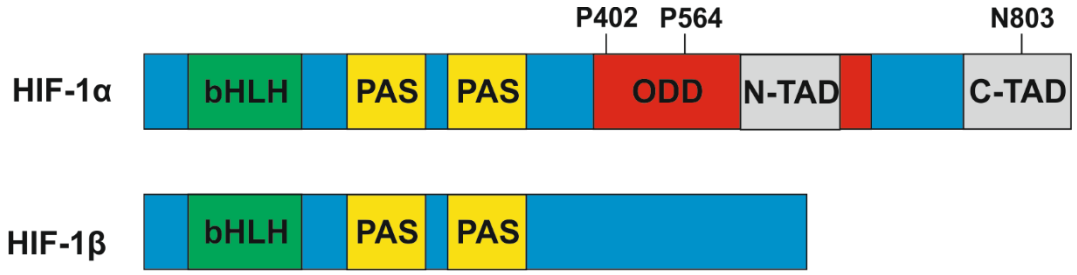

Figure 1: Protein structure of HIF-1α and HIF-1β including domains and modification sites. HIF-1α and HIF-1β both possess a basic helix-loop-helix (bHLH) and a Per-ARNT-Sim (PAS) domain for interaction with DNA and with each other respectively. HIF-1α possesses an oxygen-dependent degradation (ODD) domain containing an N-terminal transactivation domain (N-TAD). The ODD domain includes two conserved prolines (P402 and P564), which can be hydroxylated by prolyl-4-hydroxylase domain enzymes. HIF-1α also possesses a C-terminal transactivation domain (C-TAD) with a conserved asparagine (N803), which can be hydroxylated by Factor Inhibiting HIF-1.

There are multiple variants described for HIF-3α. Full length HIF-3α includes bHLH and PAS domains, an ODD domain as well as a N-TAD, but not a C-TAD domain. Full length HIF-3α is described to have only limited function in the hypoxia response, which is typically mediated by HIF-1α and -2α (Gu et al., 1998). Shorter variants of HIF-3α, such as the inhibitory PAS domain protein (IPAS), have been described to dimerize with HIFα subunits, thereby inhibiting their ability to act as a transcription factor (Makino et al., 2002).

1.4.2 HIF-target genes

Together with HIF-1β, HIFα subunits bind to hypoxia-responsive elements (HREs) in or outside promoter regions of its target genes. Those HREs consist of the sequence (A/G)CGTG, with the most abundant form being ACGTG (reviewed by (Wenger et al., 2005)).

The onset of hypoxia forces the cell to change its metabolism towards anaerobic glycolysis. For this adaptation HIF-regulated gene expression of glucose transporters (GLUT)1 and 3 increases in order to transport more glucose into the cells (Chen et al., 2001). Furthermore, several metabolic enzymes are HIF-target genes. These include for example Pyruvate dehydrogenase lipoamide kinase isoenzyme 1 (PDK-1), which inhibits the tricarboxylic acid (TCA) cycle by inhibition of pyruvate dehydrogenase (PDH). PDH is an enzyme that converts pyruvate to acetyl-CoA (Kim et al., 2006; Papandreou et al., 2006) which is then fed into the TCA cycle. Pyruvate kinase isoenzymes 1 and 2 (PKM1, 2) are also HIF-target genes. PKM2

has been shown to act as a coactivator of HIF, which promotes its transcriptional activity (Luo et al., 2011).

An important HIF-1α target gene, especially in myeloid cells, is the inducible NO synthase (iNOS) which produces NO as a defense mechanism against invading pathogens (Fang, 1997; Melillo et al., 1995; Melillo et al., 1997)). Interestingly, HIF-2α induces the expression of arginase-1, which converts L-arginine into ornithine and urea (Takeda et al., 2010). L-arginine is also needed for NO production by iNOS, which puts both enzymes in direct competition for their substrate. Anti-inflammatory macrophage polarization has been shown to correlate with increased levels of HIF-2α, while HIF-1α mediated iNOS induction primed macrophages to a pro-inflammatory phenotype (Takeda et al., 2010). HIF-1α and -2α have been shown to differ in their time course of protein stabilization upon induction of hypoxia. While HIF-1α is transiently stabilized in the early hypoxic phase, HIF-2α stabilization is also prominent in prolonged hypoxia (Holmquist-Mengelbier et al., 2006; Kong et al., 2007). This might indicate different roles for HIF-1α and HIF-2α for the different phases of macrophage activation during tissue hypoxia- with HIF-1α promoting the early inflammatory and HIF-2α mediating the subsequent regulatory and anti-inflammatory phase.

In hypoxia, cell survival and apoptosis need to be regulated in order to prevent cell necrosis and subsequent damage to the tissue. Certain factors influencing cell survival are HIF-target genes. An example of such a factor is BCL2/adenovirus E1B 19 kDa protein-interacting protein 3 (Bnip3), which mediates mitophagy (Band et al., 2009; Tracy et al., 2007). A connection between HIF and p53 signaling has furthermore been established by various researchers (reviewed by (Obacz et al., 2013). The anti-apoptotic factor B cell lymphoma-extra large (Bcl-XL) is also a direct HIF-target gene (Chen et al., 2009).

To overcome long term hypoxia, endothelial cell growth is stimulated to restore blood flow via angiogenesis. VEGF which is a potent pro-angiogenic factor is upregulated as a HIF-target gene (Connolly et al., 1989; Shweiki et al., 1992). Additionally, erythropoiesis is stimulated by the upregulation of EPO, which was the first described HIF-target gene (Semenza and Wang, 1992).

Overall, more than 100 target genes of the hypoxia-inducible factors have been described that play an important role in the adaptation to hypoxia.

1.4.3 Hypoxia-inducible factor-1 regulation

While HIF-1β is stably expressed in normoxia and hypoxia, HIFα protein levels are highly dependent on the availability of oxygen. In normoxia, HIF-1α is only present at basal levels but gets rapidly induced upon hypoxia. When hypoxic samples get reoxygenated, the level of

HIF-1α is again diminished to basal levels within minutes (Huang et al., 1998; Moroz et al., 2009).

The fast kinetics of HIF-1α protein levels suggest a regulation mechanism which is not mediated on a transcriptional level. Indeed, levels of HIFα subunits are mainly regulated via their protein stability. In normoxia these subunits are recognized by the von-Hippel Lindau tumor suppressor protein (pVHL), which is a component of an Ubiquitin E3 ligase complex (Maxwell et al., 1999). Following the recognition by pVHL, HIFα is ubiquitinated which leads to its proteasomal degradation.

pVHL can only effectively bind HIFα when conserved proline residues (HIF-1α: Pro 402 and Pro 564) in the ODD domain of HIFα are hydroxylated (Figure 1). This hydroxylation is mediated by Prolyl-4-hydroxylase domain enzymes (PHD) 1, 2 and 3 (Ivan et al., 2001; Jaakkola et al., 2001). PHDs need cofactors like 2-oxoglutarate (2-OG), Fe^{2+}, ascorbate and most importantly molecular oxygen for their enzymatic activity. Therefore, HIFα is rapidly degraded when enough oxygen is available. In hypoxia however, hydroxylation of HIFα by the PHDs is inhibited, and HIFα is no longer recognized by pVHL. HIFα gets stabilized and can then translocate into the nucleus and dimerize with the stably expressed HIF-1β to activate the expression of its target genes (Figure 2).

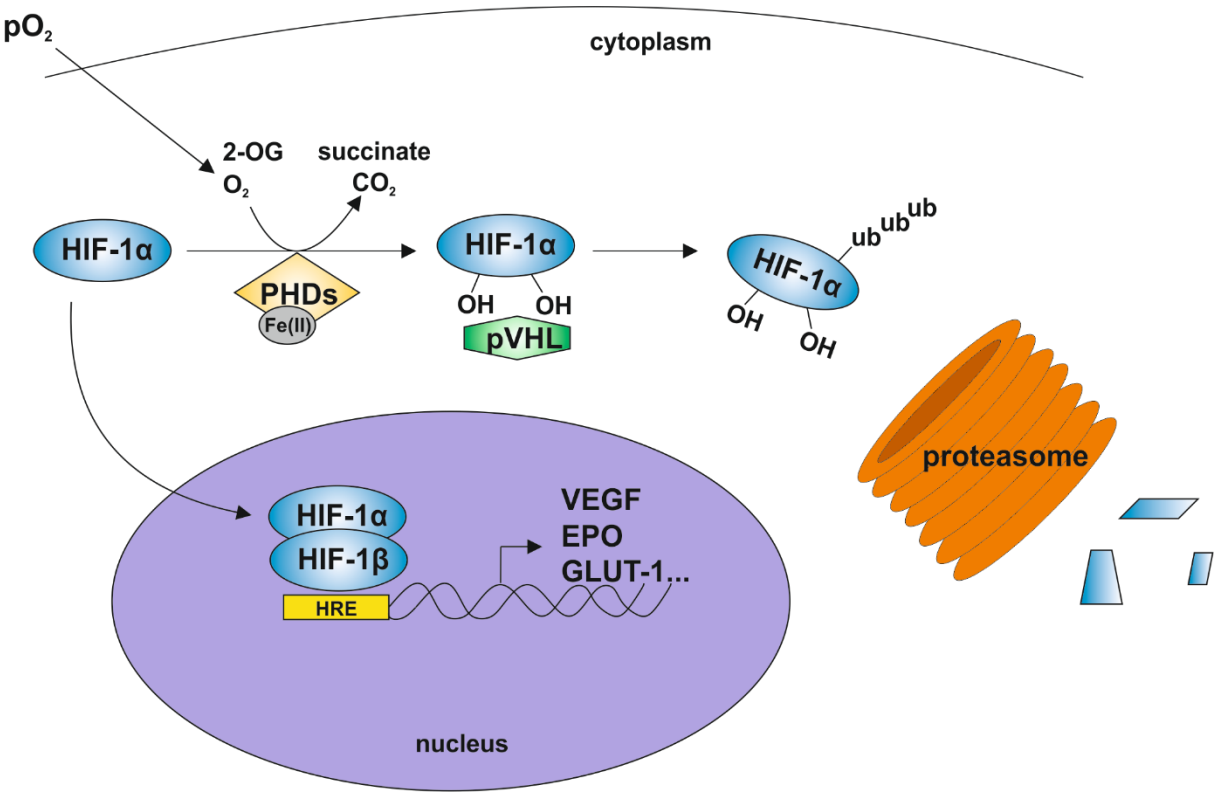

Figure 2: Overview of the oxygen-dependent degradation of HIF-1α by prolyl-4-hydroxylase domain enzymes (PHDs). HIF-1α is hydroxylated by PHDs which need the cofactors Fe(II), oxygen and 2-oxoglutarate (2-OG) for their enzymatic activity. The hydroxylated HIF-1α is recognized by von-Hippel Lindau tumor suppressor protein (pVHL), which leads to polyubiquitination of hydroxylated HIF-

1α and subsequent proteasomal degradation. When oxygen is not present at sufficient levels, HIF-1α is stabilized, translocates into the nucleus, dimerizes with HIF-1β and activates transcription of its target genes, including vascular endothelial growth factor (VEGF), erythropoietin (EPO) and glucose transporter 1 (GLUT-1), via binding to hypoxia-responsive elements (HREs) in their enhancers or promoters.

PHDs are not the only enzymes that can modify HIFα proteins. Factor inhibiting HIF (FIH)-1 is an asparaginyl hydroxylase enzyme, which hydroxylates a conserved asparagine residue (HIF-1α: Asn 803, HIF-2α: Asn 851) in the C-TAD region of HIFα (Lando et al., 2002a). This modification has been reported to inhibit HIFα association with CREB-binding protein and p300 (Lando et al., 2002b), which act as coactivators of HIF-mediated transcription (Kallio et al., 1998; Ruas et al., 2010). Similar to the PHDs, FIH-1 needs molecular oxygen to convey hydroxylation of the conserved asparagine residue. As a result, this asparagine is constantly hydroxylated in normoxia, leading to an inhibition of HIF. In hypoxia, hydroxylation can no longer take place, which leads to transactivation of gene expression. FIH-1 has furthermore been demonstrated to form a complex with HIF-1α and pVHL, which inhibits HIFs activity as a transcription factor (Mahon et al., 2001).

1.4.4 PHDs

PHD enzymes belong to a group of 2-OG-dependent dioxygenases which catalyze the hydroxylation of conserved prolines within the structure of HIF-α subunits as well as of several other proteins. PHD 1, 2 and 3 have a 42-59% structural similarity to each other (Hirsila et al., 2003) while P4H-TM, the fourth member of this enzyme family, is structurally quite different (Koivunen et al., 2007; Oehme et al., 2002). Their function as prolyl-4-hydroxylases, as well as their binding sites for Fe(II) and 2-OG are however highly conserved. Other prolyl-4-hydroxylases (P4H), like the collagen-P4H (c-P4H) enzymes utilize the same cofactors as PHDs (Hutton et al., 1966). The essential difference between those enzymes and the PHDs is the binding affinity for oxygen. PHDs all bind oxygen with a K_m-value of 230-250 µM, which is slightly above the concentration of dissolved O_2 at atmospheric conditions (Hirsila et al., 2003). This high K_m-value is a prerequisite for the oxygen sensor function of PHDs because it results in oxygen being the limiting factor, while c-P4H enzymes still work efficiently at low oxygen concentrations.

1.4.4.1 Proline-4-hydroxylation of HIF

PHD enzymes mediate the *trans*-4-hydroxylation of conserved prolines within the structure of HIFα subunits. The conserved prolines that are hydroxylated by PHDs lie in a LXXLAP amino acid motif, which is conserved (Epstein et al., 2001). However, HIFα hydroxylation can also take place when single amino acids are replaced (Huang et al., 2002; Li et al., 2004). Out of those two prolines, Pro564 (HIF-1α) is hydroxylated first. This prior hydroxylation of Pro564 then facilitates Pro402 hydroxylation (Chan et al., 2005).

In order to mediate proline-4-hydroxylation, PHDs need the cofactors Fe(II), ascorbate, molecular oxygen and 2-OG. Fe(II) is very important for the coordinated binding of the substrates HIF, 2-OG and oxygen. Binding to Fe(II) allows oxygen to attack one ketone group of 2-OG. 2-OG is decarboxylated which results in the formation of succinate and CO_2 and requires one oxygen atom from the O_2 molecule (Figure 3). The remaining oxygen atom is bound in a highly active oxo-ferryl intermediate. This intermediate captures one hydrogen atom from proline to then introduce a hydroxyl radical back to form 4-hydroxyproline (reviewed by (Berra et al., 2006; Smirnova et al., 2012)).

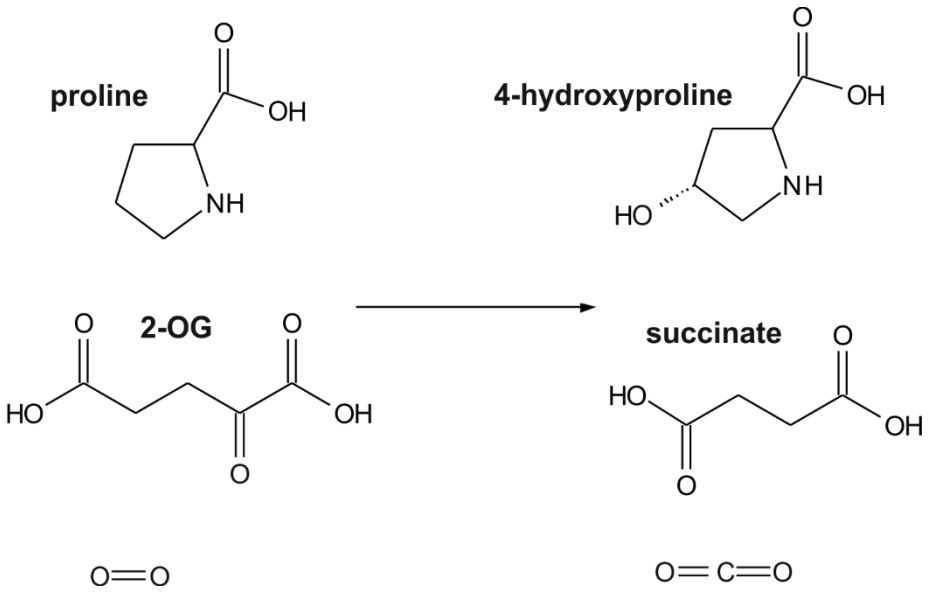

Figure 3: Prolyl-4-hydroxylation reaction. The substrate 2-oxoglutarate (2-OG) is decarboxylated by the Fe(II)-bound oxygen. This results in the formation of succinate and CO_2, which incorporates one oxygen atom of the oxygen molecule. The other oxygen atom gets integrated into proline forming a hydroxyl group at position C-4.

1.4.4.2 Differences between PHD isoform expression patterns

PHD1, 2, 3 and P4H-TM have distinct expression patterns within the cell. PHD1 is predominantly located in the nucleus (Metzen et al., 2003). The transport of PHD1 into the nucleus is mediated via a nuclear localization sequence (NLS) in a α/β-importin-dependent manner (Steinhoff et al., 2009). In contrast to that, PHD2 is actively transported out of the nucleus via a nuclear export sequence (NES) and is mostly present in the cytoplasm (Metzen et al., 2003; Steinhoff et al., 2009). PHD3 is localized both in the cytosol and the nucleus (Metzen et al., 2003).

In contrast to PHD1, 2 and 3, P4H-TM (called PH4 by (Oehme et al., 2002)) has a transmembrane domain and is localized in the endoplasmatic reticulum (ER) facing its lumen (Koivunen et al., 2007; Oehme et al., 2002). Despite this location, P4H-TM overexpression or knock down still have an influence on HIF-1α levels *in cellulo* and on EPO levels *in vivo* (Hyvarinen et al., 2010; Laitala et al., 2012) and it is capable of hydroxylating HIFα *in vitro*

(Koivunen et al., 2007). It however remains unknown how P4H-TM exhibits those effects from inside the ER-lumen.

PHD2 is the most abundantly expressed isoform in different organs and cell types compared to the other PHDs (Appelhoff et al., 2004). In contrast to that, both PHD1 and PHD3 are widely expressed at low levels, but show high expression levels only in a few distinct tissues. While PHD1 is highly expressed in hormone-responsive tissues and is the only PHD present in the testis, PHD3 is highly present in the adult heart and brain, as well as in various embryonic tissues (Lieb et al., 2002). The clear differences in expression pattern both intracellular and between different tissues already hints at non-redundant functions of the three isoforms.

1.4.4.3 Different roles of the PHDs in the hydroxylation of HIFα

PHD1, 2 and 3 differ distinctly from each other in their role for HIFα stabilization. PHD2 is the most abundantly expressed isoform and has a dominant role in regulating HIFα protein stability in normoxia (Appelhoff et al., 2004; Berra et al., 2003). PHD3 is a HIF-target gene which gets highly induced in hypoxia, presumably as part of a negative feedback loop (del Peso et al., 2003; Pescador et al., 2005). Indeed, PHD3 retains more of its enzymatic activity in hypoxia than PHD1 and 2, which makes it a potent regulator of HIF-1α in hypoxia (Appelhoff et al., 2004; Ginouves et al., 2008). PHD2 is also a HIF-target gene and moderately induced in hypoxia, while PHD1 is not upregulated in hypoxia or in some cell lines even downregulated (Appelhoff et al., 2004; Berra et al., 2003; Epstein et al., 2001; Metzen et al., 2005). Instead, transcription of PHD1 is induced by the estrogen-receptor in hormone-sensitive cells (Seth et al., 2002).

It is furthermore suggested that PHD2 targets preferentially HIF-1α while PHD3 shows a stronger activity towards HIF-2α (Appelhoff et al., 2004). PHD2 and 3 show an equally high activity for hydroxylation of HIF-1, 2 and 3α in pVHL capture assays, while PHD1 activity is significantly lower (Tuckerman et al., 2004). Also, the activity of the three PHDs towards the two conserved prolines is different. PHD3 is almost incapable of hydroxylating Pro402 on HIF-1α, while PHD1 and 2 are both capable of doing so (Hirsila et al., 2003). Furthermore, PHD3 seems to identify Pro564 by the amino acid sequence in the immediate proximity, while PHD1 and 2 both recognize it by its general location (Chan et al., 2005).

1.4.4.4 PHD1

PHD1 homozygous knock out mice are viable and do not show any obvious phenotypes. Upon induction of hind limb ischemia, myofibers from PHD1$^{-/-}$ mice are protected from lethal damage by a metabolic shift towards anaerobic glycolysis (Aragones et al., 2008). This metabolic shift also caused a more beneficial response in PHD1$^{-/-}$ mice upon hepatic

ischemia-reperfusion damage (Schneider et al., 2010) and in a stroke model (Quaegebeur et al., 2016).

Apart from HIFα, PHD1 can also hydroxylate other substrates. Hypoxia-mediated induction of NF-κB signaling has been shown to be mediated by PHD1. PHD1 hydroxylates a proline in an LXXLAP sequence of IKKβ (Cummins et al., 2006). In addition to its influence on NF-κB signaling, PHD1 also influences inflammation *in vivo*. In a model of inflammatory bowel disease, $PHD1^{-/-}$ mice had a better survival rate than wild type littermates, which was mediated by an enhanced endothelial barrier function and decreased enterocyte apoptosis (Tambuwala et al., 2010). Also, human biopsies of ulcerative colitis were found to have increased PHD1 RNA and protein levels, which correlated with increased pro-inflammatory TNFα and IL-8 levels (Van Welden et al., 2013).

1.4.4.5 PHD2

PHD2 seems to have a vital role for physiological processes, especially in the cardiovascular system. Homozygous deletion of PHD2 leads to embryonically lethal defects in heart and placenta formation of mice (Takeda et al., 2006). In contrast to that, heterozygous PHD2 knock out mice ($PHD2^{+/-}$), in which PHD2 RNA levels are decreased by half, are viable without any gross defects (Mazzone et al., 2009). Mice in which a homozygous PHD2 knock out is induced after early embryogenesis develop polycythemia and dilated cardiomyopathy with a drastically decreased life span (Minamishima et al., 2008). In humans, loss-of-function mutations of PHD2 have been described to lead to a form of familial erythrocytosis (Percy et al., 2007; Percy et al., 2006).

PHD2 plays an important role in vessel formation and maintenance. Conditional $PHD2^{-/-}$ knock out mice showed altered vessel morphology and erythema (Takeda et al., 2006). In cell culture, endothelial cell proliferation was inhibited by overexpression of PHD2, which was mediated independently of PHD2´s hydroxylase activity (Takeda and Fong, 2007). In the context of tumor metastasis, injection of tumor cells into $PHD2^{+/-}$ mice led to better oxygenated tumors and vessels showed less angiogenesis and an improved endothelial barrier (Mazzone et al., 2009). The normalization of the vessels might have led to the drastic decrease in metastasis formation that was observed.

In myeloid-specific PHD2 knock out mouse models, the lack of PHD2 led to decreased pro-inflammatory cytokine expression (Ikeda et al., 2013; Mamlouk et al., 2014). Expression of anti-inflammatory cytokines was unchanged or slightly downregulated in PHD2-deficient macrophages. In a model of increased afterload, this effect correlated with reduced cardiac hypertrophy and fibrosis. Tissue sections of these hearts showed decreased invasion of macrophages into the heart muscle compared to wild type mice (Ikeda et al., 2013). In a

tumor model, decreased cytokine levels correlated with a decrease in tumor growth, which originated from both increased proliferation and cell death rates (Mamlouk et al., 2014).

The function of PHD2 in myeloid cells has also been studied in mice with a global PHD2 haplodeficieny. In a model of hind limb ischemia, downregulation of PHD2 mRNA expression by 50% led to a M2-like polarization of macrophages, which stimulated smooth muscle cells and thereby improved arteriogenesis (Takeda et al., 2011). This effect could not be seen in a homozygous myeloid-speciic PHD2 knock out. Furthermore, upon induction of hind limb ischemia in wild type mice, PHD2 levels in macrophages were shown to be decreased by half by the action of angiopoietin-1, which in a feed-forward loop led to induction of TIE2, the angiopoietin-receptor (Hamm et al., 2013).

1.4.4.6 PHD3

Besides HIFα, PHD3 can also mediate the stability of other proteins. These proteins include for example activating transcription factor 4 (ATF-4), β-adrenergic receptor, non-muscle actin and PKM2 (Koditz et al., 2007; Luo et al., 2011; Luo et al., 2014; Xie et al., 2009). A recent publication employed a substrate trap mediated by dimethyloxaloylglycine (DMOG), combined with a mass spectrometry approach, to identify more substrates of PHD3. In total, 388 putative PHD3 substrates were identified, of which many still need to be confirmed by independent methods (Rodriguez et al., 2016).

A global murine knock out of PHD3 produces viable $PHD3^{-/-}$ offspring, which show a sympathetic dysfunction. This resulted in decreased blood pressure and hypersensitivity to adrenergic agonists (Bishop et al., 2008).

The role of PHD3 in myeloid cells is only partially understood. The above mentioned global PHD3 knock out showed an increased lethality when challenged with LPS in a model of abdominal sepsis. This was linked to increased macrophage infiltration into different organs and with higher plasma cytokine levels. The authors referred this to a pro-inflammatory polarization of the macrophages as a result of increased NF-κB signaling due to HIF-1α stabilization (Kiss et al., 2012). In a myeloid-specific PHD3 knock out, however, no pro-inflammatory polarization could be observed in fully differentiated bone marrow-derived macrophages (BMDM) (Swain et al., 2014). Instead, $PHD3^{-/-}$ BMDM showed an increased differentiation rate, which most likely also caused the higher cytokine expression observed by Kiss and colleagues in not fully differentiated macrophages. Additionally, $PHD3^{-/-}$ macrophages were protected against apoptosis in stress conditions, such as starvation. In neutrophils, PHD3 deficiency led to enhanced apoptosis selectively in hypoxia by upregulation of the pro-apoptotic Siva1 (Walmsley et al., 2011). There are furthermore reports that observe an inhibitory effect of PHD3 on NF-κB signaling (Fu and Taubman, 2010; Fujita et al., 2012; Kiss et al., 2012; Xue et al., 2010). In PHD3-deficient BMDM

however, no regulation of NF-κB signaling could be observed in basal conditions, while NF-κB activity was decreased in PHD3-deficient BMDM upon stimulation with LPS (Swain et al., 2014). The effect of PHD3$^{-/-}$ macrophages on sterile inflammation has not been studied so far.

1.5 Aim of the thesis

Ischemic diseases such as peripheral artery disease and myocardial infarction are characterized by a hypoxic and ischemic insult to the muscle tissue. This then leads to necrosis, followed by a sterile inflammation. Innate immune cells, such as macrophages and neutrophils, are vital for the clearance of cell debris and the initiation of wound healing. However, prolonged inflammation can have detrimental effects on organ function.

HIFs, which mediate the response of cells towards hypoxia, also regulate properties of myeloid cells like macrophage polarization into pro- or anti-inflammatory types and neutrophil survival. HIFs are tightly regulated on protein level by proteasomal degradation, which is dependent on hydroxylation mediated by PHD 1, 2 and 3. PHD enzymes utilize molecular oxygen for the hydroxylation of HIF, which makes them the oxygen sensors of the cell. Their role for myeloid cells such as macrophages is only partially understood.

PHD3 has been demonstrated to be a pro-apoptotic factor in macrophages, while in an infectious inflammation model, lack of PHD3 led to an increased inflammation. In the setting of a sterile inflammation however, no data about the specific role for PHD3 in macrophages have been reported so far. The aim of the thesis was therefore to study the role of PHD3 for the tissue response to ischemia in a myeloid-specific PHD3 knock out model *in vivo* via the surgical induction of hind limb ischemia. The following questions were addressed:

1. Does a myeloid-specific PHD3 knock out alter the course of inflammation after hind limb ischemia?
2. How does a myeloid-specific PHD3 knock out influence clinical parameters such as reperfusion recovery, angiogenesis, motor function and fibrosis after hind limb ischemia?
3. Are alterations in the course of inflammation based on an altered macrophage functions, such as polarization, apoptosis or migration capacity?
4. How do PHD3$^{-/-}$ macrophages after hind limb ischemia differ from wild type cells in their RNA expression?
5. Can the differentially regulated genes alter macrophage behavior?

PHD2-haplodeficiency has been implicated with macrophage polarization and increased arteriogenesis. *In vitro* data show a metabolic impairment in PHD2-deficient macrophages, which is linked to decreased phagocytosis and migration. In order to study whether these

effects had an influence on sterile inflammation *in vivo*, where both phagocytosis and migration play a vital role, a myeloid-specific knock out mouse was studied in a model of myocardial infarction. The following questions were addressed:

1. How does myeloid PHD2-deficiency affect heart function after myocardial infarction?
2. Is the course of inflammation altered in myeloid-specific PHD2-deficient mice after myocardial infarction?

2. Material and methods

2.1 Material

2.1.1 Antibodies, isotype controls and cell dyes used for flow cytometry

All antibodies were purchased from Biolegend with the exception of CD120b (BD Horizon) and its respective isotype control (BD Horizon). All cell dyes used for flow cytometry were purchased from Biolegend.

Table 1: Antibodies for flow cytometry.

Antibody	Coupled fluorophore	Raised in	Final concentration [µg/ml]	Clone	Catalog number
Anti-mouse CD16/CD32	none	Rat	10	93	101319
Anti-mouse/ human CD11b	APC	Rat	0.4	M1/70	101211
Anti-mouse/ human CD11b	PE/Cy7	Rat	0.1	M1/70	101215
Anti-mouse Ly-6G	FITC	Rat	0.1	127605	127605
Anti-mouse F4/80	FITC	Rat	2	BM8	123107
Anti-mouse F4/80	PE	Rat	0.4	BM8	123109
Anti-mouse I-Ab^{b}	PE	Rat	0.4	AF6-120.1	116407
Anti-mouse CD86	PE	Rat	0.4	GL-1	105007
Anti-mouse CD120b	BV421	Hamster	0.4	TR75-89	564088
Anti-mouse CD206	PE/Cy7	Rat	0.4	C068C2	141719
Anti-mouse CD120a	PE	Armenian hamster	0.4	55R-286	113003

Table 2: Isotype controls for flow cytometry.

Isotype control	Coupled fluorophore	Control for	Final concentration [µg/ml]	Clone	Catalog number
Rat IgG2b, κ isotype ctrl	APC	CD11b-APC	0.4	RTK4530	400611
Rat IgG2b, κ isotype ctrl	PE/Cy7	CD11b-PE/Cy7	0.1	RTK4530	400617
Rat IgG2a, κ isotype ctrl	FITC	Ly-6G-FITC	0.1	RTK2758	400505
Rat IgG2a, κ isotype ctrl	FITC	F4/80-FITC	2	RTK2758	400505
Rat IgG2a, κ isotype ctrl	PE	I-Ab^{b}-PE, CD86-PE	0.4	RTK2758	400507
Hamster IgG1, λ1 isotype ctrl	BV421	CD120b-BV421	0.4	G235-2356	562919
Rat IgG2a, κ isotype ctrl	PE/Cy7	CD206-PE/Cy7	0.4	RTK2758	400521
Armenian hamster IgG isotype ctrl	PE	CD120a-PE	0.4	HTK888	400907

Table 3: Cell dyes used for flow cytometry.

Dye	Coupled fluorophore	Dilution	Catalog number
Annexin V	Pacific Blue	1:50	640917
Zombie fixable Viability kit	FITC	1:1000	423111

2.1.2 Antibodies used for immunofluorescence and Western blot

Antibodies used for immunofluorescence on cryosections and for Western blotting are listed below.

Table 4: Antibodies used for immunofluorescence.

Antibody	Raised in	Dilution	Company	Catalog number
Isolectin GS-IB4, Alexa-488	Griffonia simplicifolia	1:200	Invitrogen	I21411
Vinculin	Rabbit	1:100	Sigma	V9264-200UL
TR-coupled anti mouse	Goat	1:200	Santa Cruz	Sc-2781

Table 5: Antibodies used for Western blots.

Antibody	Raised in	Dilution	Company	Catalog number
Anti-HIF-1α	Mouse	1:1000	Novus Biologicals	NB-100-479
Anti-PHD2	Mouse	1:1000	Novus Biologicals	NB-100-2219
Anti-PHD3	Rabbit	1:500	Novus Biologicals	NB-100-303
Anti-β-Actin	Mouse	1:10000	Sigma	A5441
HRP-coupled anti-rabbit	Goat	1:1000	Santa Cruz Biotechnology	Sc-2004
HRP-coupled anti-mouse	Goat	1:1000	Santa Cruz Biotechnology	Sc-2005

2.1.3 Primer lists

Genotyping of mice was performed in a PCR using the following primers (table 5) at the indicated annealing temperatures. Gene expression of cells was tested using primers for qRT-PCR in table 6. For detection of miRNA-511, commercially available primers were used.

Table 6: Primers for genotyping.

Name	Sequence		Annealing temperature [°C]
Cre	fw	5´-GTT CGC AAG AAC CTG ATG GAC A-3´	60
	rev	5´-CTA GAG CCT GTT TTG CAC GTT C-3´	
$PHD2^{flox}$	fw	5´-CTC ACT GAC CTA CGC CGT GT-3´	53
	rev	5´-CGC ATC TTC CAT CTC CAT TT-3´	

PHD3^{flox}	fw	5´-CCA CGT TAA CTC TAG AGC CAC TGA-3´	58
	rev	5´-ATG GCC GCT GTA TCA CCT GTA T-3´	

Table 7: Primers for qRT-PCR.

Gene of interest	Sequence		Annealing temperature [°C]
Cyp2s1	fw	5´-TGC TCC TGC TGA GAT ACC CT-3´	58
	rev	5´-GAA GCA AGT GGT CCT CGT GA-3´	
IL-6	fw	5´-GTG GGC CAC CAG CAG CTC AG-3´	58
	rev	5´-GCT GGT GAC AAC CAC GGC CT-3´	
IL-12b	fw	5´-CTT CAT CAG GGA CAT CAT CAA ACC A-3´	58
	rev	5´-CCT TTG CAT TGG ACT TCG GT-3´	
iNOS	fw	5´-AAG TCC AGC CGC ACC ACC CT-3´	62
	rev	5´-TCC GTG GCA AAG CGA GCC AG-3´	
MCP-1	fw	5´-GCT CAG CCA GAT GCA GTT AAC GCC C-3´	58
	rev	5´-CCT TCT TGG GGT CAG CAC AGA CCT-3´	
PHD2	fw	5´-TTG CTG ACA TTG AAC CCA AA-3´	60
	rev	5´-GGC AAC TGA GAG GCT GTA GG-3´	
PHD3	fw	5´-GGC CGC TGT ATC ACC TGT AT-3´	60
	rev	5´-TTC TGC CCT TTC TTC AGC AT-3´	
Rbm4	fw	5´-CAC TGT TGG AGA GGG CTA CG-3´	60
	rev	5´-TTC CTG GGG ACT GAA TGC AC-3´	
S12	fw	5´-GAA GCT GCC AAG GCC TTA GA-3´	60
	rev	5´-AAC TGC AAC CAA CCA CCT TC-3´	
TNF-α	fw	5´-GAC CCT CAC ACT CAG ATC ATC TTC-3´	58
	rev	5´-CCA CTT GGT GGT TTG CTA CGA-3´	

Table 8: Primers for miRNA detection by qRT-PCR.

Primer	Catalog number	Company
Universal Adaptor primer	P01011A	GeneCopoeia
Mmu-miR-511-3p	MmiRQP3338	GeneCopoeia
Mmu-miR-511-5p	MmiRQP1067	GeneCopoeia
Mouse snRNA U6	MmiRQP9002	GeneCopoeia

2.1.4 Kits

The following kits were used for the studies of cytokine levels and gene expression analyses.

Table 9: Kits used.

Name	Order number	Company
Cytometric bead array	552364	BD Biosciences
SensiMix^{TM} SYBR$^{®}$ Low-ROX kit	QT625-05	Bioline
First Strand cDNA Synthesis kit	K1612	Thermo Fisher Scientific
All-in-One miRNA First-Strand cDNA Synthesis Kit	AMRT-0060	GeneCopoeia
DNase I kit	04716728001	Roche
Immobilon Western	WBKLS0500	Merck Millipore

Chemiluminescent HRP Substrate		
Prostaglandin E2 ELISA Kit	ab136948	abcam
PCR Master Mix (2x)	K0171	Thermo Fisher Scientific
Protonex™ Red-600 Latex Bead Conjugate	ABD-21209	biomol

2.1.5 Cell lines

All cell lines were purchased from ATCC.

Table 10: Cell lines used to create conditioned medium.

Cell line	Origin	Original publication	Specification
L929	Murine, connective tissue	(Sanford et al., 1948)	#CCL-1
MDA-MB231	Human, breast cancer	(Cailleau et al., 1974)	#HTB-26

2.1.6 Cell culture media

All cell culture ingredients were purchased from PAN Biotech (Aidenbach, Germany) with the exception of β-mercaptoethanol, which was purchased from Carl Roth GmbH (Karlsruhe, Germany).

Table 11: Composition of cell culture media used.

Medium	Ingredients	Catalog number
Neutralization medium	Dulbecco´s modified eagle medium (DMEM) 15% fetal calf serum (FCS) 100 U/ml penicillin 100 µg/ml streptomycin	P04-03590 3302-P271806 P06-07100 P06-07100
Culture medium	DMEM 10% fetal calf serum 0.2 mM glutamine 0.2 M HEPES 0.1 mM sodium pyruvate 50 U/ml penicillin 50 µg/ml streptomycin	P04-03590 3302-P271806 P04-80100 P05-01100 P04-43100 P06-07100 P06-07100
Pluznik´s medium	DMEM 30% L929-conditioned medium 10% fetal calf serum 5% horse serum 0.1 mM sodium pyruvate 50 U/ml penicillin 50 µg/ml streptomycin 0.00005% β-mercaptoethanol	P04-03590 3302-P271806 B30-0702 P04-43100 P06-07100 P06-07100 4277.1
Starvation medium	DMEM 50 U/ml penicillin 50 µg/ml streptomycin	P04-03590 P06-07100 P06-07100

2.1.7 Buffers and staining solutions

The following buffers and staining solutions were prepared according to the information provided below.

Table 12: Ingredients of buffers and their concentrations.

Buffer	Ingredients	Catalog number	Company
Phosphate buffered saline (PBS)	137 mM NaCl 2.7 mM KCl 10 mM Na_2HPO_4 1.8 mM KH_2PO_4	9265.2 6787.1 4984.1 3904.1	Carl Roth GmbH Carl Roth GmbH Carl Roth GmbH Carl Roth GmbH
Mowiol solution	3% glycerine 1.33% mowiol 0.133 M Tris pH 8.5 0.1% DABCO	3783.2 81381-50G 5429.3 0718.1	Carl Roth GmbH Sigma Aldrich Carl Roth GmbH Carl Roth GmbH
Picro-sirius red	0.1% Direct Red 80 Picric acid	365548-5G 3E-086	Sigma Aldrich Waldeck
Tail lysis buffer for genotyping	25 mM NaOH 0.2 mM EDTA	6771.1 8043.2	Carl Roth GmbH Carl Roth GmbH
Neutralization buffer For genotyping	40 mM Tris/HCl pH 5.0	9090.1	Carl Roth GmbH
TBE 0.5x	45 mM Tris 45 mM Boric acid 1 mM EDTA pH 8.0 In dH_2O	5429.3 6943.1 8043.2	Carl Roth GmbH Carl Roth GmbH Carl Roth GmbH
Washing buffer for flow cytometry	0.1% Bovine serum albumin (BSA) 0.01% NaN_3 In PBS	A1391,0500 K305.1	AppliChem Carl Roth GmbH
Digestion buffer for hind limb tissue	450 U/ml collagenase IV 1.2 U/ml dispase II In PBS	C4-22 P10-032100	Merck Millipore PAN Biotech
Digestion buffer for heart tissue	600 U/ml collagenase IV 1.2 U/ml dispase II In PBS	C4-22 P10-032100	Merck Millipore PAN Biotech
Peritoneal macrophage buffer	0.5% BSA 2 mM Ethylenediamine-tetraacetic acid (EDTA) In PBS	A1391,0500 8043.2	AppliChem Carl Roth GmbH
Blocking solution immunofluorescence	10% Normal goat serum 0.1% Triton-X 100 In PBS	Sc-2043 3051.3	Santa Cruz Carl Roth GmbH
Cell lysis buffer	400 mM NaCl 10 mM Tris/HCl, pH 8.0 1 mM EDTA, pH 8.0 0.1% Triton-X 100 In dH_2O	9265.2 9090.1 8043.2 3051.3	Carl Roth GmbH Carl Roth GmbH Carl Roth GmbH Carl Roth GmbH
2x SDS sample buffer	100 mM Tris/HCl pH 6.8 4% SDS 0.2% bromphenol blue 20% glycerine 5% β-mercaptoethanol In H_2O	9090.1 4360.2 A512.1 3783.2 4277.1	Carl Roth GmbH Carl Roth GmbH Carl Roth GmbH Carl Roth GmbH Carl Roth GmbH
5x SDS	125 mM Tris	5429.3	Carl Roth GmbH

electrophoresis buffer	1.25 M glycine 0.5% SDS In H_2O, pH 8.3	3908.2 4360.2	Carl Roth GmbH Carl Roth GmbH
Western blot transfer buffer	25 mM Tris 192 mM glycine 10% SDS 20% methanol In H_2O	5429.3 3908.2 4360.2 4627.5	Carl Roth GmbH Carl Roth GmbH Carl Roth GmbH Carl Roth GmbH
Enhanced chemiluminescence (ECL) solution	100 mM Tris/HCl, pH 8.5 90 mM coumaric acid 250 mM luminol 0.009% H_2O_2	9090.1 C-9008 4203.1 H1009	Carl Roth GmbH Sigma Carl Roth GmbH Sigma
Ponceau S solution	0.1% Ponceau 5% acetic acid	P7170 3738.5	Biorad Carl Roth GmbH

2.1.8 Chemicals

The following chemicals were used for experiments.

Table 13: List of chemicals used.

Chemical	Order number	Company
Agarose Broad Range	T846.3	Carl Roth GmbH
Gene Ruler DNA ladder 1kb	SM0311	Thermo Scientific
Roti Safe Gel Stain	3865.1	Carl Roth GmbH
Chloroform	3313.1	Carl Roth GmbH
Isopropanol	6752.4	Carl Roth GmbH
Ethanol	9065.4	Carl Roth GmbH
Xylol	9713.1	Carl Roth GmbH
TRIzol	15596018	Ambion
Dako Diluent	S0809	Dako
Tissue-Tek O.C.T.	4583	Sakura
Acetone	9372.1	Carl Roth GmbH
Methanol	4627.5	Carl Roth GmbH
Hoechst	D1306	Thermo Scientific
Roti Histokitt	T160.1	Carl Roth GmbH
RNase-free water	R0581	Thermo Scientific
Paraformaldehyde	0335.1	Carl Roth GmbH
Percoll	17-0891-02	GE Healthcare
Phenol/Chloroform/Isoamylalcohol	A156.3	Carl Roth GmbH
Evan´s Blue	E2129-10G	Carl Roth GmbH
2,3,5-Triphenyltetrazolium chloride	T8877-56	Sigma
10x Hank´s balanced salt solution	P04-49100	PAN Biotech

2.1.9 Equipment

The following equipment was used for experiments.

Table 14: Surgery equipment.

Consumable	Order number	Company
0.9% NaCl solution	2000277	Braun Melsungen AG
Ketamine 10%	04-03-9264/23	Medistar

Xylariem (Xylazine)	1246626/11	Ecuphar
Forene (Isoflurane) 100% (v/v)	B506	Abbvie
500 mg/ml Novaminsulfon (Metamizol)	PZN-03530402	Ratiopharm
Heparin 25000 I.U/5 ml	PZN-03862340	Rotexmedica
Prolene thread 9-0	8889-H	Ethicon
Silk thread 6/0	4208	Resorba
26 gauge Sterican needle	4665427	Braun Melsungen AG
25 gauge Sterican needle	4657675	Braun Melsungen AG
Omnifix 40 solo syringe	9161309V	Braun Melsungen AG
Thilo-Tears gel (eye crème)	530/28292-2	Alcon Pharma GmbH
K^+ EDTA tubes	41.1395.005	Sarstedt
Lithium heparin tubes	41.1502.005	Sarstedt

Table 15: Consumables.

Consumable	Company
Superfrost coverslide	Thermo Scientific
Menzel coverslide	Thermo Scientific
Eppendorf cups	Sarstedt
Cell culture dish 100, Standard	Sarstedt
Petri dish 100, with cams	Sarstedt
Petri dish 35, with cams	Sarstedt
Round bottom polystyrene tubes (flow cytometry)	Falcon
70 µm Cell Strainer	Falcon
40 µm Cell Strainer	Falcon
Pipette tips: 10 µl, 200 µl, 1000 µl	Sarstedt

2.1.10 Devices

The following devices were used for experiments.

Table 16: Lab and surgery devices.

Instrument	Application	Company
RotaRod Advanced V4.3.0	Motor function	TSE Systems GmbH
Vevo 2100 Imaging system	Ultrasound	Visualsonics
PeriScan PIM3 Laser Dopper	Perfusion hind limb ischemia	Perimed
Stemi 2000-c microscope	Surgery	Zeiss
Hot plate ST983	Surgery	Vogel
Mantis Elite microscope	Surgery	Vision Engineering
Mini Vent Type 845	Surgery- Ventilation	Hugo Sachs Elektronik
Vapor 19.3 Halothane	Surgery- gas mix	Drägerwerk AG
Elektrotom B50	Surgery	Martin
Bipolar forceps	20195-020	Erbe
KL1500 LCD	Surgery-light source	Schott
Surgical instruments		F.S.T.
FACS Canto II	Flow cytometry	Beckton Dickinson
FACS Aria III	Cell sorting	Beckton Dickinson
Centrifuge 5810R for falcons	Cell culture	Eppendorf
Hera Safe clean bench	Cell culture	Thermo Electron Cooperation

Sci-tive Hypoxia workstation	Single cell migration	Baker Ruskinn
Nikon ECLIPSE TS100	Single cell migration	Nikon
Digital Sight DS-L3 screen	Single cell migration	Nikon
AE30 Inverted Microscope	Cell culture	Motic
5415R Centrifuge for tubes		Eppendorf
Primus 96 PCR cycler	PCR	PeqLab
Mx300P light cycler	qRT-PCR	Stratagene
Fume hood		Köttermann
NanoDrop 2000c	RNA concentration	Thermo Scientific
Microm HM560 cryotome	Cryosections	Thermo Scientific
Microm HM 355S microtome	Paraffin sections	Thermo Scientific
Zeiss microscope, 40x	Imaging	Zeiss
Nikon microscope SMZ 1500	Imaging	Nikon
Digital Sight camera	Imaging	Nikon
Gene Flash Gel Documentation	Genotyping PCR	Syngene Bio Imaging
Fine scale AC 2115		Sartorius
Universal scale		Sartorius
Neubauer counting chamber	Cell culture	Marienfeld

Table 17: Software.

Software	Application	Reference
PIMSoft	Laser Doppler Imaging	Perimed
Flowing software 2.5.1	Flow cytometry	Perttu Terho, Turku Centre for Biotechnology, Finland
RotaRod V4.3.0 (4965)	Motor function assay	TSE Systems GmbH
FCAP Array software	Cytokine bead assay	BD Biosciences
DeSeq^2 software	RNA sequencing	Bioconductor
Pro Size software	Fragment analysis	Advanced Analytical Technologies
FACS DIVA software	Flow cytometry	Beckton Dickinson
Graph Pad prism	Data analysis	GraphPad Software
Corel Draw	Data display	Corel Cooperation
MxPro	qRT-PCR analysis	Agilent Technologies
Axiovision	Acquiring of images	Zeiss
ImageJ	Image analysis	NIH
NanoDrop software	RNA concentration	Thermo Scientific

2.2 Methods

2.2.1 Mouse models

2.2.1.1 Myeloid-specific PHD3 knock out mice

PHD3$^{flox/flox}$ mice were kindly provided by Prof. Guo-Hua Fong (Center for Vascular Biology, University of Connecticut Health Center, Farmington, CT, USA). In these mice, PHD3 exon 2 is flanked by loxP sites. Generation and detailed characterization of the mice are described elsewhere (Takeda et al., 2006). All animals in this study were backcrossed to C57BL/6 mice at least five times. PHD3$^{flox/flox}$ mice were crossed with LysMcre mice (Clausen et al., 1999), which were purchased from the Jackson Lab to generate PHD3$^{flox/flox}$ × LysMcre$^{+/-}$ mice within two generations. PHD3$^{flox/flox}$ × LysMcre$^{+/-}$ mice were then crossed with PHD3$^{flox/flox}$

mice to obtain PHD3$^{-/-}$ mice (PHD3$^{flox/flox}$ × LysMcre$^{+/-}$) and littermate control wild type mice (PHD3$^{flox/flox}$ × LysMcre$^{-/-}$). The initial breeding of PHD3$^{flox/flox}$×LysMcre$^{+/-}$ mice was performed by Dr. Katja Farhat, a former Postdoc of the Institute of Cardiovascular Physiology.

2.2.1.2 Myeloid-specific PHD2 knock out mice

All animals in this study were backcrossed to C57BL/6 mice at least five times. PHD2$^{flox/flox}$ mice were kindly provided by Prof. Ben Wielockx (Dresden University, Germany). In these mice, PHD2 exons 2 and 3 are flanked by loxP sites. Generation and detailed characterization of the mice are described elsewhere (Singh et al., 2013). PHD2$^{flox/flox}$ × LysMcre$^{+/-}$ mice were crossed with PHD$^{flox/flox}$ mice to obtain PHD2$^{-/-}$ (PHD2$^{flox/flox}$ × LysMcre$^{+/-}$) mice and littermate control wild type mice (PHD2$^{flox/flox}$ × LysMcre$^{-/-}$). The initial breeding of PHD2$^{flox/flox}$ × LysMcre$^{+/-}$ mice was performed by Dr. Katja Farhat, a former Postdoc of the Institute of Cardiovascular Physiology.

2.2.1.3 Genotyping

Tail biopsies from 3-4 week old mice were incubated in 75 µl tail lysis buffer for 60 min at 95 °C. The alkaline lysis of the tissue was stopped by incubating the samples on ice for 10 min and adding the same amount of genotyping neutralization buffer.

To test for the presence of a cre recombinase or floxed PHD2 or PHD3 allele, a polymerase chain reaction (PCR) was performed. 5 µl of DNA-containing lysate was mixed with 12.5 µl PCR Master Mix (2x) and 0.1 pmol/µl reverse and forward primers for PHD2^{flox}, PHD3^{flox} or cre recombinase and H_2O in a final volume of 25 µl. The PCR was run according to the following temperature settings:

Table 18: Temperature profile for genotyping PCRs.

Step	Temperature [°C]			Time [sec]		
	Cre	PHD2^{flox}	PHD3^{flox}	Cre	PHD2^{flox}	PHD3^{flox}
Initial denaturation	94	94	94	240	120	180
Denaturation	94	94	94	30	15	30
Annealing	60	53	58	30	25	60
Elongation	72	72	72	75	30	60

The sequence of denaturation annealing and elongation steps was repeated for 30 (Cre, PHD2^{flox}) or 40 (PHD3^{flox}) cycles. The PCR product was mixed with 5 µl Orange G and loaded on a 1.5% agarose-gel in 0.5x TBE buffer containing Roti Safe together with a 1 kb DNA ladder to estimate product size. The PCR product for cre recombinase was around 350 bp long, the one for PHD2^{flox} 400 bp (wild type no band), and the one for PHD3^{flox} 840 bp (wild type band at 400 bp). Bands were visualized in a UV gel documentation station.

2.2.2 Surgery techniques and associated analyses

2.2.2.1 Hind limb ischemia

Peripheral artery disease (PAD) occurs most commonly after formation of an atherosclerotic plaque in an artery supplying the leg, which can ultimately lead to its complete occlusion. An established model to study PAD in mice is the permanent ligation of the femoral artery (Limbourg et al., 2009; Niiyama et al., 2009). The femoral artery of the mouse is the main supplier of blood and nutrients to the hind limb muscles. It originates from the common iliac artery and enters the thigh as common femoral artery behind the inguinal ligament. It then gives rise to several collaterals, among those the proximal caudal femoral artery which supplies the adductor muscles superficially as well as the medial hamstring muscles (Kochi et al., 2013). This artery was referred to as arteria profunda femoris by Limbourg and colleagues (Limbourg et al., 2009).

Ligation of only the femoral artery proved to be a valid model to study both arteriogenesis and angiogenesis in murine models of hind limb ischemia (Limbourg et al., 2009). However, the induction of ischemia is rather mild and, depending on the mouse strain, not always sufficient. It has been demonstrated before that especially mice with a C57Bl/6 background are more resistant towards induction of ischemia which is most likely caused by strain-dependent differences in collateral vasculature (Greenberg et al., 2008). This is why in this study I ligated both femoral artery and proximal caudal femoral artery proximally to the bifurcation. After a second ligation at the knee joint, the femoral artery was completely removed without damaging the associated femoral vein and nerve. This caused a sufficient drop in perfusion, which was only partially recovered until day 28 after surgery.

All animal experiments were performed according to the German animal protection law and approved by the Niedersächsisches Landesamt für Verbraucherschutz und Lebensmittelsicherheit in Oldenburg (animal experimentation number 33.9-42502-04-11/0413). 8-12 week old male wild type and PHD3$^{-/-}$ mice underwent hind limb ischemia. To induce anesthesia, mice were injected with a mixture of ketamine (75 mg/kg body weight) and xylazine (15 mg/kg body weight) in 0.9% NaCl-solution. Mice were fixed underneath a microscope on a hot plate (37 °C) using adhesive tape. The right leg was disinfected using 70% ethanol and a small incision was made on the level of the knee joint. The femoral artery was separated from the accompanying vein and nerve and ligated using a silk thread (6/0). The artery was then cauterized at the distal side of the ligation. A second incision was made just below the groin. Again, the femoral artery was separated from the accompanying vein and nerve, and a second ligation was done proximal of the bifurcation of femoral artery and the proximal caudal femoral artery. Both femoral artery and proximal caudal femoral artery

were cauterized at the distal side of the ligation. The femoral artery was then removed and the two incisions were closed using prolene thread.

Mice received metamizol to relieve them from pain caused by the surgery and the following ischemia. Metamizol was given 2 days before surgery until 5 days after surgery via the drinking water in a final concentration of 1.33 mg/ml.

Mice that showed severe signs of indisposition (lethargy, weight loss over 20%) and mice that developed a severe necrosis spreading to the whole limb were excluded from the study.

2.2.2.2 Laser Doppler imaging

Laser Doppler imaging is a widely used and non-invasive method to quantify blood flow. A low power laser beam (658 nm) that penetrates the skin around 200-300 µm deep is used to scan the tissue (Jakobsson and Nilsson, 1993). Moving objects like erythrocytes scatter the light waves and change their wavelength (Dopplershift) while resting objects scatter the light waves without changes in wavelength. The Dopplershift can be detected by a photo-detector and transformed into color-coded images which represent the perfusion of the upper skin levels of the tissue. Only the hairless hind paws were analyzed, and not the whole limb, because the fur can influence the recording. Measuring the paws has been shown to correlate well with the perfusion mediated by the femoral artery (Limbourg et al., 2009).

The perfusion in hind paws was analyzed via laser Doppler imaging while mice were anesthetized (ketamine 75 mg/kg body weight, xylazin 15mg/kg body weight in 0.9% NaCl-solution). Mice were placed on a hot plate at 37 °C and their paws were fixed in the scanning region (3.2 cm width and 2.1 cm height) with adhesive tape. Pictures were taken before and directly after surgery, as well as on the day of tissue isolation. Mice were additionally analyzed on day 7, 14 and 21 after surgery if they were studied for 28 days.

Color-coded images were analyzed using the PIMsoft software. Regions of interest (ROI) were drawn around the hind paws with a maximum of 5% difference in area between right and left paw. The mean perfusion values of the ligated leg were then normalized to the values of the unligated leg.

2.2.2.3 Assessing motor function

Motor function was assessed before and after hind limb ischemia to evaluate whether one group recovered faster after surgery. Two different methods were used to assess motor function:

2.2.2.3.1 Grading system

In order to evaluate to which degree mice made use of the operated leg, the mouse was placed in a cage and observed while freely moving around. The bottom of the cage was

covered with paper to avoid slipping. The ability to move the ligated leg was graded according to the following parameters (adapted from (Rishi et al., 2015)):

Table 19: Grading scores for impairment of leg movement after hind limb ischemia.

Grade	Description
1	Inability to move the whole limb
2	Inability to move the foot
3	Mouse makes a claw, cannot spread toes
4	Ability to move the foot and toes, but tendency to adopt a relieving posture
5	No impairment at all

Mice were checked before surgery and once every postsurgical day until day 7, when none of the tested mice showed any impairment anymore.

2.2.2.3.2 RotaRod running test

A RotaRod system is a device with a rotating rod, on which a rodent can be placed in order to measure running capacity. In the RotaRod system used here (RotaRod Advanced, TSE) the rod was accelerated in order to test which maximum speed a mouse can still run. Mice that could not keep up anymore fell onto a grid, which was detected by a light sensor. The maximum speed at which the mice were still able to keep themselves on the rod was recorded.

Mice had to get used to the RotaRod device before the experiment. In order to get them acquainted with the system and reduce the influence of learning behavior on the outcome of the experiment, mice were trained prior to the surgery. The following table gives an overview over the training program and the recording program:

Table 20: Running schedule for mice on the RotaRod system.

Program	Time [min]	Speed [rpm] From	To	Remarks
Training day 1	30	10	10	
Training day 2	15	10	10	
	10	None		Mouse was placed back into the cage to rest
	4	10	40	4 runs
Recording day	5	10	10	Warm up
	4	10	40	4 recorded runs

Mice were trained for two days before surgery. 4 recorded runs were performed one day before surgery, as well as on day 7, 14, 21 and 27. Before each recorded run, mice were allowed to adjust to the rod for 5 min at a constant speed of 10 rpm. For data analysis, the arithmetic mean of the 4 runs was calculated.

2.2.2.4 LAD ligation

A widely used model to study the effects of myocardial infarction in rodent models is the permanent occlusion of the left anterior descending artery (LAD). By occlusion of the LAD, a large part of the left ventricle at the tip of the heart is not properly perfused anymore, which ultimately leads to an inflammatory reaction, scar formation and impaired heart function.

LAD ligation surgeries were performed by Dr. Liza Swain, a Postdoc of the Institute of Cardiovascular Physiology. Animal experiments were performed according to the German animal protection law and approved by the Niedersächsisches Landesamt für Verbraucherschutz und Lebensmittelsicherheit in Oldenburg (animal experimentation number 33.9-42502-04-12/0833). 10-12 week old female wild type and PHD2$^{-/-}$ mice underwent LAD-surgery. Mice were injected with buprenorphine (0.1 mg/kg body weight) 30 min before surgery for analgesia. Narcosis was induced with a gas mixture containing 2.5-3.5% isoflurane in O_2 and maintained with 0.75-2% isoflurane in O_2. Mice were intubated and mechanically ventilated with a respiratory rate of 150 breaths/min and a breathing volume of 150 µl. After a thoracotomy, the left anterior descending artery was occluded using 9-0 prolene thread just below the left atrial auricle. Successful ligation led to a decoloring of the heart muscle distal to the ligation. Surgery wounds were then sutured and mice were extubated after they started to breathe spontaneously. Sham surgeries were performed with the same procedure as LAD surgeries just without ligation of the artery.

To relieve mice from pain, they were subcutaneously injected with buprenorphine (0.1 mg/kg body weight) twice a day for 3 days after surgery. In addition, mice received metamizol (1.33 mg/ml) 2 days before until 7 days after surgery with their drinking water. Mice that showed over 20% loss of body weight within 24 hrs, a low body temperature, signs of pain or lethargy and inability to move were excluded from the experiment.

Hearts were harvested 3 or 7 days after surgery for flow cytometric analysis (see 2.2.3.2).

2.2.2.5 Echocardiography

Echocardiography is a non-invasive method to examine the heart via ultrasound. The thickness of the heart walls as well as heart function parameters can be determined via this method.

Echocardiography was performed by Dr. Aline Jatho, a Postdoc of the Institute of Cardiovascular Physiology. Mice that underwent LAD-surgery underwent echocardiography before and 6 days after surgery. The examination was performed while the mouse was anesthetized (1% isoflurane in an O_2-mixture). 10 cardiac cycles were recorded in B-mode to visualize the long axis and the short axis of the heart. The echocardiography device was then switched to M-mode to measure the heartbeat with a high temporal resolution. Another 10

cardiac cycles were recorded in M-mode visualizing the short axis. Different parameters like thickness of the posterior and anterior walls as well as area of the lumen during diastole (Area(d)) and systole (Area(s)) and length of the long axis (L(d) and L(s)) of the heart were determined. The ejection fraction (EF [%]) describes how much blood is distributed by the heart with each heartbeat. It was calculated by the following formula:

$$EF = \frac{Vol(d) - Vol(s)}{Vol(d)} * 100$$

Vol(d) and Vol(s) are the abbreviations for the volume of the left ventricle during diastole and systole respectively. They were calculated using the following formulas:

$$Vol(d) = \left(\frac{5}{6}\right) * (Area(d) * L(d))$$

$$Vol(s) = \left(\frac{5}{6}\right) * (Area(s) * L(s))$$

The fractional area shortening (FAS [%]) describes to which degree the area of the left ventricle changes during each heartbeat. It was calculated by the following formula:

$$FAS = \frac{Area(d) - Area(s)}{Area(d)} * 100$$

2.2.2.6 Blood collection

Blood was taken from anesthetized mice (ketamine 75 mg/kg body weight, xylazine 15mg/kg body weight in 0.9% NaCl-solution). The abdominal cavity was opened with a V-cut. Intestines were shifted to the left side in order to expose the vena cava (Hoff, 2000). A 26 gauge needle was used to slowly draw blood from the vena cava. Blood was collected in K^+ EDTA tubes and spun down for 5 min at 5000 rpm to separate plasma from erythrocytes and buffy coat. Plasma was carefully separated from the other phases and stored in 50 µl aliquots at -80 °C until it was used for measuring plasma cytokines (see 2.2.3.3).

2.2.3 Flow cytometric analyses and sorting

Flow cytometry enables to characterize and distinguish cells via various optical parameters. For that, a stream of cells has to pass an argon laser. The cells are focused by the surrounding fluids so that only one cell at a time passes the laser. When meeting the cell, the laser beam is scattered into different directions which can be detected in a forward (FSC) and sideward scatter (SSC). The FSC is a measure of cell size while the SSC characterizes the intracellular complexity. Apart from that, the light from the laser excites fluorophores, by which the cells can be labelled. The resulting emission of characteristic spectra can be collected via various filters which makes it possible to label cells with different dyes simultaneously.

2.2.3.1 Flow cytometry of hind limb muscles

In order to evaluate ischemia-induced inflammation after hind limb ischemia surgery, gastrocnemicus muscles from the ligated and unligated legs were isolated. To this end, mice anesthetized with ketamine (75 mg/kg body weight) and xylazine (15 mg/kg body weight) were killed by cervical dislocation. The skin covering the lower limbs and the abdomen was disinfected using 70% ethanol and incisions were made in the abdominal zone without harming the peritoneum. Starting from those incisions, the skin was removed from the upper leg all the way down to the paw. The gastrocnemicus muscle is partially covered by the adductor, which had to be removed. Gastrocnemicus muscles were excised by detaching them at the hamstring and at the knee joint.

Muscles were then cut into small pieces, suspended in 5 ml of digestion buffer and incubated for 45 min at 37 °C and 180 rpm in a shaker. During this time, the tissue was further disrupted by pipetting the solution up and down every 15 min using first a 10 ml pipette and then a 5 ml pipette. Digestion was stopped by adding 15 ml ice cold neutralization medium. The samples were filtered through a 70 µm mesh and subsequently through a 40 µm mesh to get rid of tissue residues. The samples were centrifuged at 400 x g for 10 min. After removing the supernatant, cells were resuspended in 2 ml of washing buffer and counted using a Neubauer counting chamber.

An equal number of cells (between 300.000 and 500.000) were then distributed into FACS-tubes in 1 ml of washing buffer and centrifuged at 450 x g for 5 min. After removing the supernatant, unstained CD16/CD32 antibody was added for 15 min at 4 °C to block unspecific binding sites. After that antibodies against certain surface markers were added at the indicated final concentrations (see table 1 and 2) to identify different cell populations:

Table 21: Staining protocols to characterize and identify cells via flow cytometry.

Staining protocol	Stained surface markers	Cell characteristics	
1	Ly-6G-FITC	Leukocytes	$CD11b^+$
	$I\text{-}Ab^b$ (MHCII)-PE	Neutrophils	$Ly\text{-}6G^+$ $MHCII^{low}$ $CD11b^+$
	CD11b-PE/Cy7		
2	F4/80-FITC	Leukocytes	$CD11b^+$
	CD86-PE	Macrophages	$F4/80^+$ $CD11b^+$
	CD206-APC	M1-polarization	Geometric mean fluorescence intensity of CD86 within the $F4/80^+$ $CD11b^+$ population
	CD11b-PE/Cy7	M2-polarization	Geometric mean fluorescence intensity of CD206 within the $F4/80^+$ $CD11b^+$ population

3	F4/80-FITC	Leukocytes	$CD11b^+$
	CD11b-APC	Macrophages	$F4/80^+$ $CD11b^+$
	CD120a (TNF-R1)-PE	TNF-R1	Geometric mean fluorescence intensity within the $F4/80^+$ $CD11b^+$ population
	CD120b (TNF-R2)-BV421	TNF-R2	Geometric mean fluorescence intensity within the $F4/80^+$ $CD11b^+$ population
4	F4/80-PE	Macrophages	$F4/80^+$ $CD11b^+$
	CD11b-APC	Living cells	Annexin V^- Zombie $Green^{low}$ $F4/80^+$ $CD11b^+$
	Annexin V	Early apoptotic cells	Annexin V^+ Zombie $Green^{low}$ $F4/80^+$ $CD11b^+$
	Zombie Green	Late apoptotic cells	Annexin V^+ Zombie $Green^{high}$ $F4/80^+$ $CD11b^+$
		Dead cells	Annexin V^- Zombie $Green^{high}$ $F4/80^+$ $CD11b^+$

Samples were incubated with antibody mixtures for 30 min at 4 °C. Afterwards, cells were washed once in washing buffer or in Annexin V-staining buffer (staining protocol 4).

Cells were measured using the FACS Canto II flow cytometer. A compensation was done for all staining protocols. The compensation setup required single-stained representative samples as well as one unstained control sample. The voltage of each laser was adjusted in a way that positive and negative populations were clearly visible. Positive cell populations were gated and the compensation was calculated by the FACS Diva software.

In order to correctly distinguish positive and negative cell populations in a sample, fluorescence minus one (FMO) controls were created, using all antibodies at the given concentrations except one which was replaced by the respective IgG control.

Acquired data were analyzed using the freely available Flowing software 2.5.1 developed by Perttu Terho.

2.2.3.2 Flow cytometry of heart tissue

In order to quantify immune cells after the induction of myocardial infarction, hearts were isolated from mice that underwent LAD or a sham operation. Mice were killed by cervical dislocation under anesthesia and hearts were extracted. Hearts were flushed once with 1 ml 0.9% NaCl solution by cannulating the aorta under the microscope.

Hearts were dissected into very small pieces. Minced hearts were suspended in digestion buffer and incubated at 37°C for 45 min at 180 rpm in a shaker.

Further processing of the tissue was performed as described above for hind limb muscles, with the addition of an erythrocyte lysis step, which was implemented after the first centrifugation. After this centrifugation step, the supernatant was removed and cells were resuspended in 10 ml 0.2% NaCl solution. After 15 sec, an equal amount of 1.6% NaCl solution was added and cells were centrifuged at 400 x g for 10 min at 4 °C. After that the supernatant was removed and cells were resuspended in 2 ml washing buffer, counted and processed as described above. Staining protocols 1 and 2 were used to identify populations of leukocytes, neutrophils, macrophages and macrophage polarization.

2.2.3.3 Flow cytometric measurement of cytokines from plasma

In order to evaluate systemic signs of inflammation after hind limb ischemia surgery, the abundance of pro- and anti-inflammatory cytokines was tested in blood plasma. Plasma taken from mice 1, 3, 5 and 7 days after surgery was evaluated, as well as plasma from resting mice, which served as negative control.

Cytokines were detected using a cytometric bead assay kit (BD Biosciences). In short, plasma was incubated with a mix of beads that specifically bound to the cytokines IL-6, IL-10, MCP-1, IFN-ɣ, TNF or IL-12p70, respectively. In order to detect the cytokine-bound beads, a PE-labelled detection reagent was added. After 2 hrs of incubation, beads were washed and measured using the FACS Canto II flow cytometer. Different cytokine beads could be differentiated by their distinctively different intensity in the APC channel. Abundance of cytokines was measured via the mean fluorescence intensity in the PE channel. Cytokine concentrations were determined with the help of a calibration curve using the inflammation standard provided by the kit. Data were analyzed using the FCAP Array™ software.

2.2.3.4 RNA sequencing

Macrophages were isolated from the gastrocnemicus muscle of mice 5 days after hind limb ischemia surgery as described above (2.2.3.1). Tissue lysates were washed one time in washing buffer and then stained with antibodies against F4/80-PE and CD11b-APC. Doublets were discriminated using SSC-A vs SSC-W gating. The cell population positive for both markers was selected and sorted via a FACS Aria III flow cytometer into 1 ml of TRIzol.

RNA was isolated according to the manufacturer´s instructions. In short, 200 µl of chloroform was added to the sample to generate a phase separation. After centrifugation at 12000 x g for 15 min at 4 °C, the upper aqueous phase was transferred to a new tube and RNA was precipitated by adding 500 µl isopropanol and incubating the sample at -20 °C overnight. After centrifugation at 12000 x g for 30 min at 4 °C, the supernatant was removed and the RNA pellet was washed by adding 500 µl of 75% ethanol and centrifugating the sample at 12000 x g for 10 min at 4 °C. The supernatant was removed and this step was repeated a

second time. The pellet was dried at 37 °C and subsequently dissolved in 10 µl of RNase-free water and stored at -80 °C until it was further processed.

The quality of the isolated RNA was assessed by measuring the RIN (RNA Integrity Number) using a Fragment Analyzer via PROSize 2.0 software. RNA was prepared for sequencing using the TruSeq total RNA Sample Preparation Kit (Illumina). In short, a RNA library was prepared according to the following steps: rRNA was depleted, RNA was fragmented and cDNA was synthesized using random primers. The 3´-end was adenylated and adaptors were ligated to the cDNA. The modified cDNA was further amplified in a PCR reaction using primers complementary to the adaptor sequence to enrich cDNAs that were successfully linked to adaptors. This RNA library was then sequenced using the Illumina technique.

The results of the total RNA sequencing were analyzed using DeSeq2 software. Only genes that showed a significant $\log_2$-fold change of more than 1 or less than -1 between the PHD3$^{-/-}$ and wild type macrophages were included in the candidate list. Statistical significance was determined using the Benjamini-Hochberg correction. Adjusted *p*-values less than 0.05 were considered statistically significant.

2.2.4 Tissue sections and staining techniques

2.2.4.1 Embedding hind limb muscles for cryosections

In order to evaluate processes like angiogenesis and fibrosis within the hind limb tissue, muscle tissue was taken 3 and 28 days after surgery to study both acute and long term effects of ischemia on muscle physiology.

The gastrocnemicus muscle was extracted from the unligated and ligated hind limb as described above. The muscle was then placed on a piece of cork with a drop of frozen Tissue-Tek. It was fixed in an upright position (distal end with the hamstring up) using needles without piercing the muscle. The muscle was then fully covered with Tissue-Tek and snap frozen in liquid nitrogen.

Tissues were sectioned using the Microm HM560 cryotome. Around 2 mm of the tissue was discarded before the first sections were collected on superfrost coverslides. 3 to 4 sections with a thickness of 10 µm were collected per coverslide. In total, 24 coverslides were taken per muscle. To ensure that also deeper areas of the muscle were represented by the sections, around 2 mm of tissue was removed without collecting it after 8 coverslides and 16 coverslides, respectively.

2.2.4.2 Immunofluorescence staining of hind limb sections

Hind limb sections were stained for endothelial cells in order to quantify capillaries and to see whether there was a differential angiogenic response between wild type and PHD3$^{-/-}$ mice.

Cryosections were dried for 60 min at room temperature. After that, they were fixed for 20 min in a 1:1 mix of acetone and methanol at -20 °C. Tissues were encircled using a fat pen and washed twice in PBS. Afterwards, they were blocked for 30 min at room temperature in blocking solution. After removing the blocking solution with a quick rinse in PBS, sections were stained for 60 min at room temperature with Alexa488-coupled isolectin GS-IB4 and an antibody against vinculin in Dako Diluent (dilutions see table 4). Slides were then washed 5 times in PBS and incubated with TR-coupled goat anti mouse antibody in Dako Diluent for 60 min at room temperature. Slides were washed 6 times in PBS and stained using Hoechst (1:500) in PBS for 10 min at room temperature. After that, sections were again washed 3 times in PBS and embedded in Mowiol solution.

Stained sections were imaged using the 40x channel of the Zeiss Observer D1 microscope. 15-20 images were taken of different areas of the muscle using the same intensity for each channel. The amount and average size of capillaries was then measured and normalized to the amount of muscle cells in the field of view using ImageJ.

2.2.4.3 Picro-sirius red staining of hind limb sections

In order to quantify the extent of fibrosis in hind limbs 28 days after surgery, cryosections were stained with picro-sirius red, which stains collagen and elastin fibers red while healthy muscle tissue appears in orange.

Slides were dried for 60 min at room temperature and then incubated two times for 7 min in xylol. Slides were then incubated for 5 min each in isopropanol, 99% ethanol, 75% ethanol, 60% ethanol and distilled water. After that, slides were incubated for 60 min in picro-sirius red staining solution. The slides were washed in 1% acetic acid in distilled water two times for 3 min to get rid of unspecific staining. Afterwards slides were incubated 3 times for 3 min in ethanol and once in xylol for 7 min. Sections were embedded in Roti Histo-kitt.

Stained sections were imaged in bright-field using the 20x channel of the Zeiss Observer D1 microscope. The whole section was imaged and analyzed towards its content of picro-sirius-positive area using ImageJ. Holes in the tissue and borders were excluded from the analysis.

2.2.4.4 Evan´s Blue staining of infarcted hearts

The staining of a freshly isolated heart with the dyes Evan´s Blue and TTC (2,3,5-triphenyltetrazolium chloride) can identify the necrotic area in the infarcted heart as well as the area of the heart, which is at risk of dying. The method of Evan´s Blue staining was performed by Dr. Anke Zieseniß, a Postdoc of the Institute of Cardiovascular Physiology, and has been described before (Vogler et al., 2015).

Mice underwent LAD surgery. After 6 hrs, mice were injected with heparin (250 IU) and killed by cervical dislocation under isoflurane anesthesia. Hearts were isolated, the aorta was

cannulated and injected with 1% Evan´s Blue. The staining solution was distributed throughout the heart via the coronary arteries and stained the well perfused areas of the myocardium in blue. Areas that were not stained blue were defined as area at risk (AAR). The left ventricle was isolated and sliced into three sections which were incubated in 2% TTC for 20 min at 37 °C. Areas that were still viable were stained in red by TTC, while the areas of necrosis (AON) stayed pale. To quantify infarct size, images of the heart sections were made using the Nikon microscope SMZ 1500. AAR and AON were defined as the average area of the slice that was not stained in blue or appeared pale, respectively. The percentage was related to the individual weight of the slice. The total infarct size was calculated as AON/total AAR.

2.2.5 Cell cultivation and associated techniques

2.2.5.1 Cultivation and differentiation of BMDMs

The bone marrow contains a vast amount of hematopoietic precursor cells, which can be differentiated into myeloid cells depending on external stimuli. In order to generate large amounts of macrophages, hematopoietic progenitors can be isolated and differentiated in cell culture into macrophages. Differentiation of macrophages in Pluznik´s medium is a well-established technique (Ichikawa et al., 1966; Weischenfeldt and Porse, 2008). Secreted factors in L929-conditioned medium such as macrophage colony-stimulating factor (M-CSF) provide the stimulus for this differentiation.

8 to 12 week old mice were killed by cervical dislocation under isoflurane anesthesia and femurs were extracted. After cleaning the bones from residue muscle tissue, bones were disinfected by incubating them in 70% ethanol and subsequently washing them in PBS. The epiphysis on both sides of the bone was cut off with a scissor and the bone was flushed with a syringe (26 gauge needle) using 10 ml culture medium. Flushed medium was collected in a 50 ml tube and was allowed to settle for 10 min in order for pieces of bone to deposit. The supernatant was then seeded in a 10 cm surface-treated cell culture dish in order to separate non-adherent monocytes from adherent cells like fibroblasts. After 24 hrs, non-adherent cells were collected and spun down at 400 x g for 10 min at 4 °C. The pelleted cells were resuspended in 50 ml of Pluznik´s medium and spread into 5 bacteria plates. Cells were cultivated in Pluznik´s medium for 7 days. During this time, the medium was changed once on day 3 of differentiation.

Cultivating the cells for 7 days in Pluznik´s medium creates a cell population which is 80 to 90% positive for the macrophage marker F4/80 which can be analyzed by flow cytometry (see 2.2.5.4).

On day 7 in Pluznik´s medium, cells were detached using 3.5 ml accutase per 10 cm plate and collected in culture medium. After a centrifugation step at 400 x g for 10 min at 4 °C, cells were resuspended in 10 ml culture medium and counted. Cells were then seeded for RNA isolation, flow cytometry or single cell migration at the cell densities mentioned in the respective chapters.

An important component of Pluznik´s medium is L929-conditioned medium which was created by culturing 4-5x10^6 L929 cells for 7 days in 50 ml Dulbecco´s modified eagle medium (DMEM) with 10% FCS and 1% P/S. The medium was then pooled and spun down at 4000 rpm for 20 min at 4 °C and the supernatant was stored in aliquots at -20 °C.

2.2.5.2 Isolation and enrichment of neutrophils

The murine bone marrow presents a suitable place to extract high amounts of functionally differentiated neutrophils (Boxio et al., 2004). In order to extract them, 8-12 weeks old mice were killed via cervical dislocation under isoflurane anesthesia. Femur and tibia of both hind limbs were collected.

Bones were cleaned from residue muscle tissue, disinfected in 70% ethanol and shortly washed in PBS. Bones were then flushed with DMEM and filtered using a 70 µm mesh to get rid of bone residues. Cell suspensions were spun down at 400 x g for 10 min at 4 °C and the pellet was resuspended in 10 ml 0.2% NaCl to lyse erythrocytes. After 15 sec, 10 ml 1.6% NaCl was added to stop the lysis and cells were again spun down as described above.

A 100% Percoll solution was prepared by mixing 9 parts of Percoll solution with 1 part of 10x Hank´s balanced salt solution (HBSS). This stock solution was then further diluted to the desired percentages in 1x HBSS. Cells were resuspended in 3 ml 50% Percoll in HBSS and carefully layered onto a gradient made of 3 ml 80% Percoll and 4 ml 65% Percoll in HBSS. Percoll gradients were then centrifugated at 1200 x g for 30 min at 4 °C without brake. Neutrophils were enriched in the interface between 50% Percoll and 65% Percoll. This layer was carefully isolated and washed several times in PBS.

In order to quantify the amount of neutrophils in this layer, a sample of the cells was stained for flow cytometry (see 2.2.5.5). The remaining cells from this layer were used for RNA isolation in triplicates, if the flow cytometric analysis showed comparable amounts of neutrophils in both wild type and PHD3$^{-/-}$ samples and a neutrophil content of above 80%.

2.2.5.3 Isolation and cultivation of peritoneal macrophages

Mature macrophages can be isolated from the peritoneal cavity. This method yields comparably little amounts of cells, however, they display a phenotype that resembles macrophages *in vivo* better than BMDM (Zhang et al., 2008).

8-12 week old mice were killed by cervical dislocation in isoflurane narcosis. A small incision was made at the abdomen without harming the peritoneal cavity. The fur was pulled apart to uncover the skin lining of the peritoneal cavity. The peritoneal cavity was injected with 4 ml 0.5% BSA, 2 mM EDTA in PBS using a 26 gauge needle. The abdomen was then massaged in order to detach cells. Using a 25 gauge needle, as much fluid as possible was retained and collected.

Cells were spun down at 400 x g for 10 min at 4 °C, resuspended in culture medium and plated on 4 petri dishes (35 mm diameter). After 90 min, cells were washed two times with PBS in order to remove non-adherent cells. After 48 hrs of cultivation, a sample of the cells was analyzed using flow cytometry (see 2.2.5.5). The rest of the cells were harvested for RNA isolation if flow cytometric analysis showed more than 80% macrophages.

2.2.5.4 Flow cytometry of BMDM

To verify BMDM differentiation and quantify expression of M1 and M2 markers, TNF-R1 and 2, 350.000 differentiated BMDM were seeded per 35 mm petri dish. Different treatments were measured in quadruplicates. Cells were seeded in starvation medium or culture medium and kept for 24 hrs in normoxia (20% O_2) or hypoxia (1% O_2). Treatment with 10^{-7} M dexamethasone was performed for 18 hrs.

Cells were detached using 350 µl accutase and transferred into flow cytometry tubes. After washing them once in washing buffer, cells were blocked for 15 min using unstained CD16/CD32 antibody and then stained according to staining protocol 2 and 3 and measured using the FACS Canto II as described above (2.2.3.1).

2.2.5.5 Flow cytometry of peritoneal macrophages and neutrophils

The purity of isolated peritoneal macrophages and bone marrow-derived neutrophils was analyzed via flow cytometry.

Around 200.000 peritoneal macrophages were cultured for 48 hrs in 35 mm petri dishes and detached using 350 µl accutase. 100.000 neutrophils were taken from the enriched neutrophil layer of the Percoll gradient. After washing the cells several times in PBS, macrophages and neutrophils were blocked for 15 min using unstained CD16/CD32 antibody and then stained according to staining protocol 1 for neutrophils and 2 for peritoneal macrophages. Staining and measurement procedures were performed as described above (2.2.3.1).

2.2.5.6 RNA isolation

RNA was isolated from BMDM seeded in a 6-well at a density of 750.000 cells per well. Peritoneal macrophages were seeded at approximately 250.000 cells per 3.5 cm petri dish for RNA isolation. RNA was isolated from approximately $1x10^6$ neutrophils.

RNA was extracted making use of the acid guanidinium thiocyanate-phenol-chloroform extraction method (Chomczynski and Sacchi, 1987). In short, the chaotropic guanidinium thiocyanate enabled separation of proteins from nucleic acids upon phenol phase separation with chloroform.

Before RNA isolation, macrophages were washed twice in PBS, while neutrophils were washed several times in PBS and spun down at 400 x g for 5 min at 4 °C. After removing the PBS, cells were lysed in 500 µl TRIzol, which is a commercially available guanidinium thiocyanate-phenol mixture. Cell lysates were transferred into e-cups and 200 µl of chloroform was added. After mixing the samples shortly on a vortex, they were spun down at 1200 x g for 15 min at 4 °C to separate the aqueous RNA-containing upper phase from the protein-containing organic phase. The upper phase was then mixed with 1 volume of isopropanol and incubated at -20 °C for 20 min to precipitate RNA. Neutrophil and peritoneal macrophage samples were allowed to incubate over night at -20 °C to increase RNA yield. RNA was then pelleted by a centrifugation step at 12000 x g for 20 min at 4 °C and washed twice in 750 µl 75% ethanol. After removing the ethanol, pellets were dried, resuspended in 13 µl autoclaved H_2O and incubated for 10 min at 56 °C. RNA quality and concentration were determined using a NanoDrop. RNA was stored at -80 °C or directly transcribed into cDNA.

2.2.5 7 cDNA synthesis

RNA was transcribed into cDNA using a reverse transcriptase from the Moloney Murine Leukemia Virus supplied by the First strand cDNA synthesis kit. In short, 1 µg RNA was mixed with Oligo dT (5 µM) primers and incubated at 65 °C for 10 min in order to anneal the primers to the RNA. After that, the following substances were added to the sample:

Table 22: Reaction mix for cDNA synthesis.

Substance	Final concentration
M-MuLV Reverse Transcriptase	1 U/µl
RiboLock RNase Inhibitor	1 U/µl
5x Reaction Buffer	1x
dNTP Mix	0.5 mM

The reaction mix was then incubated at 37 °C for 60 min in order for the cDNA synthesis to take place and at 70 °C for 10 min to inactivate the enzyme. Samples were diluted 1:2 with autoclaved H_2O and stored at -20 °C or directly used for qRT- PCR.

2.2.5.8 cDNA synthesis for miRNA

miRNAs are small non-coding RNAs which are usually around 20-25 bp long. In order to study their expression, an adaptor-sequence was ligated into the cDNA to allow for binding of a forward and a reverse primer during the following qRT-PCR.

RNA was isolated from BMDM as described above (2.2.5.6). After that, a treatment with DNase was performed to degrade DNA. The following reaction mix was prepared:

Table 23: Reaction mix for DNase treatment.

Substance	Final concentration
RNA in RNase-free H_2O	
DNase Incubation buffer	1x
DNase I	0.5 U/µl
RNase OUT	4 U/µl
RNase-free H_2O	Ad 50 µl

Samples were then incubated at 37 °C for 20 min. RNase-free water was added to a final volume of 200 µl and the same volume of phenol/chloroform/isoamyl alcohol (24:25:1 mixture) was added. Samples were vortexed and centrifuged at 13,000 x g for 2 min. The upper aqueous phase was transferred into a new cup and RNA was precipitated by incubating it in 1 volume isopropanol and 1:10 volume 3 M sodium acetate (pH 4.8) for 30 min at -20 °C. Samples were spun down at 13000 x g for 30 min at 4 °C, and the supernatant was removed. The pellet was washed twice with 75% ethanol, resuspended in 13 µl RNase-free water and incubated at 56 °C for 10 min. RNA was kept at -80 °C or directly used for cDNA synthesis.

1 µg of RNA was transcribed into cDNA using the All-in-One miRNA First-Strand cDNA Synthesis Kit. This kit contains Poly A Polymerase which adds a poly-A tail to 3´-ends of all RNAs. Oligo-dT adaptors can then bind to the poly-A tails and the RNA is reversely transcribed into cDNA. In short, a reaction mix containing the following ingredients was prepared:

Table 24: Reaction mix for cDNA synthesis out of miRNA.

Reagent	Volume/Final concentration
RNA	1 µg
Poly A Polymerase	0.1 U/µl
RTase Mix	1 µl
PAP/RT Buffer	1x
Spike-in control	1 µl
RNase-free H_2O	Ad 25 µl

Samples were incubated at 37 °C for 60 min in order to synthesize cDNA and at 85 °C for 5 min to inactivate the enzymes. Samples were diluted 1:2 with RNase-free H_2O and stored at -20 °C or directly used for qRT-PCR.

2.2.5.9 qRT- PCR

The expression levels of genes can be quantified and compared using quantitative realtime polymerase chain reaction (qRT-PCR). During this reaction, transcript amplification is

detected by the fluorescent dye SYBR green which intercalates with double-stranded DNA. Fluorescence intensity directly correlates with transcript abundance and increases with every amplification cycle, making it possible to compare expression levels of different genes. The SensiMix™ SYBR® Low-ROX kit was used according to the manufacturer´s instructions. In short, the following reaction mix was prepared:

Table 25: Reaction mix for SYBR green qRT-PCR.

Substance	Amount [µl]	Final concentration
SensiMix™ SYBR® Low-ROX kit	12.5	1x
Primer fw	0.5	0.1 pmol/µl
Primer rev	0.5	0.1 pmol/µl
cDNA	1	1:50
H_2O	10.5	

For miRNA detection, the Universal Adaptor primer as well as the miRNA-specific primer were added in a final concentration of 0.2 µM. The qRT-PCR reaction was run in 96-well plates in the Stratagene Mx3000p light cycler following this temperature profile:

Table 26: Temperature profile for qRT-PCR.

Step	Temperature [°C]	Time [min]	Cycles
Initial activation	95	10:00	1
Amplification	95	00:15	40
	Annealing temperature	00:20	
	72	00:30	
Dissociation curve	95	1:00	1
	Annealing temperature	0:30	
	95	0:30	

The annealing temperatures for the respective genes are given in the primer list (table 7). Analysis was done using the MxPro software. C_T-values represent the cycle number, at which the amplification curve of the respective gene crosses the threshold. C_T-values of the house keeping gene S12 were subtracted from C_T-values of genes of interest to get ΔC_T-values. The mean of the wild type control was then subtracted from these values in order to normalize them. $\Delta\Delta C_T$-values were then calculated by inserting normalized ΔC_T-values into the following formula:

$$\Delta\Delta C_T = 2^{-\Delta C_T}$$

The resulting $\Delta\Delta C_T$-values present the fold change of the expression of the gene of interest in all samples compared to the wild type control.

2.2.5.10 Protein isolation

In order to extract proteins from BMDM, $4x10^6$ cells were seeded in culture medium or starvation medium in surface-treated 10 cm dishes for 48 hrs. Cells were incubated in normoxia (20% O_2) or hypoxia (1% O_2) for 24 hrs. After that, cells were washed once in PBS and lysed by adding 175 µl cell lysis buffer. Cells were scraped from the dishes and incubated in the cell lysis buffer for 10 min on ice. Cell lysates were centrifugated at 13000 x g for 20 min at 4 °C and the supernatant was collected. Cell lysates were either directly processed or stored at -80 °C.

2.2.5.11 Measuring protein concentration

Protein concentration in BMDM cell lysates was determined using the Bradford method. In short, 1 µl of sample was placed in a 96-well plate and a standard curve was prepared ranging from 0.5 µg to 6 µg BSA. 200 µl 1:5 Protein Assay Reagent was added to each well and the absorbance at 595 nm was measured in the Bio-Rad Microplate Reader. 80 µg of protein per sample was used for Western blot.

2.2.5.12 SDS-Polyacrylamide gel electrophoresis

Protein samples were incubated with 1 volume 2xSDS sample buffer for 10 min at 95 °C. This sample buffer contains sodium dodecyl sulfate (SDS) which, together with β-mercaptoethanol, denaturates proteins by disrupting non-covalent bonds. SDS also gives proteins a negative charge by associating with them. This allows the separation of proteins via an electrical field in the following polyacrylamide gel electrophoresis. Smaller proteins can migrate faster through the gel, while bigger proteins are held back by the pores of the polyacrylamide-gel, resulting in protein separation according to their size.

Samples and a PageRuler protein marker were loaded onto a polyacrylamide gel composed of a 4% stacking gel, and a 10% or 12% running gel (see table 25). 10% running gels were used to obtain Western blots of HIF-1α, while 12% running gels were used for detection of all the other proteins.

Table 27: Composition of stacking and running gels for SDS-polyacrylamide gel electrophoresis.

Compound	4% stacking gel	10% running gel	12% running gel
H_2O	2.7 ml	11.9 ml	9.9 ml
30% acrylamide mix	0.67 ml	10 ml	12 ml
1 M Tris/HCl (pH 6.8)	0.5 ml	-	-
1.5 M Tris/HCl (pH 8.8)	-	7.5 ml	7.5 ml
10% SDS	0.04 ml	0.3 ml	0.3 ml
10% ammonium persulfate	0.04 ml	0.3 ml	0.3 ml
TEMED	0.004 ml	0.012 ml	0.012 ml

The SDS-PAGE was run at a constant current of 40-45 mA with a maximum voltage of 300 V.

2.2.5.13 Western blot

Proteins were transferred from the polyacrylamide gel onto a nitrocellulose membrane using a semi-dry blotting technique. Again, the negative charge of proteins after association with SDS was utilized to ensure transfer. Gel, nitrocellulose membrane and filter paper were soaked in Western blot transfer buffer and stacked between the anode and cathode of the PerfectBlue Semi-Dry Electroblotter. Negatively charged proteins travelled towards the positive anode and were transferred onto the membrane. Western blotting was performed at a constant current of 2 mA/cm^2 for 1 hr.

Successful transfer was evaluated by reversibly staining the proteins attached to the nitrocellulose membrane in Ponceau S staining solution. Afterwards, the membrane was washed in PBS to get rid of the Ponceau staining and incubated in 5% milk for 60 min at room temperature to block unspecific binding sites for antibodies.

The membrane was subsequently incubated in 5% milk containing a primary antibody at the dilution listed above (table 5) over night at 4 °C. After that, the membrane was washed three times in PBS to get rid of unbound antibodies. The membrane was then incubated in 5 % milk containing horseradish peroxidase (HRP)-coupled secondary antibody which would recognize the respective primary antibody for 2 hrs at room temperature.

In order to detect β-actin, the membrane was washed three times and incubated in 10 ml enhanced chemiluminescence (ECL) solution, which contains substrates for the horseradish peroxidase. The membrane was imaged using the LAS3000 Imager. For all other proteins, a commercially available chemiluminescent HRP substrate solution (Merck Millipore) was used. X-ray films were exposed to the membrane with varying exposure times to visualize protein bands.

2.2.5.14 Single cell migration

Migration is a substantial feature of macrophages as they have to migrate into areas of inflammation. Migration capacity was measured using a single cell migration approach which studied random migration.

Differentiated BMDM were seeded at a density of 100.000 cells/well in a 6-well. Migration of cells was then monitored by taking pictures of an arbitrarily chosen field of interest at a 10x magnification. Pictures were taken every 10 min over a period of 6 hrs.

Images were stacked and cells were tracked using the manual tracking plugin for ImageJ as well as the chemotaxis plugin. Cells that wandered out of the field of view were excluded from the analysis.

Cells were either measured in fresh culturing medium as a control condition or in MDA-MB231-conditioned medium, which presents a migration stimulus.

In order to create MDA-MB231-conditioned medium, $1x10^6$ MDA-MB231 cells were cultured in 10 ml DMEM + 10% FCS and 1% P/S for 4 days. The medium was then spun down at 4000 rpm for 20 min at 4 °C and the supernatant was stored at -20 °C in aliquots.

2.2.5.15 Prostaglandin E2 (PGE2) secretion

Prostaglandin E2 levels were measured using a chemiluminescent ELISA kit. In short, endogenous PGE2 competes with PGE2 coupled to alkaline phosphatase (AP) for the interaction with a PGE2-specific antibody. This antibody was then caught by a capture antibody at the bottom of the well. The chemiluminescence measured upon addition of AP-substrate inversely correlates with the amount of endogenous PGE2 in the samples.

Prostaglandin secretion was measured in BMDM supernatant, which was isolated after 24 hrs of cultivation in normoxia or hypoxia with culture medium or in starvation medium. Cells were cultivated at a density of 750.000 per well in 6-well plates. The supernatant was removed and centrifuged for 20 min at 12000 x g at 4 °C to pellet floating particles and transferred to a new cup. Samples were either used directly or stored at -80 °C. For the assay, 100 µl supernatant was used according to the manufacturer´s instructions.

2.2.5.16 Phagocytotic capacity

Phagocytotic capacity was measured using labelled latex beads, which emitted red fluorescent signals in the acidic environment of the phagosome. In short, BMDMs were seeded at a density of 300.000 in a 35 mm petri dish and cultivated for 24 hrs in normoxia or hypoxia in normal culture medium or in starvation medium. Treatment with PGE2 was performed for 18 hrs at a final concentration of 100 pg/ml. Cells were incubated with latex beads for 4 hrs, after which they were detached using 350 µl accutase. Cells were centrifuged at 400 x g, washed once with PBS and subsequently analyzed for their uptake of beads using the FACS Canto II flow cytometer. Uptake of beads was measured in % phagocytotic cells.

2.2.6 Statistics

If not indicated otherwise, statistical significance was calculated by using an unpaired two-tailed student´s T-test. A significant difference between two means was defined by a *p*-value smaller than 0.05. Error bars in graphs indicate the standard error of the mean (SEM).

3. Results

3.1 Characterization of myeloid-specific conditional PHD3 knock out mice

The goal of the study was to investigate the role of PHD3 in macrophage-mediated inflammation after an ischemic insult. In order to dissect macrophage-mediated effects from those of other cell types, a mouse model with a myeloid-specific knock out of PHD3 was studied. Mice with a heterozygous expression of the cre recombinase under the control of the lysozyme M promoter (LysMcre$^{+/-}$) were crossed with mice that had a floxed PHD3 gene (PHD3$^{flox/flox}$, Figure 4B). This led to excision of exon 2 of PHD3 in cells expressing lysozyme M in LysMcre$^{+/-}$xPHD3$^{flox/flox}$ mice (called PHD3$^{-/-}$ mice hereafter). Lysozyme M is mainly expressed in myeloid cells such as macrophages and granulocytes and to a lower degree in dendritic cells (Clausen et al., 1999). Mice expressing the floxed PHD3 gene but no cre recombinase were used as wild type controls (LysMcre$^{-/-}$xPHD3$^{flox/flox}$, called wild type hereafter).

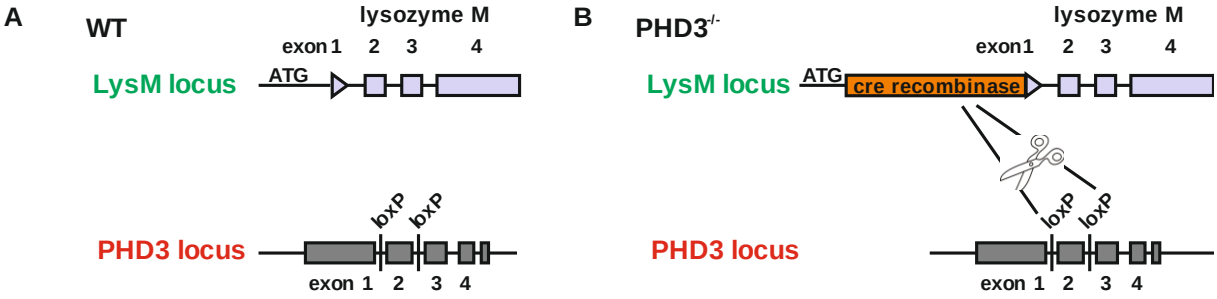

Figure 4: Myeloid-specific conditional knock out of PHD3. Mice expressing cre recombinase under the control of the lysozyme M promoter were crossed with mice in which exon 2 of the PHD3 locus was homozygously flanked by loxP sites. (A) LysMCre$^{-/-}$xPHD3$^{flox/flox}$ mice were used as wild type controls. In LysMcre$^{+/-}$xPHD3$^{flox/flox}$ mice (B), excision of exon 2 took place in myeloid cells.

I confirmed that indeed both *in vitro* differentiated BMDM and isolated peritoneal macrophages showed a knock out of PHD3 by testing their RNA expression level via qRT-PCR (Figure 5A) compared to wild type mice. Neutrophils isolated from the bone marrow displayed a PHD3 knock out as well. Residual expression of PHD3 in all cell populations could be the result of contamination with non-myeloid cells. In case of neutrophils, flow cytometry analysis showed that the tested population contained around 80% neutrophils (Figure 5C). For peritoneal and bone marrow-derived macrophages, purity was always above 85% (Figure 5B). Also, an inefficient recombination could be a possible reason why there was still a residual PHD3 expression in the PHD3$^{-/-}$ cells.

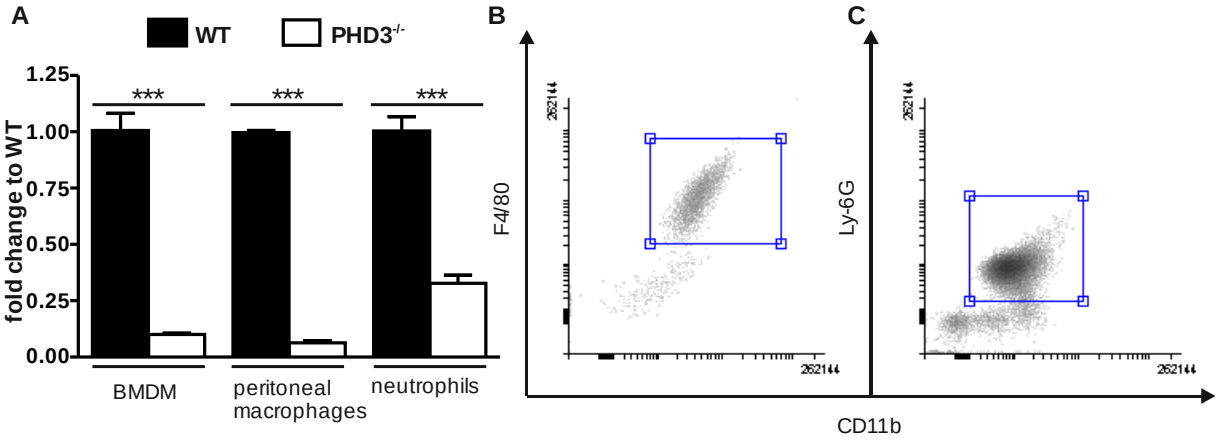

Figure 5: Confirmation of the myeloid knock out of PHD3 on RNA level. (A) RNA expression was analyzed in bone marrow-derived macrophages (BMDM), peritoneal macrophages and neutrophils relative to the house-keeping gene S12 and normalized to the respective wild type cells. Results are representative of at least 3 independent experiments. Neutrophil PHD3 expression levels are representative of 2 independent experiments. Bars show mean ± SEM, *** $p<0.001$. The purity of isolated peritoneal macrophages (B) and neutrophils (C) were tested via flow cytometry using the markers F4/80 and CD11b (macrophages) or Ly6G and CD11b (neutrophils) for the identification of the respective cell population.

As BMDM yield high enough cell numbers to test protein expression, in contrast to peritoneal macrophages and neutrophils, I analyzed HIF-1α, PHD2 and PHD3 protein levels under different culture conditions including hypoxia and starvation in a Western blot (Figure 6). Fully differentiated BMDM were incubated for 48 hrs in starvation medium or in normal cell culture medium. Incubation in hypoxia was performed for 24 hrs. The respective normoxia control samples were kept in normoxia for this time. Incubating the cells in hypoxia led to a robust HIF-1α stabilization with no apparent difference between wild type and PHD3$^{-/-}$ BMDM. In normoxia, HIF-1α is hardly detectable due to its high turnover. Interestingly, knock out of PHD3 did not lead to a HIF-1α stabilization in normoxia, suggesting that PHD3 is not the main regulator of HIF-1α stability in normoxia. PHD2 protein levels were not upregulated in PHD3$^{-/-}$ cells to compensate for the loss of PHD3.

PHD3 protein levels are hardly detectable in normoxia. The HIF-target gene PHD3 is highly upregulated in hypoxia, which leads to a strongly visible band in the wild type sample, while the PHD3$^{-/-}$ sample displays only a faint band. Starvation led to a mild HIF-1α stabilization in normoxic samples but did not significantly alter protein levels between wild type and PHD3$^{-/-}$ samples.

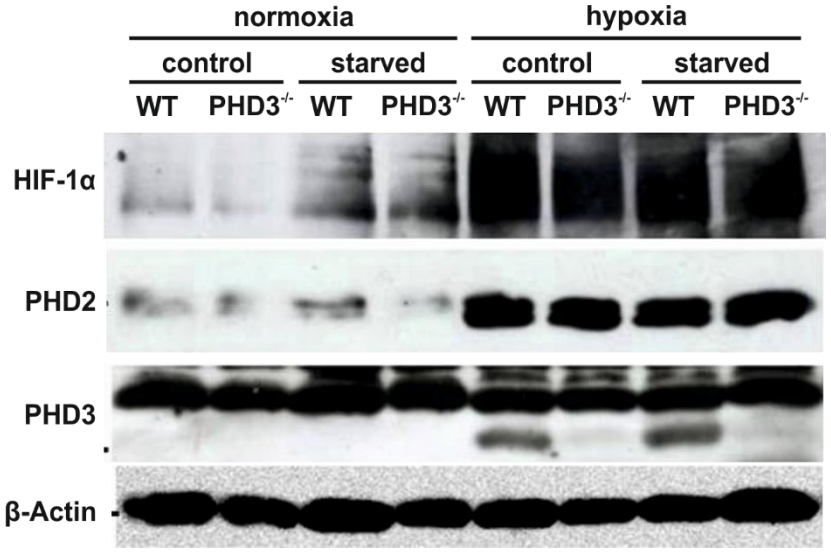

Figure 6: Confirmation of the knock out of PHD3 in BMDM on protein level. Western blot of protein lysates from BMDM was performed. Cells were incubated for 48 hrs in starvation or normal culture medium (control) and incubated in hypoxia (1% O_2) or normoxia (20% O_2) for 24 hrs. Protein levels of HIF-1α, PHD2 and PHD3 were studied, β-Actin levels were examined as loading control. Results are representative of 3 independent experiments.

To test whether the myeloid-specific knock out of PHD3 was indeed myeloid-specific, different organs were isolated from wild type and PHD3$^{-/-}$ mice. RNA was isolated and tested for PHD3 expression. None of the organs of PHD3$^{-/-}$ mice, including the gastrocnemicus muscle (GM), heart, skin, spleen, liver, kidney, lung and brain, showed a downregulation of PHD3 mRNA (Figure 7), indicating that the myeloid-specific knock out strategy via cre expression in lysozyme M-expressing cells does not "leak" to off-target tissues. This is in line with an earlier characterization of the myeloid-specific knock out in the LysMcre^{+} mice (Clausen et al., 1999).

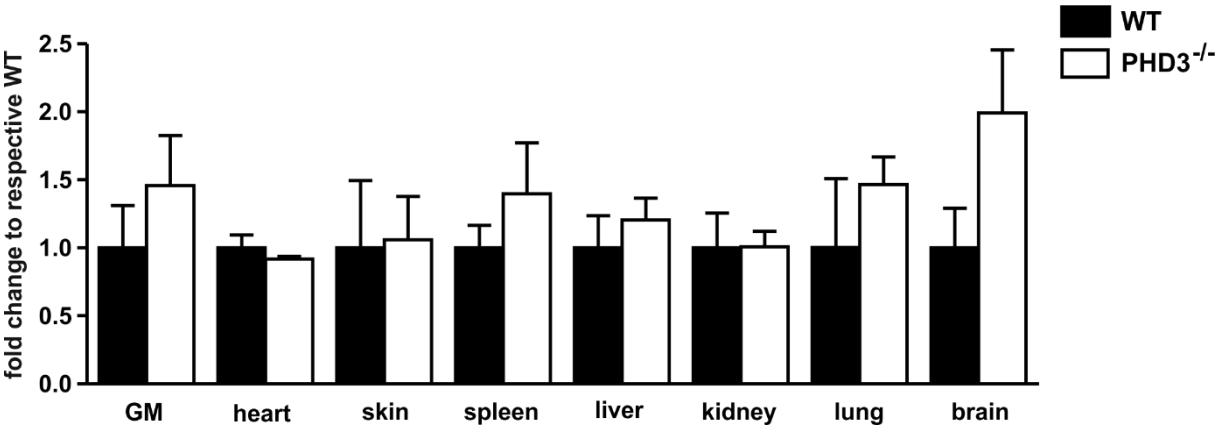

Figure 7: Expression of PHD3 in non-myeloid tissues. PHD3 expression was analyzed via qRT-PCR in different tissues including the gastrocnemicus muscle (GM) isolated from n=3 wild type and n=4 PHD3$^{-/-}$ mice and displayed normalized to the respective wild type. Bars show mean ± SEM.

In summary, the myeloid-specific conditional knock out mouse model shows a clear reduction in PHD3 RNA-level in both macrophage and neutrophil populations, as well as

strongly decreased protein levels in BMDM in hypoxia. The fact that HIF-1α protein levels are not influenced by the PHD3 knock out is in line with unchanged expression of HIF-target genes analyzed earlier in the group of Cardiovascular Physiology (Swain et al., 2014) which suggests that HIF-signaling is unchanged in PHD3 knock out BMDM. Analysis of different tissues shows no knock out of PHD3 in off-target tissues and suggests a myeloid-specific expression of the cre recombinase.

3.2 Leukocyte infiltration into the ischemic muscle is blunted in PHD3$^{-/-}$ mice

Members of the PHD enzyme family, especially PHD3 have previously been associated to changes in behavior of innate immune cells, such as neutrophils (Walmsley et al., 2011) or macrophages (Kiss et al., 2012), where a global PHD3 knock out led to increased inflammation in a model of abdominal sepsis. I now wanted to elucidate the role of PHD3 in macrophages for ischemia-induced sterile inflammation.

In order to test for leukocyte infiltration and clearance after hind limb ischemia, mice underwent surgery and GMs were isolated on day 1, 3, 4, 5 and 7 after surgery. Muscles were digested and tissue lysates were stained for markers of different subpopulations, such as macrophages (F4/80$^+$ CD11b$^+$) and neutrophils (Ly6G$^+$ CD11b$^+$), as well as for markers of macrophage polarization (CD86, CD206).

Analyzing leukocyte numbers (Figure 8A) via CD11b surface expression revealed that inflammation in the GM peaks around day 4 and is mostly cleared away at day 7. On day 4 and 5, a significantly lower number of infiltrating leukocytes were found in the myeloid-specific PHD3 knock out compared to wild type controls.

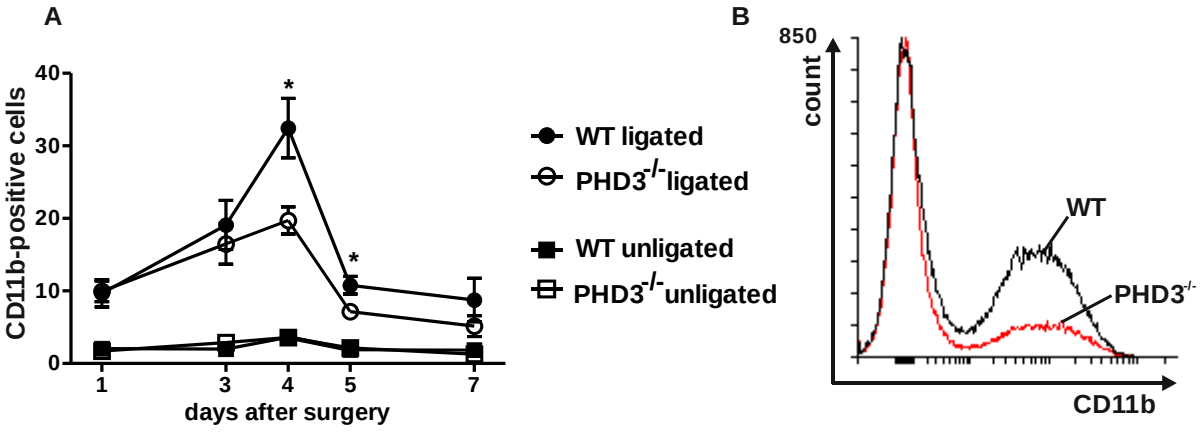

Figure 8: Leukocyte infiltration in the ischemic muscle after hind limb ischemia in PHD3$^{-/-}$ mice. Leukocyte infiltration was analyzed via flow cytometry over the course of 7 days after surgery within the gastrocnemicus muscle. Cell populations are displayed as % of total cell population within the tissue lysates of unligated and ligated legs of wild type and PHD3$^{-/-}$ mice. (A) Leukocytes were identified as CD11b$^+$ cells. (B) Exemplary histogram of CD11b expression within the cell population isolated from a wild type (black line) and a PHD3$^{-/-}$ (red line) mouse 4 days after surgery. In total, the following numbers of mice were analyzed per group: day 1 wild type=6, PHD3$^{-/-}$=7, day 3 wild type=5, PHD3$^{-/-}$=8, day 4 wild type=15, PHD3$^{-/-}$=15, day 5 wild type=7, PHD3$^{-/-}$=6, day 7 wild type=6, PHD3$^{-/-}$ =8 mice. Graph (A) represents mean ± SEM (* p<0.05, ** p<0.01).

The leukocyte population which is responsible for the blunted inflammatory phenotype seemed to be macrophages, which were first detectable 3 days after surgery. At this time point wild type and PHD3$^{-/-}$ macrophages were still abundant at similar levels. At day 4 and 5 however, PHD3$^{-/-}$ macrophages were present at significantly lower numbers compared to wild type macrophages (Figure 9).

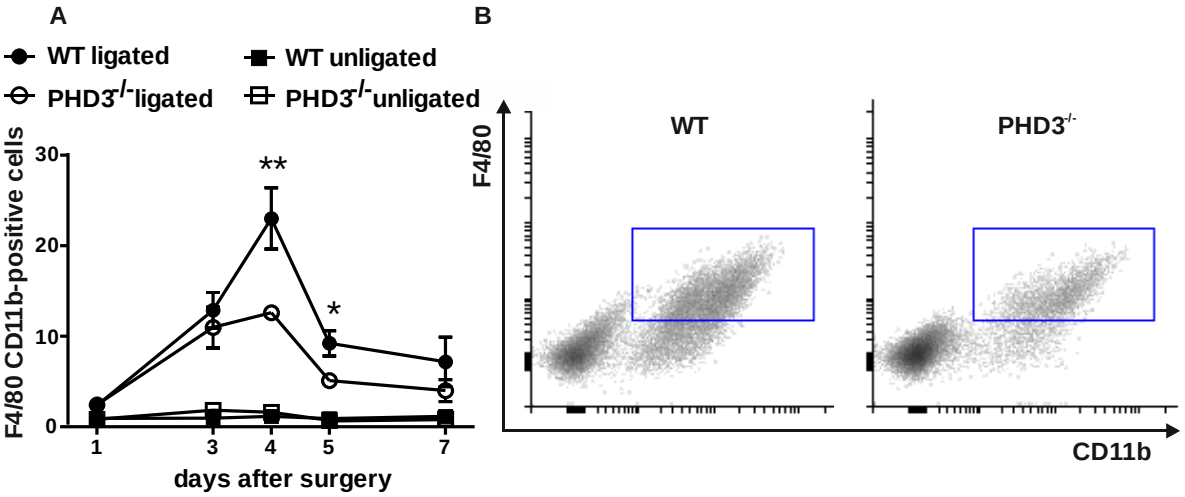

Figure 9: Macrophage infiltration in the ischemic muscle after hind limb ischemia in PHD3$^{-/-}$ mice. Macrophage infiltration was analyzed via flow cytometry over the course of 7 days after surgery within the gastrocnemicus muscle. (A) Macrophages were identified as F4/80^{+} CD11b^{+} cells. (B) Density plots are shown of an exemplary wild type (left graph) and PHD3$^{-/-}$ (right graph) sample 4 days after surgery. In total, the following numbers of mice were analyzed per group: day 1 wild type=6, PHD3$^{-/-}$=7, day 3 wild type=5, PHD3$^{-/-}$=8, day 4 wild type=15, PHD3$^{-/-}$=15, day 5 wild type=7, PHD3$^{-/-}$=6, day 7 wild type=6, PHD3$^{-/-}$=8 mice. Graph (A) represents mean ± SEM (* p<0.05, ** p<0.01).

To analyze whether the macrophage reaction was blunted due to a secondary effect caused by neutrophils, this cell population was also studied (Figure 10). Neutrophil levels did not show any significant difference on day 1 or day 3 after surgery, which present the main days of their presence within the ischemic muscle tissue.

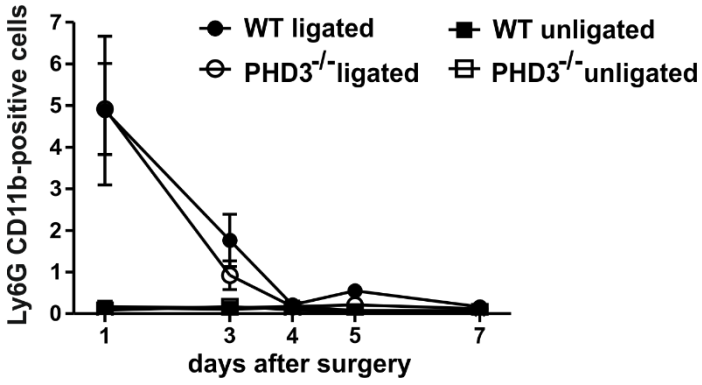

Figure 10: Neutrophil infiltration in the ischemic muscle after hind limb ischemia in PHD3$^{-/-}$ mice. Neutrophils were identified as Ly6G^{+} MHCII^{low} CD11b^{+} cells. In total, the following numbers of mice were analyzed per group: day 1 wild type=6, PHD3$^{-/-}$=7, day 3 wild type=5, PHD3$^{-/-}$=8, day 4 wild type=15, PHD3$^{-/-}$=15, day 5 wild type=7, PHD3$^{-/-}$=6, day 7 wild type=6, PHD3$^{-/-}$=8 mice. Graph represents mean ± SEM (* p<0.05, ** p<0.01).

The macrophage population was additionally analyzed regarding their expression of pro-inflammatory (M1) or anti-inflammatory (M2) markers. CD86 was used as a marker for M1-polarization while CD206 was used as a marker for M2-polarization. CD86 levels within the macrophage population did not change significantly between wild type and PHD3$^{-/-}$ (Figure 11A and 11C). CD206 levels, however, showed a clear induction from day 3 to day 4 and 5, indicating that wound healing processes are already being induced in this stage (Figure 11B and 11D). PHD3$^{-/-}$ macrophages, compared to macrophages from wild type littermates, displayed a higher expression of CD206 both at day 4 and at day 5.

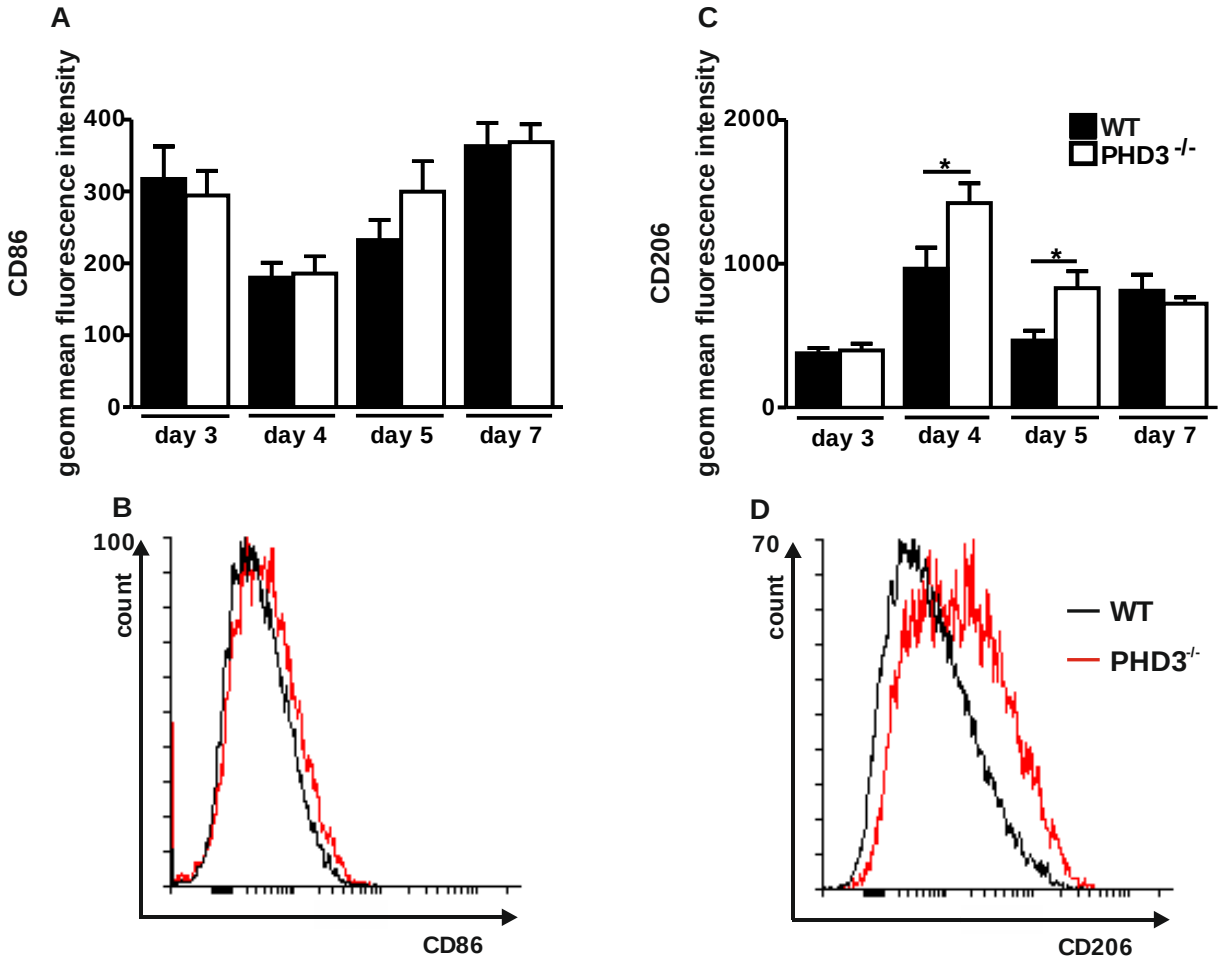

Figure 11: Macrophage polarization in PHD3$^{-/-}$ mice. Macrophage polarization was analyzed via expression of CD86 (M1-marker) or CD206 (M2-marker) within the F4/80^{+} CD11b^{+} population. M1 (A) and M2-marker (B) expression was measured as mean fluorescence intensity within the F4/80^{+} CD11b^{+} macrophage population. Exemplary histograms are shown for one wild type (black line) and one PHD3$^{-/-}$ (red line) mouse (C and D). In total, the following numbers of mice were analyzed per group: day 1 wild type=6, PHD3$^{-/-}$=7, day 3 wild type=5, PHD3$^{-/-}$=8, day 4 wild type=15, PHD3$^{-/-}$=15, day 5 wild type=7, PHD3$^{-/-}$=6, day 7 wild type=6, PHD3$^{-/-}$=8 mice. Bars represent mean ± SEM (* $p<0.05$, ** $p<0.01$).

Taken together, these data suggest a blunted inflammatory response in the ischemic muscle after hind limb ischemia caused mainly by the macrophage population in myeloid-specific PHD3$^{-/-}$ mice. A more anti-inflammatory polarization, as suggested by the expression levels of CD206, may additionally contribute to confine the inflammatory reaction.

3.3 Cytokine levels in the blood are unchanged between wild type and PHD3$^{-/-}$ mice after hind limb ischemia

Strong inflammatory reactions result in cytokine secretion by immune cells to the blood stream. In order to test whether plasma cytokines levels are elevated after hind limb ischemia, peripheral blood was taken 1, 3, 5 or 7 days after surgery, covering the whole time period of the inflammatory reaction in the hind limb muscle.

Plasma was isolated from wild type and PHD3$^{-/-}$ blood and tested using a cytometric bead assay to analyze concentrations of the cytokines IL-6 (Figure 12A), MCP-1 (Figure 12B) and TNF (Figure 12C). As a reference, plasma from resting age and gender-matched mice was used. IL-6 showed a clear increase in concentration 1 day after surgery as well as elevated levels on day 3 and 5 after surgery, however, there was no difference visible between wild type and PHD3$^{-/-}$ mice. Also, TNF and MCP-1 levels showed slightly increased cytokine concentrations after surgery compared to the resting control, though standard deviations were quite high. They however also did not show a significant difference between plasma concentrations of wild type and PHD3$^{-/-}$ mice. Of note, cytokine concentrations were in general rather low, which implies that the inflammatory reaction was well defined to the ischemic muscle with rather little systemic impact.

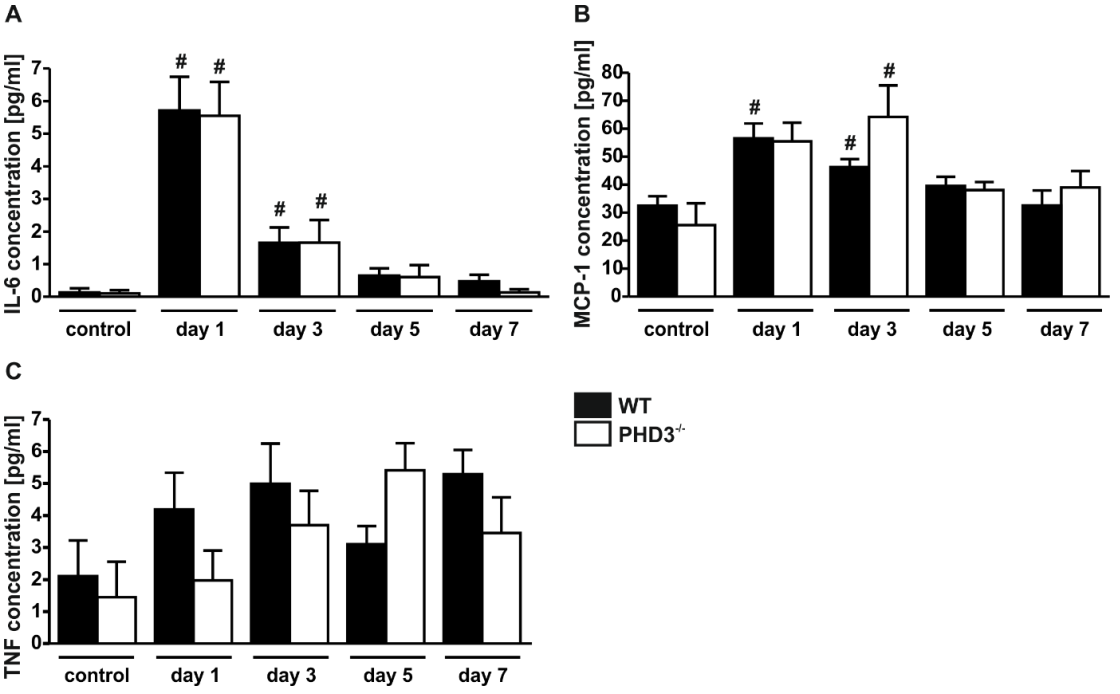

Figure 12: Plasma concentration of pro-inflammatory cytokines of wild type and PHD3$^{-/-}$ mice. IL-6 (A), MCP-1 (B) and TNF (C) concentration [pg/ml] in plasma of resting control mice as well as 1, 3, 5 and 7 days after hind limb ischemia surgery were measured using a cytometric bead assay. The following numbers of mice were used per group: control wild type=5, PHD3$^{-/-}$=4, day 1 and 3 n=6 for all groups, day 5 and 7 wild type=6, PHD3$^{-/-}$=5. Bars represent mean ± SEM. P<0.05 # (comparing plasma from an operated group to the resting control)

3.4 Reperfusion recovery stays unchanged between wild type and PHD3$^{-/-}$ mice

Macrophages are not only important for the early phases of inflammation, they also mediate wound healing processes like angiogenesis and arteriogenesis. To investigate, whether a knock out of PHD3 influences the properties of macrophages responsible for these aspects, I analyzed perfusion recovery after hind limb ischemia surgery measured via laser Doppler imaging (Figure 13A and B).

Mice underwent hind limb ischemia surgery and were analyzed before, directly after as well as on day 1, 3, 5, 7, 14, 21 and 28 after surgery. Both wild type and PHD3$^{-/-}$ mice showed after an initial sharp drop a steep increase of perfusion within 7 days. Perfusion recovered up to 70-80% until day 28. There was no significant difference in perfusion recovery at any of the investigated time points between the two groups. In addition, the development of necrotic toe nails, which is an indicator for insufficient paw perfusion, was analyzed. Toe nails of a small number of mice were stained black around day 2 after surgery (Figure 13C). This was a non-reversible effect that did not impair foot or limb movement and was closely monitored. The number of necrotic toe nails per paw was documented and it was quantified how many of the mice per genotype developed 1, 2, 3, 4 or 5 black toe nails on the paw of the operated leg. There was no significant difference between wild type and PHD3$^{-/-}$ mice to whether they developed necrotic toes or not.

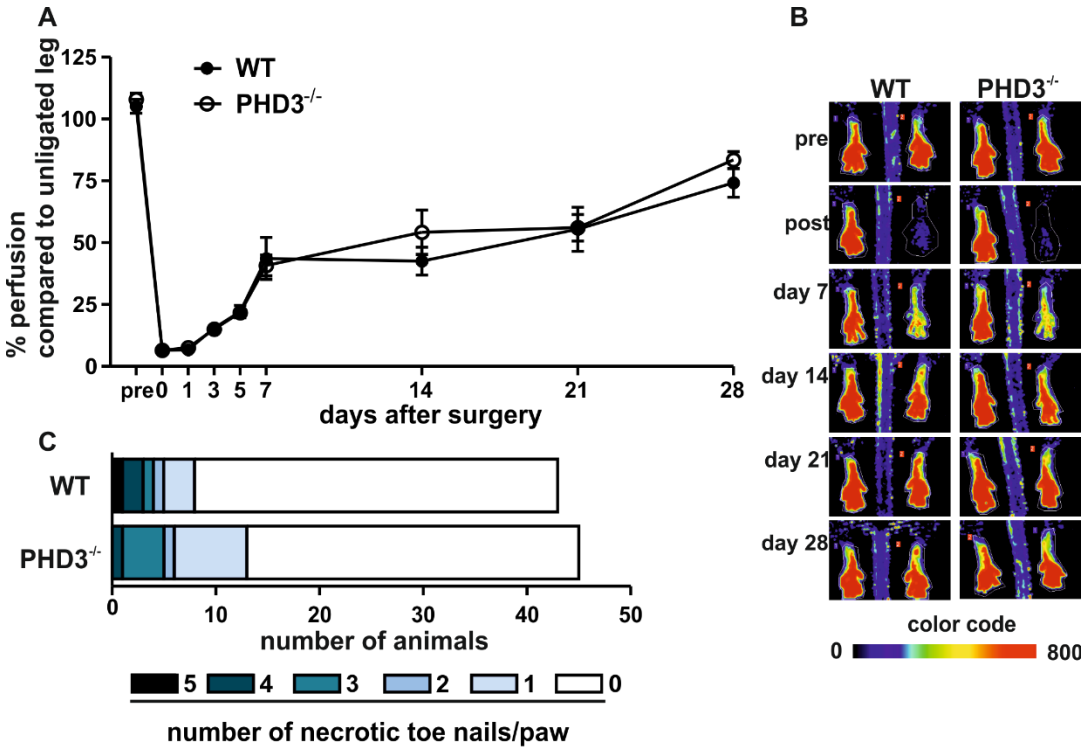

Figure 13: Perfusion recovery after hind limb ischemia in wild type and PHD3$^{-/-}$ mice. (A) Perfusion was measured from laser Doppler images before, directly after and 1, 3, 5, 7, 14, 21 and 28 days after surgery. Perfusion was measured as signal intensities per image and normalized to the value of the unligated leg of each animal. Groups included day 0 wild type=32, day 0 PHD3$^{-/-}$=32, day 1 wild type=13, day 1 PHD3$^{-/-}$=18, day 3 wild type=23, day 3 PHD3$^{-/-}$=24, day 5 wild type=22, day 5

PHD3$^{-/-}$=22, day 7 wild type=7, day 7 PHD3$^{-/-}$=15, day 14, 21, 28 wild type=7, PHD3$^{-/-}$=7 mice. Graph shows mean ± SEM. (B) Exemplary images of laser Doppler measurements are depicted, color code represents the amount of perfusion measured (arbitrary intensity units). (C) Number of necrotic toe nails counted per paw per animal comparing wild type and PHD3$^{-/-}$ mice.

Taken together, these results suggest that processes leading to perfusion recovery are not differentially influenced by PHD3$^{-/-}$ macrophages as there was no significant difference in perfusion recovery nor in development of necrotic toes.

3.5 Angiogenesis after hind limb ischemia is unchanged between wild type and PHD3$^{-/-}$ mice

The acquired perfusion data suggest that processes like angiogenesis and arteriogenesis are not altered by a myeloid-specific knock out of PHD3. This result deviates from previously published data in a global PHD3 knock out, where PHD3$^{-/-}$ mice had an ameliorated perfusion recovery after hind limb ischemia (Rishi et al., 2015). Therefore I wanted to confirm my finding with an independent method. The model of hind limb ischemia applied here leads to a permanent ligation of the femoral artery, and additionally ligates one main branch of the artery which could be used as a collateral for arteriogenesis, the proximal caudal femoral artery. Therefore, possible arteriogenic effects are highly limited by this surgery technique and thus were not studied in depth.

I chose to evaluate angiogenesis on cryosections of GM. Mice underwent hind limb ischemia and after 3 or 28 days, muscles were extracted. Blood vessels such as capillaries were visualized via isolectin IB4 staining. The extent of angiogenesis was quantified by analyzing average capillary size (Figure 14A) and capillary number (Figure 14B) in relation to the number of muscle cells.

Both at day 3 and day 28 the number of capillaries and their average size were significantly increased in ligated legs of both groups compared to their unligated controls, indicating that the applied analysis technique was able to detect angiogenic effects. However, no significant difference could be observed when comparing wild type and PHD3$^{-/-}$ mice, neither in the acute inflammatory phase (day 3) nor in the healing phase (day 28).

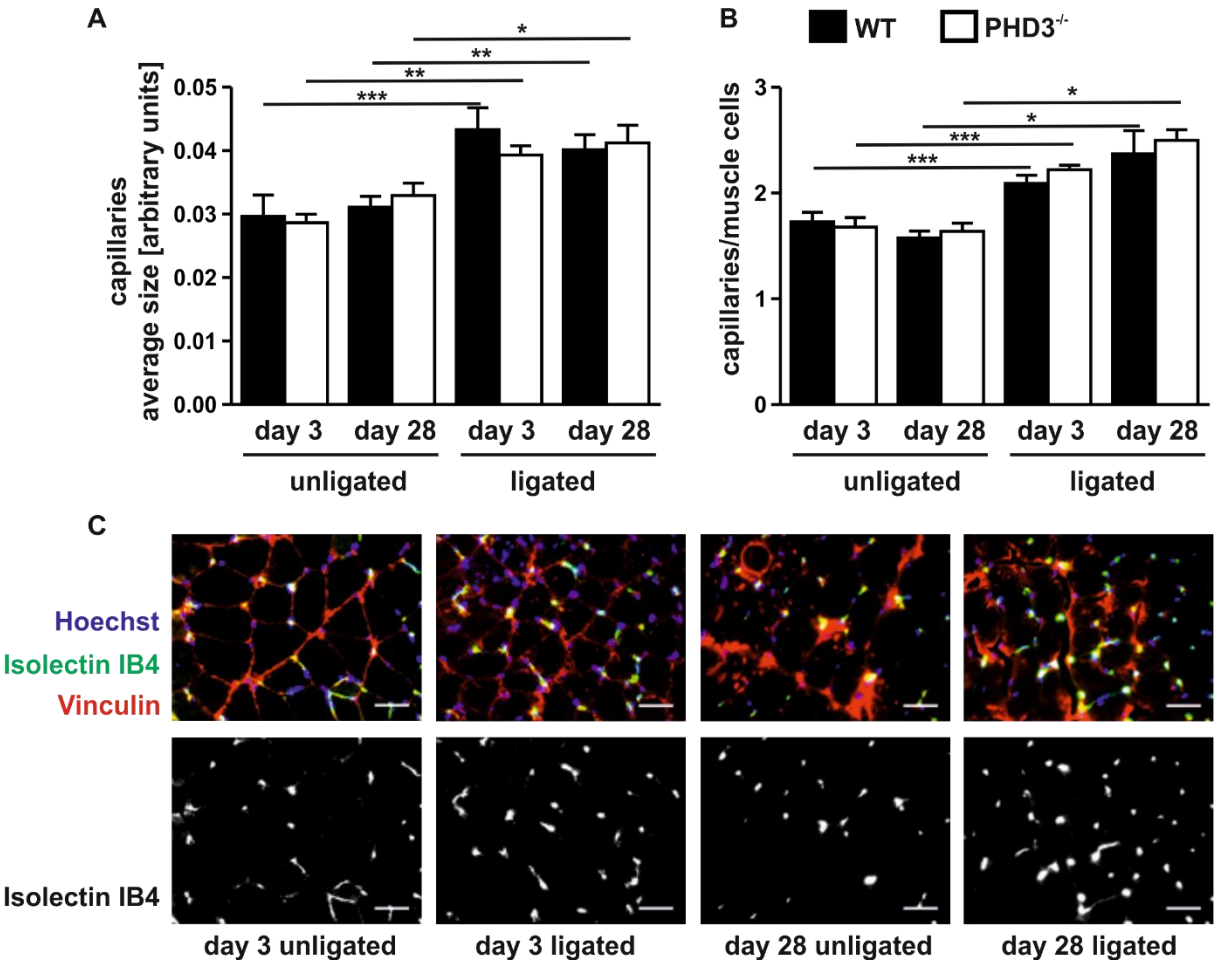

Figure 14: Angiogenesis in PHD3$^{-/-}$ mice after hind limb ischemia. Angiogenesis was analyzed on cryosections of the gastrocnemicus muscle (GM) 3 and 28 days after hind limb ischemia surgery in unligated and ligated legs. Average size (A) and capillary number per muscle cells (B) were analyzed using ImageJ. Groups include for day 3 wild type = 5, PHD3$^{-/-}$ = 7 mice and for day 28 7 mice per group. Bars present mean ± SEM, * p<0.05, ** p<0.01, *** p<0,001. Exemplary images of stained sections on day 3 and 28 for the unligated and ligated leg are displayed in (C). Capillaries are visualized by Isolectin IB4, while muscle cells were detected with an antibody against vinculin and cell nuclei were stained with Hoechst. Scale bars represent 50 µm.

In conclusion, no differences towards angiogenic effects were observed between wild type and PHD3$^{-/-}$ mice. This finding is in line with the above shown perfusion data.

3.6 Fibrotic processes are inhibited in PHD3$^{-/-}$ mice while motor function is unaltered after hind limb ischemia

The course of a sterile inflammation can influence processes like wound healing strongly. Fibrosis, which is characterized by an excessive production of extracellular matrix proteins by activated fibroblasts, can be the result of a prolonged inflammatory reaction of the tissue. Also, the effectiveness of wound healing can have a direct influence on organ performance, in case of the leg for example in running performance.

In order to test, whether the decreased inflammatory reaction towards hind limb ischemia in PHD3$^{-/-}$ mice influences the restoration of tissue homeostasis and development of fibrosis,

mice underwent hind limb ischemia and were examined until day 28 towards impairment of their motor function. At day 28, GM were extracted and the amount of fibrosis was quantified via picro-sirius red staining on tissue sections.

Quantification of picro-sirius red-positive area on tissue sections of ligated and unligated legs revealed a higher content of fibrotic tissue in wild type mice compared to PHD3$^{-/-}$ (Figure 15A, B). GM of ligated legs from PHD3$^{-/-}$ mice showed only a mild increase in comparison to the unligated leg. This suggests that fibrotic processes are inhibited in PHD3$^{-/-}$ mice.

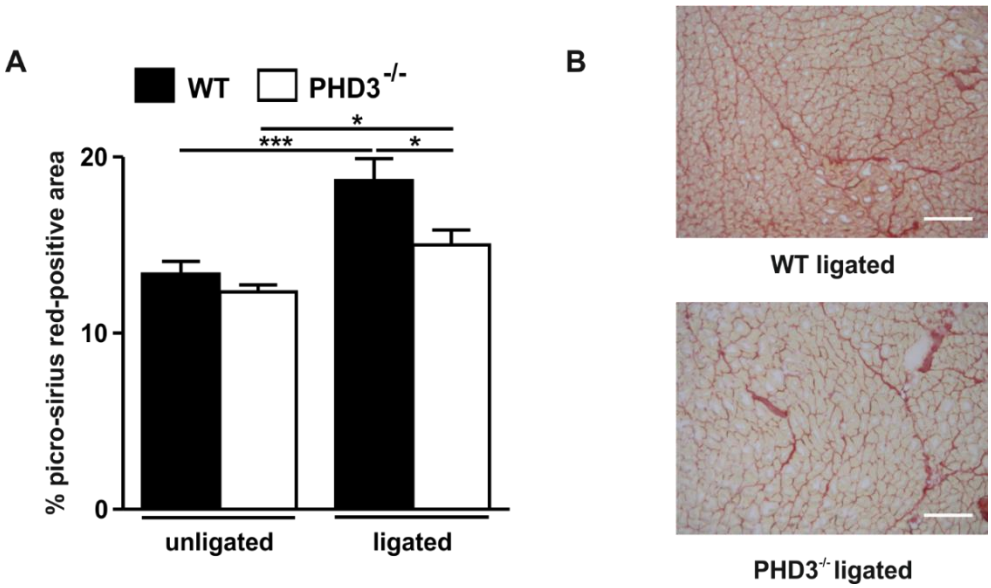

Figure 15: Fibrosis quantification on tissue sections of PHD3$^{-/-}$ mice. Fibrosis was quantified via picro-sirius red staining of hind limb muscles 28 days after surgery. (A) Sections of 3 different areas of the hind limb muscle were stained with picro-sirius red and the whole tissue section was imaged in a 20x magnification. Quantification of the picro-sirius red area per tissue region was performed using ImageJ. Groups of 7 wild type and 7 PHD3$^{-/-}$ mice were analyzed. Bars show mean ± SEM, * $p<0.05$ *** $p<0.001$. (B) Exemplary pictures of a wild type and a PHD3$^{-/-}$ ligated hind limb muscle in 20x magnification. Scale bar represents 200 µm.

Motor function in mice was assessed in order to see whether the change in the course of inflammation impacts on a clinical parameter such as the ability to move the leg and foot after surgery. Mice were graded according to a grading system adapted from (Rishi et al., 2015). In detail, the ability to move the limb was graded in 5 scores: 5 for no impairment, 4 for mice who frequently adopted a relieving posture, 3 for mice that made a claw, 2 for mice that could not move the foot, 1 for mice that could not move the whole limb. The grading was performed during the first week after surgery (Figure 16). In most mice, impairment was only clearly visible within the first days after surgery. Until day 7, all mice had recovered their abilities to move their foot to a degree where no impairment was visible anymore. Overall, no differences were observed in the motor function scores of wild type and PHD3$^{-/-}$ mice.

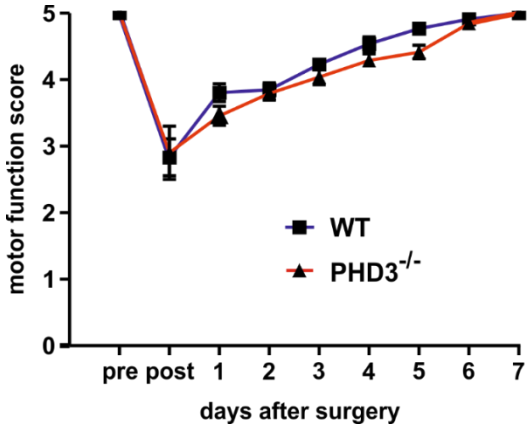

Figure 16: Motor function after surgery analyzed via a grading system. Motor function was analyzed via a grading system (5=no impairment, 4=relieving posture, 3=making a claw, 2=not able to move the foot, 1=not able to move the limb) within the first 7 days after hind limb ischemia surgery. Groups include wild type=13 and PHD3$^{-/-}$=12 mice. Graph shows mean ± SEM.

Motor function was additionally determined using a RotaRod system (Figure 17). Performance was measured before and up to 27 days after surgery. Mice showed a mild drop of performance, measured as maximum speed, 2 days after the surgery, from which they partially recovered. Until day 28, the performance of mice decreased slightly. In order to see whether this was caused by the surgery or just an aging or learning effect, a resting age and gender-matched group of mice underwent the same setup until day 21. Control mice performed significantly better on day 14 and 21 compared to wild type (only day 14) or PHD3$^{-/-}$ mice, which indicates that the decrease of performance is indeed due to the surgery. There was no significant difference between wild type and PHD3$^{-/-}$ mice at any of the time points. However, the individual performances, partially influenced by mouse behavior, strongly varied within wild type and PHD3$^{-/-}$ groups.

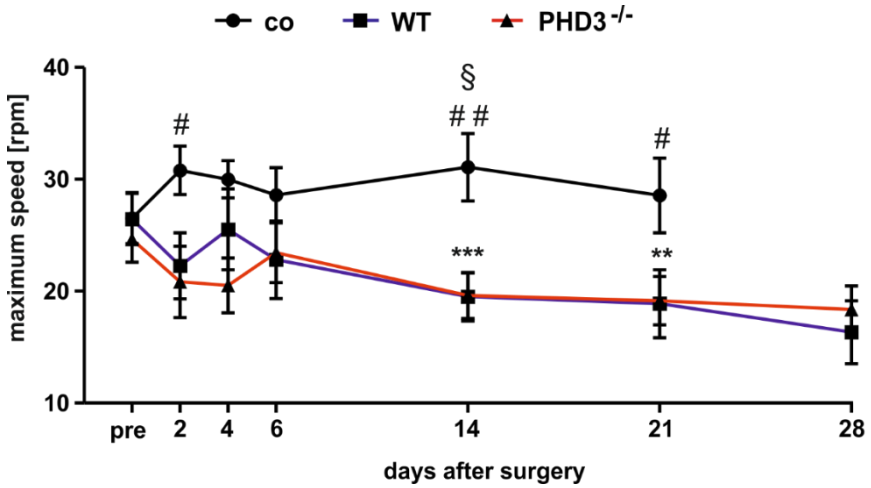

Figure 17: Motor function after surgery analyzed via a running test. Motor function was analyzed via the maximum speed mice ran on a RotaRod. Analysis includes co=5 (resting control mice), wild type=7 and PHD3$^{-/-}$=7 mice. Graph shows mean ± SEM, */#/§ p<0.05; **/##/§§ p<0.01; ***/###/§§§p<0.001. * shows significance between wild type pre value and the value of the respective day. § shows significance between the control group and wild type group at the respective day. # shows significance between the control group and PHD3$^{-/-}$ group at the respective day.

In summary, the absence of a difference in motor function between wild type and PHD3$^{-/-}$ groups could either be the result of high variation between the mice or by a rather mild effect on wound healing which did not translate into a detectable better outcome of running performance.

3.7 Analysis of cell death and migration in PHD3$^{-/-}$ macrophages

The observed blunted inflammatory reaction of macrophages in PHD3$^{-/-}$ mice after hind limb ischemia surgery could be caused by a differential behavior of the macrophages. I hypothesized that it could be either caused by a migratory phenotype that impairs their further migration into the tissue at later days, or by an apoptosis phenotype.

In a previous study (Swain et al., 2014), the group of Cardiovascular Physiology could show that under stress conditions such as serum deprivation and treatment with pro-apoptotic factors, PHD3$^{-/-}$ BMDM are protected against apoptosis. In order to investigate apoptosis and cell death of tissue macrophages after hind limb ischemia, lysates of hind limb muscles underwent flow cytometric analysis to characterize the macrophage population (Figure 18A). The lysates were stained with a live-dead marker (Zombie green) and Annexin V, which identifies apoptotic cells (Figure 18B). Within the macrophage population, the intensities for Zombie green and Annexin V were analyzed to differentiate between living, early and late apoptotic as well as dead cells according to their staining. In total, there was no difference in the relative amount of living, early apoptotic, late apoptotic or dead cells between wild type and PHD3$^{-/-}$ samples (Figure 18C), suggesting that cell death of macrophages is not involved in the blunted inflammation after hind limb ischemia surgery.

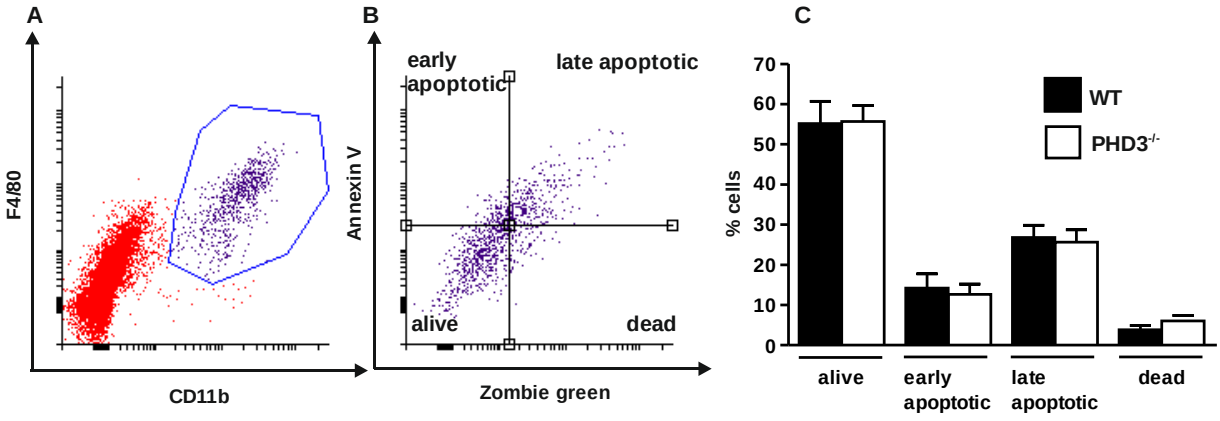

Figure 18: Apoptosis rates in PHD3$^{-/-}$ macrophages isolated from the gastrocnemicus muscle. Cell death was analyzed within the macrophage population on day 4 after surgery. (A) Macrophages were identified according to their F4/80 and CD11b expression. (B) Gating strategy for identifying dead (Annexin V^{-} Zombie green^{high}), late apoptotic (Annexin V^{+} Zombie green^{high}), early apoptotic (Annexin V^{+} Zombie green^{low}) and living cells (Annexin V^{-} Zombie green^{low}). Gates were set using FMO (fluorescence minus one) controls. (C) Analysis of macrophage population of wild type and PHD3$^{-/-}$ mice, differentiating between live, early and late apoptotic and dead cells. Bars represent mean ± SEM. The groups represent wild type=6, PHD3$^{-/-}$=8 mice.

In order to test migration as a potential cause for a change in inflammation, peritoneal macrophages (PM) as well as BMDMs from wild type and PHD3$^{-/-}$ mice were studied. Cells were seeded at a low density and pictures were taken every 10 min for a period of 6 hrs. The average accumulated distance that the cells covered during this time was measured via ImageJ. During this time, cells were either kept in normal culture medium (FCS) or in MDA-MB231-conditioned medium, which serves as a migratory stimulus. No difference in migration was observed between wild type and PHD3$^{-/-}$ cells neither in normal culture medium nor in MDA-MB231-conditioned medium (Figure 19).

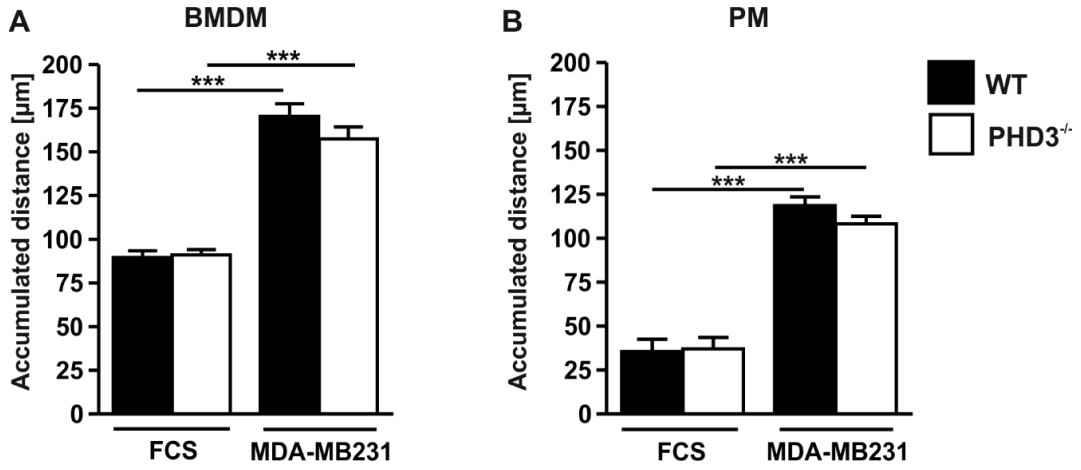

Figure 19: Cell migration in wild type and PHD3$^{-/-}$ BMDM and PM. Migration of BMDM (A) and peritoneal macrophages (PM, B) was analyzed using a single cell migration assay. Images were made every 10 min over a time period of 6 hrs and accumulated distance was calculated using ImageJ. During the time of image acquisition, cells were kept in normoxia, either in normal culture medium (FCS) or in MDA-MB231-conditioned medium to stimulate migration. Results are representative for 3 independent experiments. Bars show mean ± SEM, *** p<0.001.

In summary, both apoptosis and migration do not seem to mediate the blunted macrophage inflammatory reaction in PHD3$^{-/-}$ mice.

3.8 RNA sequencing of sorted macrophages reveal 10 differentially regulated genes between PHD3$^{-/-}$ and wild type mice

Previous data from an unbiased transcriptome screen in BMDM from PHD3$^{-/-}$ and wild type control mice could not show any differentially regulated genes when cells were cultured in culture medium in normoxia or hypoxia for 48 hrs (Swain et al., 2014). As BMDM are a limited model to study macrophage behavior in ischemic inflammatory situations like hind limb ischemia, I decided to isolate macrophages from hind limb muscles after hind limb ischemia surgery. As the peak of the inflammation on day 4 showed a high standard deviation (Figure 9), I chose to isolate macrophages from the tissue on day 5 after the surgery, where the individual differences in inflammation are less prominent in both wild type and PHD3$^{-/-}$ mice. In order to do this, I sorted F4/80^{+} CD11b^{+} macrophages from tissue

lysates and isolated RNA for sequencing, which was performed with the help of the transcriptome analysis lab (TAL, UMG Göttingen).

Between 5000 and 50000 macrophages were successfully isolated from each muscle (Figure 20).

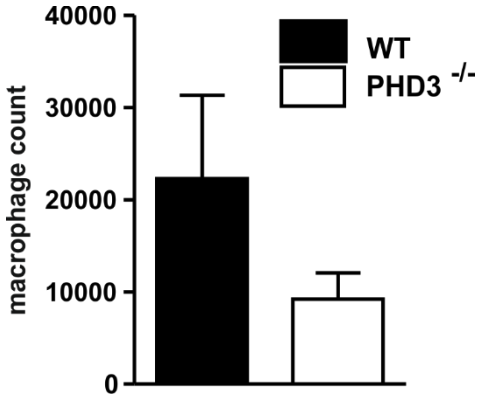

Figure 20: Macrophage count of samples used for RNA sequencing. Macrophages were sorted from the gastrocnemicus muscle (GM) 5 days after surgery. In total, sorted macrophages from 5 wild type and 5 PHD3$^{-/-}$ mice were used. Graph displays mean ± SEM.

Due to the low amount of macrophages, a DNase treatment of the isolated RNA was not possible prior to cDNA library preparation. This caused a considerable DNA contamination within the samples that might have influenced the outcome of this experiment. In addition, 2 of the samples handed in showed a high contamination rate with bacterial and viral DNA. Both samples were excluded from the analysis resulting in the comparison of 3 wild type and 5 PHD3$^{-/-}$ samples. In total, 10 candidate genes were successfully identified to be significantly regulated between wild type and PHD3$^{-/-}$ macrophages.

Among the significantly regulated genes there are 4 that are upregulated (Figure 21): Lysozyme 1, miR-511, the Ensembl gene ENSMUSG00000063254 as well as RNA binding motif protein 4 (Rbm4). The microRNA miR-511 was recently associated with anti-inflammatory properties in a mouse model of septic shock (Puimege et al., 2015). Rbm4 can form a complex with Argonaute-2 and specifically degrade mRNA of IL-6 and TNF-α (Brudecki et al., 2013). An upregulation of Rbm4 could therefore potentially lead to less IL-6 or TNF-α mRNA. However, both IL-6 and TNF-α mRNAs were not downregulated in our screen. ENSMUSG00000063254 is a transcript for which no function has been described yet.

In total, 6 genes were found to be significantly downregulated in this screen. Among those identified is Lysozyme 2, which could be explained by the knock out strategy of the PHD3$^{-/-}$ mice that express cre recombinase under the control of the Lysozyme 2 (also called Lysozyme M) promoter. This could interfere with endogenous Lysozyme 2 expression and additionally explain the upregulation of Lysozyme 1 as a compensatory mechanism of the

macrophages to retain enough Lysozyme. Other downregulated genes include pleckstrin homology like domain family A member 3 (Phlda3), Collagen type 8 alpha 1, the predicted genes GM23153 and GM22567 as well as Cytochrome P450 family 2 subfamily S member 1 (Cyp2s1). Among these candidates, the only one directly associated with inflammation is Cyp2s1. This cytochrome P450 epoxygenase was found to be highly expressed in pro-inflammatory M1-macrophages and in inflammatory settings such as atherosclerosis (Fromel et al., 2013). The biologic function of Cyp2s1 has been described to be catalyzing the reaction of prostaglandin G2 and H2 (PG2, PH2) to 12-Hydroxyheptadecatrenoic acid (12-HHT). PGG2 and PGH2 can also serve as substrates for prostaglandin E2 (PGE2)-production. PGE2 is a potent inflammatory regulator which has been shown to induce M2-polarization in macrophages and inhibit the NLRP3 inflammasome (Sokolowska et al., 2015; Strassmann et al., 1994).

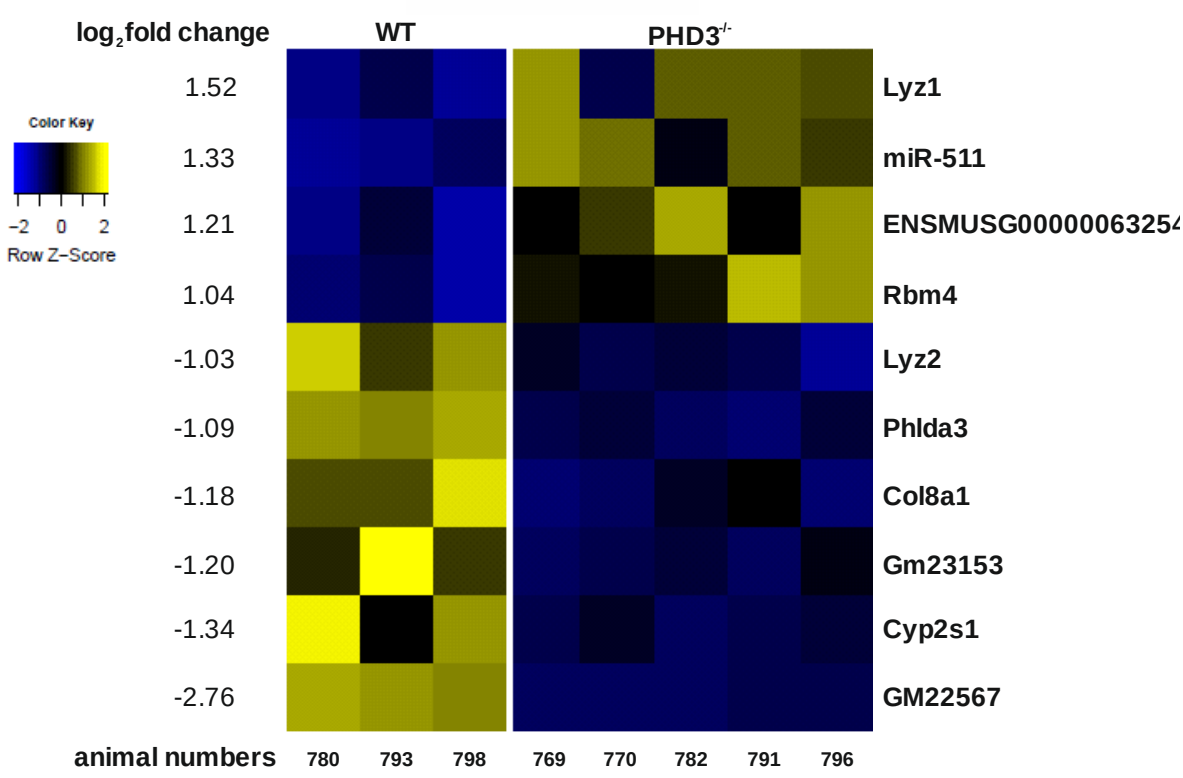

Figure 21: Heatmap of a RNA sequencing screen using macrophages sorted from the hind limb tissue 5 days after surgery. Macrophages from 3 wild type and 5 PHD3$^{-/-}$ mice were analyzed. The heatmap displays the genes that were differentially regulated with a $\log_2$ fold change of ±1 in PHD3$^{-/-}$ macrophages compared to wild type.

To conclude, the RNA sequencing underwent some technical difficulties, however also provided 10 significantly regulated genes. Out of those, especially miR-511, as well as Rbm4 and Cyp2s1 present promising targets.

To confirm the differential expression of the regulated genes for miR-511, Cyp2s1 and Rbm4, RNA was isolated from macrophages of an independent set of wild type and PHD3$^{-/-}$ mice 5 days after hind limb ischemia surgery. The expression of Rbm4, Cyp2s1 and PHD3

was studied via qRT-PCR (Figure 22). miR-511 has two mature sequences, miR-511-3p and 5p. The expression of both of them was analyzed via qRT-PCR as well.

The miR-511 sequences miR-511-3p and miR-511-5p were found to be equally- though in the case of miR-511-5p not significantly- upregulated which confirms the upregulation observed in the RNA sequencing analysis. Cyp2s1 showed a distinct but not significant downregulation in PHD3$^{-/-}$ macrophages compared to wild type cells which was also in line with the RNA sequencing analysis. PHD3 was also less expressed in PHD3$^{-/-}$ compared to wild type macrophages though not in a significant way. Rbm4, which was significantly upregulated in the RNA sequencing results, was slightly downregulated in this experiment.

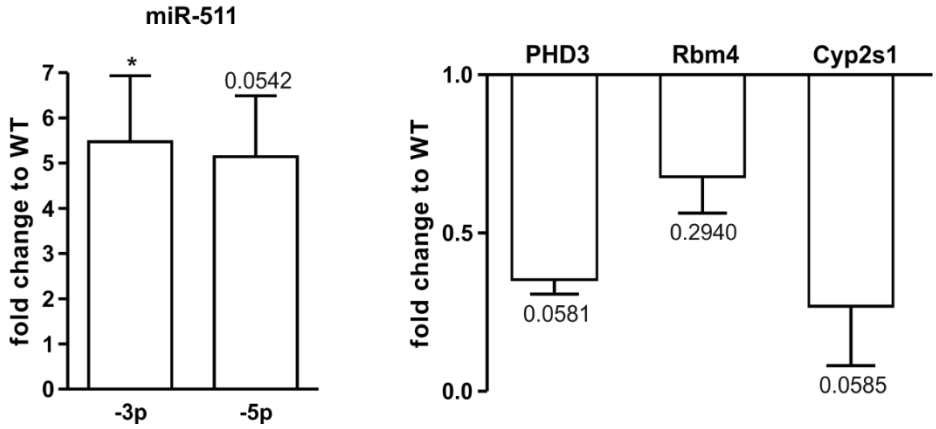

Figure 22: Confirmation of the RNA sequencing results in macrophages sorted from the gastrocnemicus muscle 5 days after hind limb ischemia. Macrophages from n=4 wild type and PHD3$^{-/-}$ mice were sorted and RNA expression of miR-511-3p and miR-511-5p was analyzed via qRT-PCR. RNA expression was normalized to the house-keeper U6 snRNA. Macrophages from n=5 wild type and n=4 PHD3$^{-/-}$ mice were sorted and RNA expression of Rbm4, PHD3 and Cyp2s1 was analyzed via qRT-PCR. The RNA expression was normalized to the house-keeping gene S12. Graphs show mean ± SEM, * $p<0.05$, p-values higher than 0.05 are indicated.

In summary, both miR-511 and Cyp2s1 expression showed marked though not significant regulation, which confirms the RNA sequencing results. PHD3 was non-significantly downregulated which was already the case in the RNA sequencing. The RNA sequencing result of Rbm4 could however not be confirmed. To see whether these results could also be reproduced in cell culture, the expression of miR-511 and Cyp2s1 were additionally studied in BMDM.

3.9 miR-511 expression and TNF-R1 levels in macrophages

miR-511 is one of the 10 significantly regulated genes in PHD3$^{-/-}$ macrophages identified by a RNA sequencing approach. miR-511 has previously been shown to downregulate TNF-R1 expression (Puimege et al., 2015), which decreased the inflammatory reaction in a model of septic shock. I hypothesized that miR-511 upregulation could mediate a similar phenotype in PHD3$^{-/-}$ macrophages, potentially causing the decrease in inflammation observed after hind limb ischemia. As miR-511 has been shown to be transcriptionally regulated by the glucocorticoid receptor (GR), I additionally treated BMDM with dexamethasone, a steroid which can bind the GR, in order to stimulate miR-511 expression.

I tested TNF-R1 expression on macrophages isolated from hind limb muscles 4 days after hind limb ischemia surgery (Figure 23A). I observed a slight but not significant decrease of TNF-R1 expression on PHD3$^{-/-}$ macrophages compared to cells isolated from wild type littermates. In order to see whether this was a general effect, expression of the TNF-R isoform TNF-R2 was tested as well (Figure 23B). TNF-R2 levels also slightly decreased, although this protein has not been reported to be a miR-511 target.

I next tested miR-511 expression in BMDM to see whether I could confirm a differential expression of it in a cell culture model (Figure 23C and D). As normal culture conditions did not reveal any changes in expression between wild type and PHD3$^{-/-}$ BMDM in a previous transcriptome screen (Swain et al., 2014), I cultured the cells in normal and in starvation medium in normoxia as well as hypoxia, to mimic the *in vivo* ischemic conditions. Additionally, I treated cells with dexamethasone to increase miR-511 transcription. However, none of the tested conditions revealed a significant upregulation of miR-511-3p or -5p, the two mature sequences of miR-511 in PHD3$^{-/-}$ BMDM.

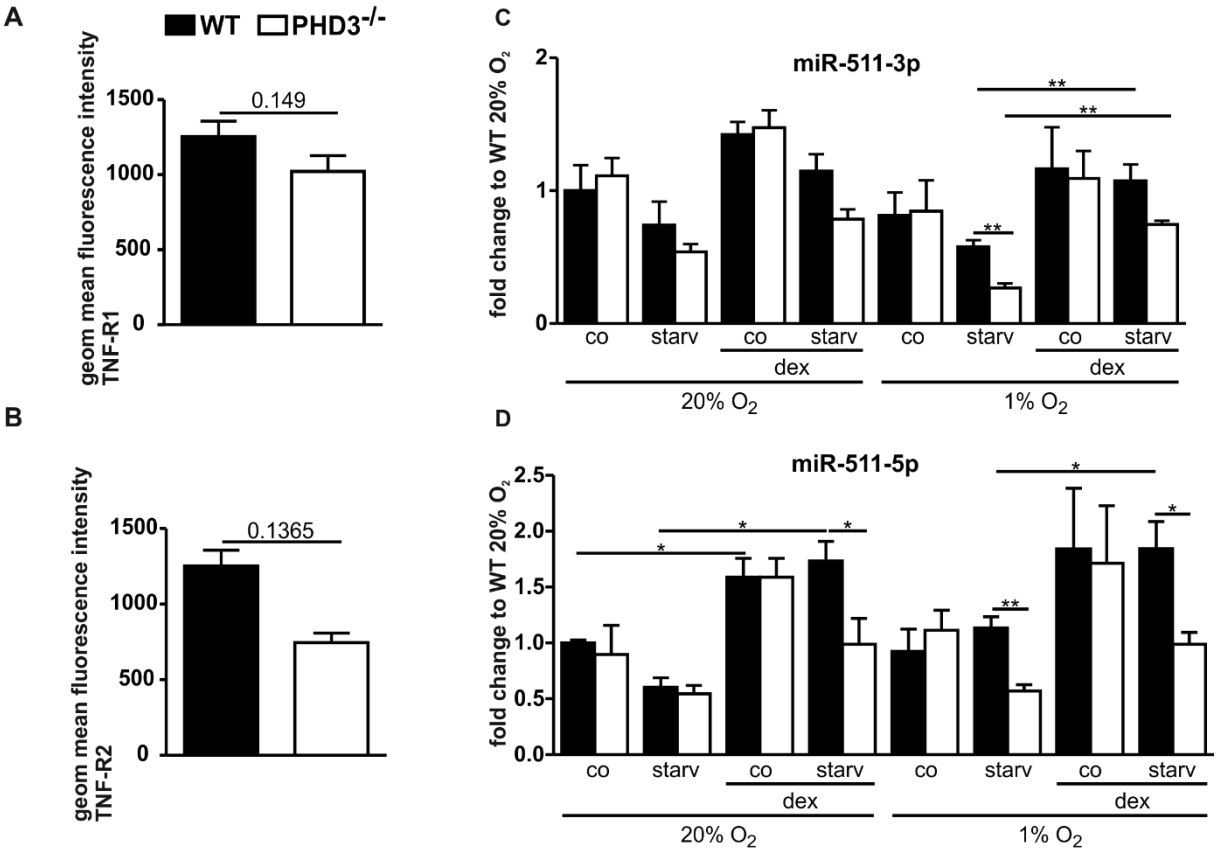

Figure 23: TNF-R1 and miR-511 expression in PHD3$^{-/-}$ macrophages. Flow cytometric analysis of TNF-R1 (A) or TNF-R2 (B) expression in the F4/80^{+} CD11b^{+} macrophage population isolated from the GM 4 days after surgery. The experiment includes wild type=8 and PHD3$^{-/-}$=8 mice. Graphs represent the geometric mean fluorescence intensity for each marker as mean ± SEM. Expression analysis via qRT-PCR of the two mature miR-511 sequences miR-511-3p (C) and -5p (D) in BMDM. Cells were cultured for 24 hrs in normoxia (20% O_2) or hypoxia (1% O_2) in normal culture medium (co) or in starvation medium (starv). Dexamethasone was added in a final concentration of 10^{-7} M for 18 hrs. Bars show mean ± SEM, * $p<0.05$, ** $p<0.01$. Experiment is representable for three independent experiments.

In conclusion, a differential regulation of miR-511 could not be mimicked *in vitro*, and TNF-R1 expression on macrophages *in vivo* did not reveal any significant difference which indicates that there is no relevant influence of miR-511 on the inflammatory reaction, at least not via TNF-R1.

3.10 Cyp2s1 expression is downregulated in PHD3$^{-/-}$ BMDM

Cyp2s1 is one of the candidates of the RNA sequencing which was significantly downregulated in PHD3$^{-/-}$ macrophages sorted from the ischemic tissue. The function of Cyp2s1 is only partially understood. In macrophages, Cyp2s1 is responsible for catalyzing the reaction of prostaglandin G2 and H2 to 12-HHT (Fromel et al., 2013), an agonist for the leukotriene B4 receptor 2 (BLT2) (Liu et al., 2014). Apart from that, Cyp2s1 is highly inducible by pro-inflammatory cytokines such as IFN-ɣ and LPS, which is why it is proclaimed as a marker for pro-inflammatory macrophages.

As the RNA sequencing data suggested a downregulation of Cyp2s1 in PHD3$^{-/-}$ macrophages, I analyzed in BMDM whether Cyp2s1 was indeed downregulated on RNA level and whether this coincided with an anti-inflammatory phenotype based on the expression of pro-inflammatory cytokines such as TNF-α, IL-6 and IL-12b (Figure 24). In order to mimic the ischemic situation after hind limb ischemia *in vitro*, I cultivated BMDM for 24 hrs in normoxia or hypoxia in normal culture medium or starvation medium. Cyp2s1 was significantly downregulated in hypoxia combined with starvation, however, the expression of pro-inflammatory cytokines did not indicate a different polarization between wild type and PHD3$^{-/-}$ BMDM in these conditions.

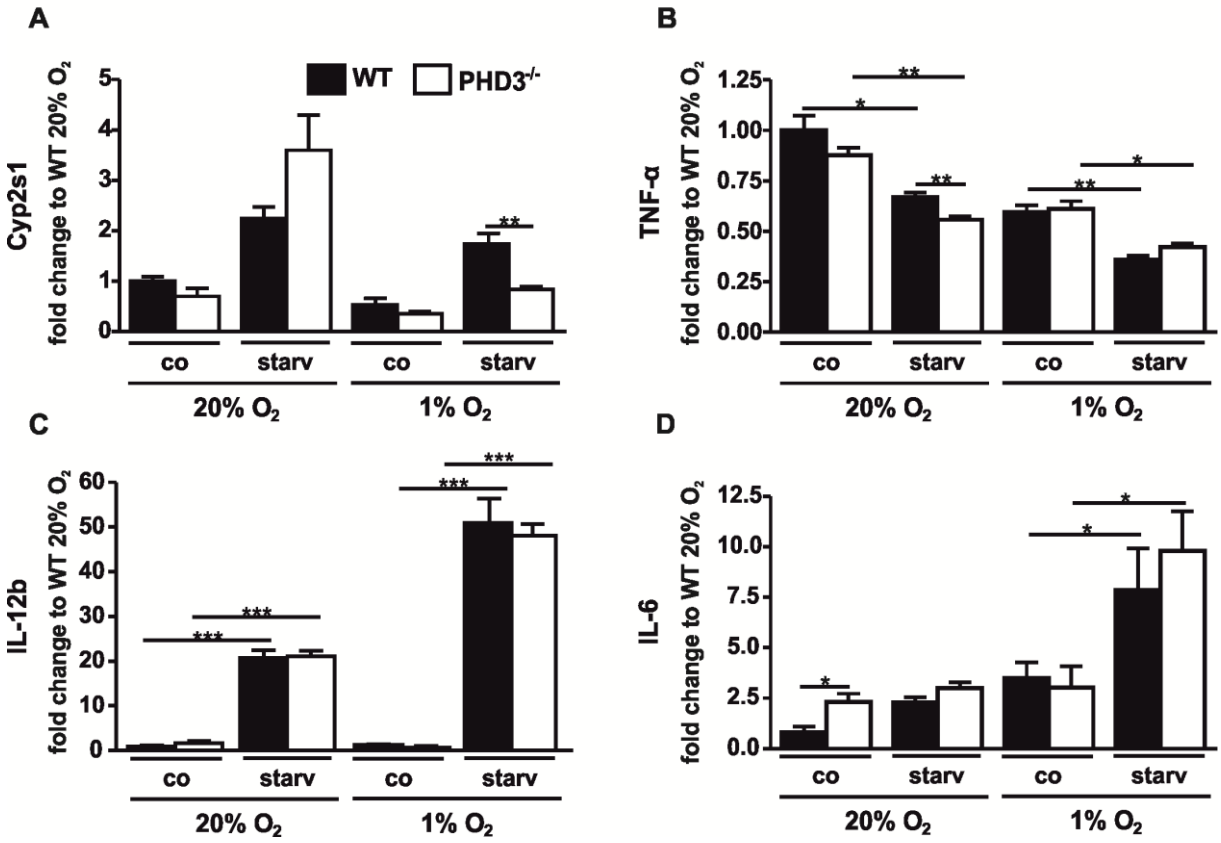

Figure 24: Cyp2s1 is downregulated in PHD3$^{-/-}$ BMDM. The RNA expression of Cyp2s1 (A), TNF-α (B), IL-12b (C) and IL-6 (D) was analyzed via qRT-PCR. Cells were either incubated for 24 hrs in normoxia (1% O_2) or hypoxia (20% O_2) and either in normal culture conditions (co) or in starvation medium (starv) for 24 hrs. Values were normalized to the wild type 20% O_2 control sample. Bars show the mean ± SEM with * p<0.05, ** p<0.01, *** p<0.001. Graphs are representative for n=3 independent experiments.

In summary, the downregulation of Cyp2s1 in sorted PHD3$^{-/-}$ macrophages identified in a RNA sequencing could be mimicked in PHD3$^{-/-}$ BMDM when cultured in starvation medium in hypoxia. However, this downregulation was not an indicator for a downregulation of pro-inflammatory M1-markers such as TNF-α, IL-6 and IL-12b.

3.11 Prostaglandin E2 secretion is upregulated in PHD3$^{-/-}$ BMDM

Cyp2s1 utilizes prostaglandin (PG) G2 and H2 as substrates for 12-HHT production. PGG2 and PGH2 also serve as a substrate for PGE2 synthesis. By spending the starting material for PGE2 synthesis for 12-HHT synthesis, Cyp2s1 could potentially be able to limit PGE2 synthesis. PGE2 is a potent mediator of inflammation, which can prime macrophages towards M2-poarization (Strassmann et al., 1994). The observed downregulation of Cyp2s1 in PHD3$^{-/-}$ macrophages might therefore lead to increased PGE2 levels, as more substrates are present for PGE2 synthesis.

I therefore tested PGE2 secretion by performing an ELISA on cell culture supernatants of PHD3$^{-/-}$ and wild type BMDM cultivated in hypoxia in normal or starvation medium (Figure 25). While there was no apparent difference in normal culture medium, PHD3$^{-/-}$ BMDM secreted significantly more PGE2 compared to wild type BMDM when incubated in starvation medium.

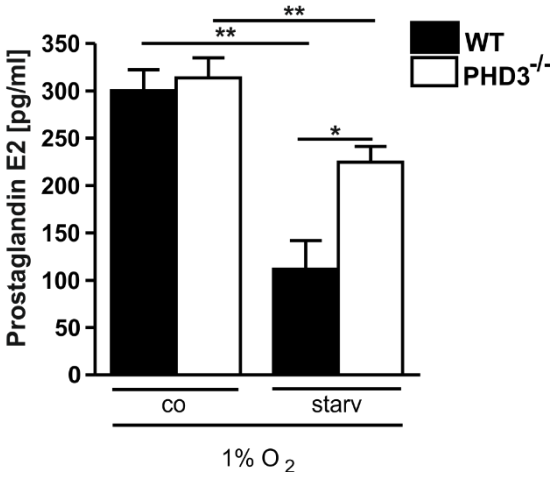

Figure 25: Prostaglandin E2 (PGE2) secretion is upregulated in PHD3$^{-/-}$ BMDM. PGE2 levels were measured with an ELISA in the supernatant of PHD3$^{-/-}$ and wild type BMDM incubated in hypoxia (24 hrs) in normal culture medium (co) or in starvation medium (starv). The displayed results are representative for n=3 experiments. Bars show mean ± SEM with * p<0.05, **<0.01.

The increased PGE2 secretion of PHD3$^{-/-}$ BMDM in hypoxia and starvation correlates with the downregulated Cyp2s1 expression observed in these culture conditions. While Cyp2s1 was not regulated in hypoxia in normal culture medium, PGE2 secretion was also not altered. Increased PGE2 secretion could be a possible explanation for the blunted inflammatory reaction of macrophages after hind limb ischemia, as Cyp2s1 levels were also found to be significantly downregulated in isolated macrophages from hind limb muscles.

3.12 Phagocytosis in enhanced in PHD3$^{-/-}$ BMDM

As downregulation of Cyp2s1 has been described to induce an increase in phagocytotic capacity of macrophages (Fromel et al., 2013), I next analyzed whether the phagocytotic

capacity was differentially regulated between wild type and PHD3$^{-/-}$ BMDM in the different culture conditions. In addition, I studied whether the addition of 100 pg/ml PGE2 could increase phagocytosis. This concentration was chosen as it reflects the difference in PGE2 secretion between wild type and PHD3$^{-/-}$ BMDM in starvation and hypoxia.

BMDMs were cultivated normal culture medium or starvation medium in normoxia or hypoxia for 24 hrs (Figure 26). Treatment with PGE2 was performed for 18 hrs. The macrophages were treated with latex beads for 4 hrs, which emitted fluorescence upon phagocytosis. The percentage of phagocytotic macrophages showed no difference in normal culture medium. In starvation medium however, PHD3$^{-/-}$ macrophages showed a higher phagocytosis rate compared to wild type. This effect was independent from incubation in normoxia or hypoxia. Treatment with PGE2 did not change phagocytosis in macrophages cultivated in normal culture medium. In starvation medium, both wild type and PHD3$^{-/-}$ macrophages showed a higher phagocytosis rate upon PGE2 treatment compared to untreated controls. Interestingly, the addition of 100 pg/ml PGE2 to wild type cells in starvation elevated phagocytosis rates to approximately the level of PHD3$^{-/-}$ macrophages without treatment.

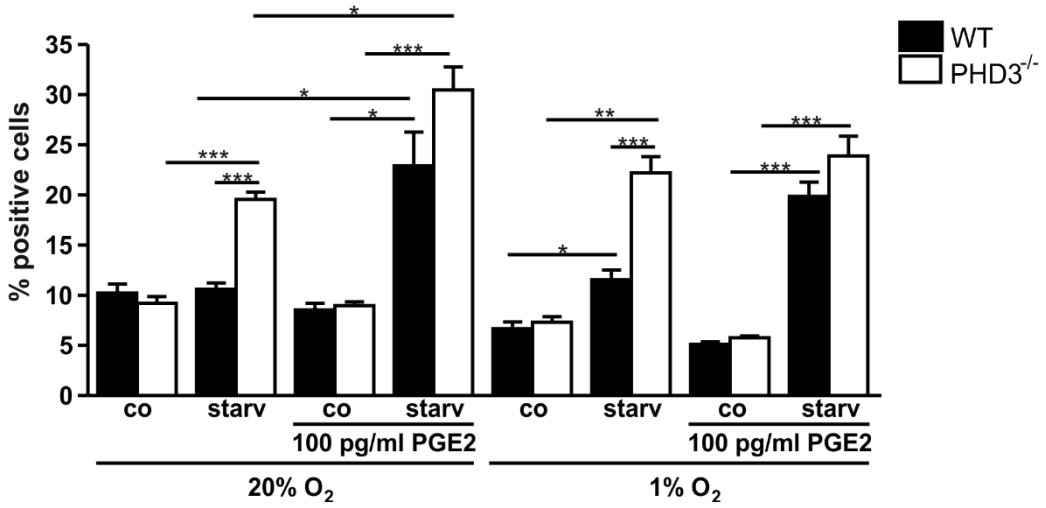

Figure 26: **Phagocytosis is elevated in PHD3$^{-/-}$ macrophages upon starvation.** PHD3$^{-/-}$ and wild type BMDMs were cultivated in starvation (starv) or normal culture medium (co) in hypoxia or normoxia for 24 hrs and treated with PGE2 for 18 hrs. Phagocytotic capacity was measured via flow cytometry based on the uptake of latex beads. The displayed data are representative for two independent experiments. Bars show mean ± SEM with * p<0.05, ** p<0.01, *** p<0.001.

This data suggest that a differential PGE2 secretion might mediate a change in macrophage behavior, leading to increased phagocytosis rates in PHD3$^{-/-}$ macrophages. Phagocytosis is a vital process for the swift clearance of apoptotic neutrophils and cell debris and therefore for the resolution of sterile inflammation. A more efficient phagocytosis might lessen the recruitment of monocytes from the blood stream to the tissue in the setting of hind limb ischemia. By this mechanism, the decreased inflammatory response of PHD3$^{-/-}$ macrophages after hind limb ischemia surgery might be explained.

3.13 Myeloid-specific conditional knock out mouse model for PHD2

A downregulation of PHD2 shifts macrophage metabolism towards anaerobic glycolysis, which is associated with impaired macrophage migration and phagocytosis *in vitro* (Güntsch et al., in revision). In order to evaluate the effects of PHD2 deficiency in macrophages *in vivo*, mice with a myeloid-specific conditional knock out of PHD2 were studied.

Mice with a heterozygous expression of cre recombinase under the control of lysozyme M promoter (LysMcre$^{+/-}$) were crossed with mice that had a floxed PHD2 gene (PHD2$^{flox/flox}$, Figure 27B). This led to excision of exon 2 and 3 in cells expressing lysozyme M in LysMcre$^{+/-}$xPHD2$^{flox/flox}$ mice (called PHD2$^{-/-}$ mice hereafter). Mice expressing the floxed PHD2 gene but no cre recombinase were used as wild type controls (LysMcre$^{-/-}$xPHD2$^{flox/flox}$, called wild type hereafter, Figure 27A). Lysozyme M is mainly expressed in myeloid cells such as macrophages and granulocytes and to a lower degree in dendritic cells (Clausen et al., 1999).

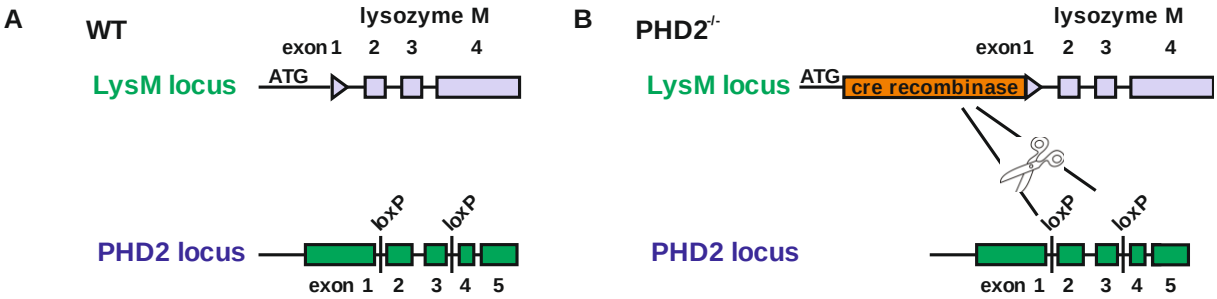

Figure 27: Myeloid-specific conditional knock out of PHD2. Mice expressing cre recombinase under the control of the Lysozyme M promoter were crossed with mice in which exon 2 and 3 of the PHD2 locus were homozygously flanked by loxP sites. In LysMcre$^{+/-}$xPHD2$^{flox/flox}$ mice (B), excision of exon 2 and 3 took place in myeloid cells while LysMcre$^{-/-}$xPHD2$^{flox/flox}$ (A) mice were used as wild type controls.

BMDM of PHD2$^{-/-}$ mice have already been successfully tested for their PHD2 knock out on both RNA and protein level (Güntsch et al., in revision).

3.14 PHD2$^{-/-}$ macrophages show a different inflammatory response after induction of myocardial infarction

Macrophages lacking PHD2 expression show an impairment of essential macrophage functions such as phagocytosis and migration *in vitro* (Güntsch et al., in revision). In order to validate whether this phenomenon would influence the inflammatory reaction caused by ischemia, PHD2$^{-/-}$ mice and their wild type littermates underwent a myocardial infarction caused by the permanent ligation of the left anterior descending coronary artery (hereafter called MI). The following inflammatory response was measured via flow cytometric analysis of heart tissue lysates. Characteristic surface markers were used in order to identify different myeloid populations such as leukocytes (CD11b^{+}), macrophages (F4/80^{+} CD11b^{+}) and neutrophils (Ly6G^{+} CD11b^{+}). Inflammatory cells were studied 3 and 7 days after surgery. In

order to verify that the induced inflammation was not an artefact from the surgery itself, sham-operated mice were included as controls.

Analysis of leukocyte and neutrophil populations after induction of a myocardial infarction did not show any differences between wild type and PHD2$^{-/-}$ mice (Figures 28A and B), neither 3 days nor 7 days after surgery. In general, inflammation was higher at day 3 than at day 7, indicating that the inflammatory reaction is already regressing at the latter time point. Sham-operated mice showed significantly lower levels of CD11b-positive and Ly6G CD11b-positive cells than the ones undergoing MI, which indicates that the inflammatory reaction is mostly caused by the infarction itself.

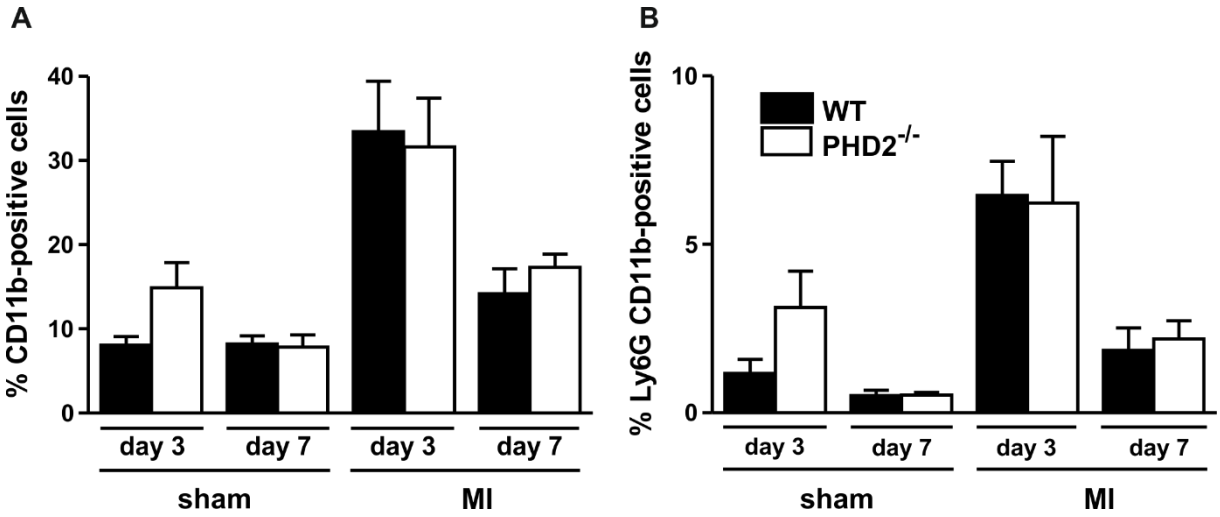

Figure 28: Leukocyte and neutrophil infiltration after myocardial infarction (MI) in PHD2$^{-/-}$ mice. (A) Leukocytes were quantified as CD11b-positive cells within tissue lysates of hearts after sham-operation or induction of MI. (B) Neutrophils were quantified as a subpopulation of leukocytes as Ly6G CD11b-positive cells. Groups include n=5 mice for day 3 and day 7 sham, n=5 for wild type day 3 and day 7 MI and n=7 for PHD2$^{-/-}$ day 3 and 7 MI. Bars show mean ± SEM.

The amount of macrophages within the tissue after MI induction differed significantly between wild type and PHD2$^{-/-}$ mice (Figure 29A). At day 3 after surgery, wild type mice showed higher numbers of macrophages compared to PHD2$^{-/-}$ mice. At day 7 however, the picture changed with PHD2$^{-/-}$ mice showing significantly higher levels of macrophages compared to wild type mice. This indicates a delayed onset of macrophage infiltration into the tissue, which could potentially be explained by the migratory defect of PHD2$^{-/-}$ macrophages, which has been observed *in vitro*.

In addition, the macrophage population was further analyzed towards their polarization into a pro-inflammatory M1 (Figure 25B) or anti-inflammatory M2 phenotype (Figure 29C). CD86 (M1-marker) and CD206 (M2-marker) expressions were analyzed via the mean fluorescence intensity within the macrophage population. No difference in expression of both M1 and M2-marker was observed between wild type and PHD2$^{-/-}$ macrophages at both time points, indicating that macrophages were not differentially polarized.

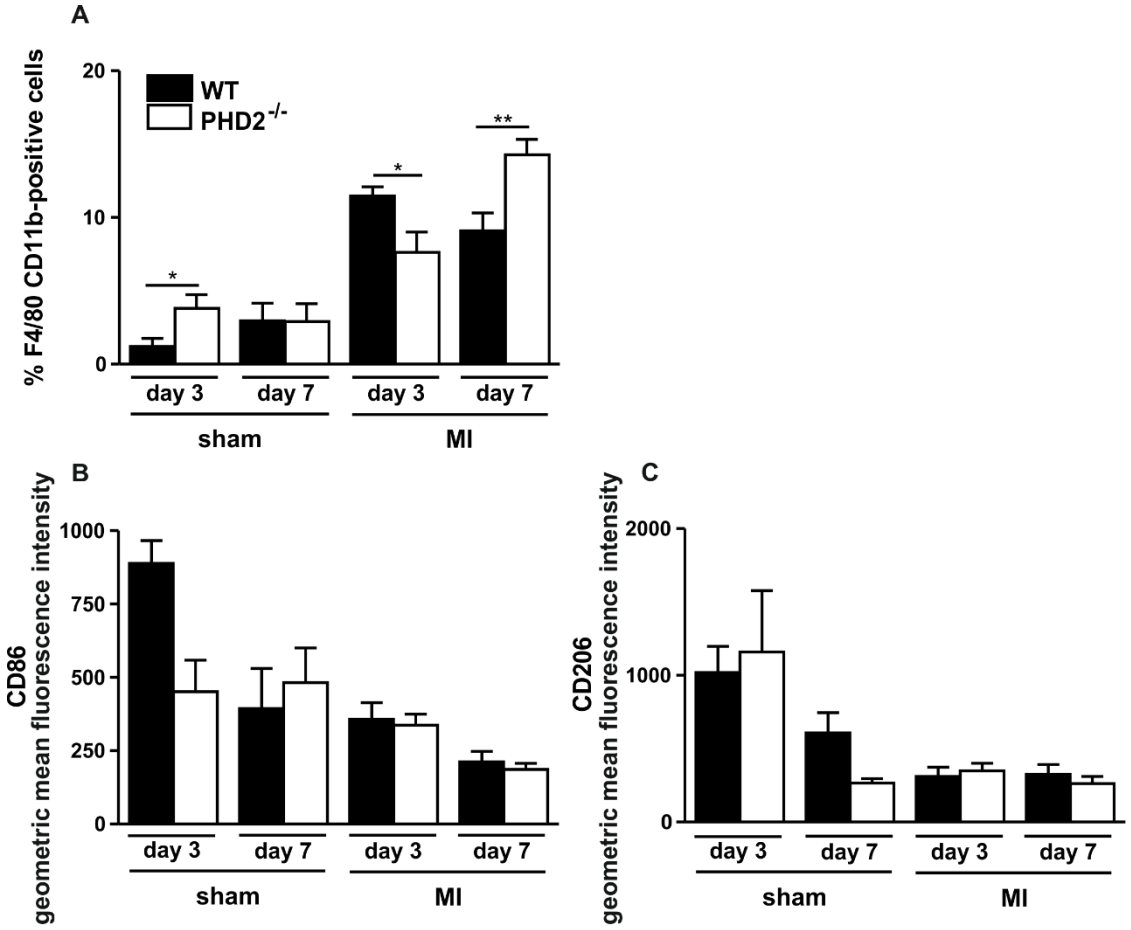

Figure 29: Macrophage infiltration after induction of MI in PHD2$^{-/-}$ mice. (A) Macrophages were identified as F4/80 CD11b-positive cells within tissue lysates of hearts after MI or sham operation. The polarization of macrophages was studied by analyzing the surface expression of CD86 (M1-marker, B) and CD206 (M2-marker, C) within the macrophage population as geometric mean fluorescence intensity. Groups include n=5 mice for day 3 and day 7 sham, n=5 for wild type day 3 and day 7 MI and n=7 for PHD2$^{-/-}$ day 3 and 7 MI. Graphs show mean ± SEM with * p<0.05, ** p<0.01.

In summary, macrophage invasion and clearance from the heart after surgical induction of a myocardial infarction was less in PHD2$^{-/-}$ at day 3 but more at day 7, indicating a delayed onset of macrophage invasion. This could potentially be caused by a migratory defect of PHD2$^{-/-}$ macrophages, which has already been observed *in vitro*. The overall leukocyte population, as well as the neutrophil population did not show any significant changes between wild type and PHD2$^{-/-}$ mice, indicating that this is a macrophage-specific effect. Also, macrophage polarization was unchanged, which goes in line with *in vitro* findings in BMDM, where M1- and M2-markers were not differentially expressed on RNA level (Güntsch et al., in revision).

3.15 PHD2$^{-/-}$ mice have a worse heart function 6 days after MI surgery

In order to analyze whether PHD2$^{-/-}$ mice had an altered clinical outcome after the induction of a myocardial infarction, echocardiography was performed 1 day before and 6 days after surgery. Heart function was analyzed via measuring the fractional area shortening, a parameter describing the change of muscle area during each contraction, and the ejection

fraction, which describes the fraction of the blood which is pumped out of the heart during each heartbeat (Figure 30).

In contrast to sham mice, both wild type and PHD2$^{-/-}$ mice showed a significant decrease of heart function after MI-surgery. Between both groups, PHD2$^{-/-}$ mice showed an even worse heart function than wild type mice. This could be caused by the prolonged inflammatory response of PHD2$^{-/-}$ macrophages.

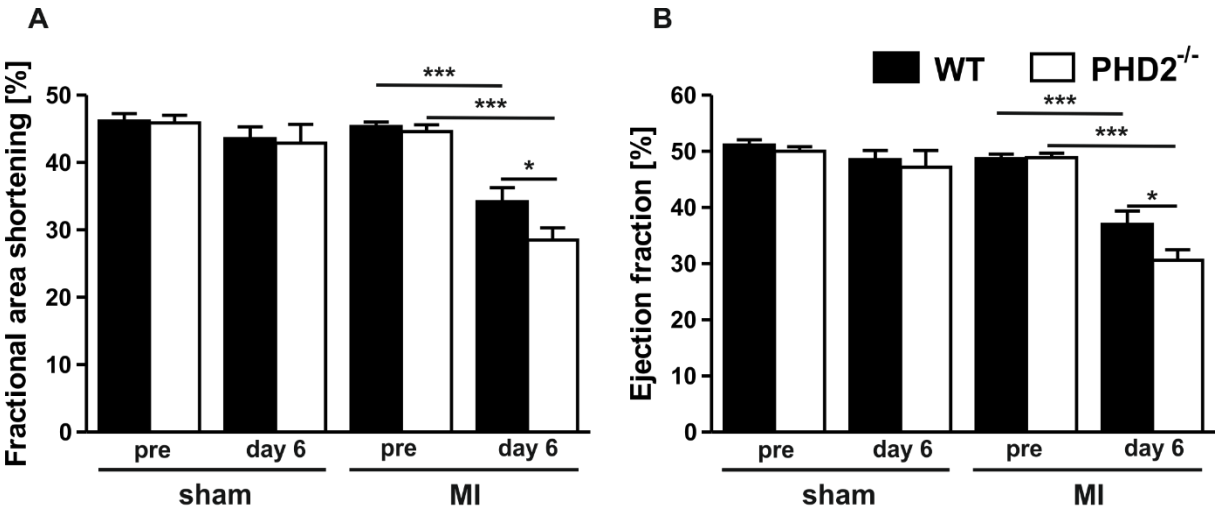

Figure 30: **Heart function in PHD2$^{-/-}$ mice after myocardial infarction.** (A) Fractional area shortening analyzed before and 6 days after surgery in sham operated and MI mice. Groups include n=9 wild type sham mice, n=8 PHD2$^{-/-}$ sham mice, n=15 wild type MI mice and n=16 PHD2$^{-/-}$ MI mice. Graphs display mean ± SEM with * p<0.05, *** p<0.001.

3.16 Initial infarction size after MI surgery is similar between wild type and PHD2$^{-/-}$ mice

In a publication including global haplodeficient PHD2$^{+/-}$ mice, the authors argue that preconditioning of the blood vessels via increased arteriogenesis at baseline would improve the outcome of PHD2$^{+/-}$ mice not only after hind limb ischemia, but also after myocardial infarction (Takeda et al., 2011). The infarction size was therefore analyzed 6 hrs after myocardial infarction (Figure 31) in order to test, whether there would be a difference visible between wild type and PHD2$^{-/-}$ mice already at this early time point.

Hearts were isolated and areas that were still perfused were stained with Evan´s blue. Area which was not stained blue was defined as area at risk (AAR, Figure 31A). Hearts were then stained with TTC, which stained the still viable areas of the AAR in red. The area which could neither be stained by Evan´s blue nor by TTC was defined as area of necrosis (AON).

Analysis of the ratio between AAR and AON did not show any significant changes between wild type and PHD2$^{-/-}$ mice (Figure 31B). Also, the total area at risk was weighed and found not to be significantly different between wild type and PHD2$^{-/-}$ mice (Figure 31D), indicating that the difference in heart function 6 days after surgery is not a product of early effects like

arteriogenic preconditioning, but has to arise later than 6 hrs after surgery, possibly by immunologically regulated processes like the invasion and clearance of macrophages.

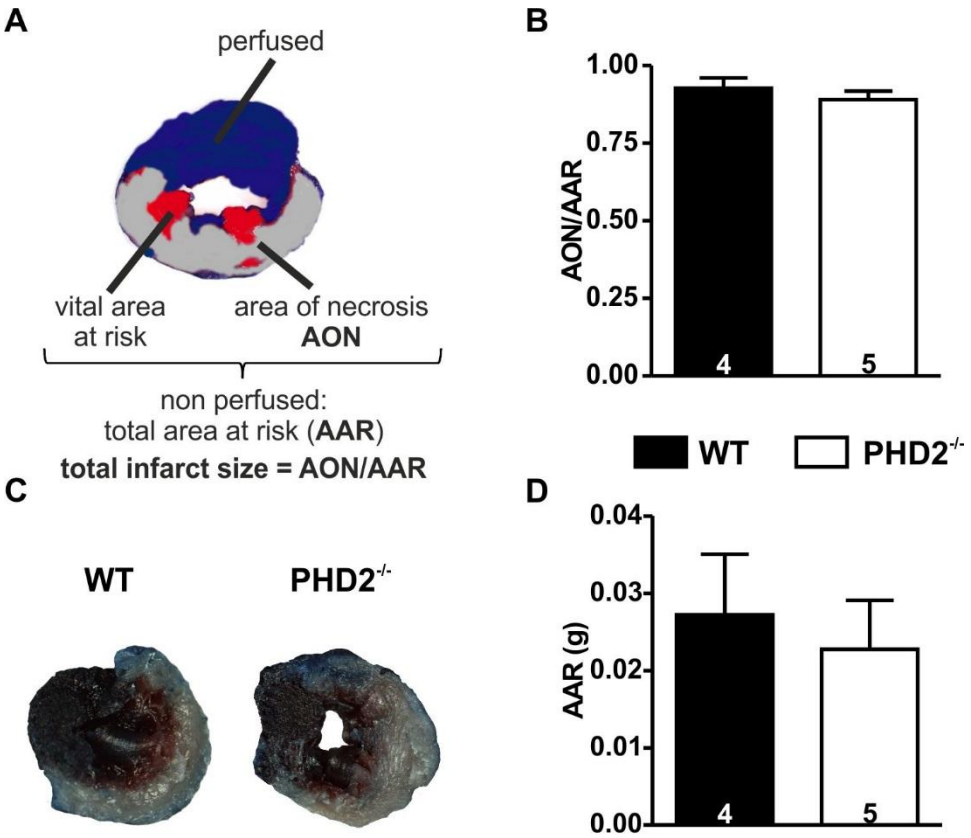

Figure 31: Initial infarction size in wild type and PHD2$^{-/-}$ mice. Infarction size was measured 6 hrs after surgery via staining the hearts with Evan´s blue and TTC. (A) The perfused area of the heart was stained with Evan´s blue. The area not stained in blue was defined as area at risk (AAR). Viable cells within the AAR could be stained in red by TTC, while the area which stayed pale was defined as area of necrosis (AON). (B) The fraction of the AON was analyzed within the AAR. (C) Analysis was based on images from infarcted hearts of wild type and PHD2$^{-/-}$ mice. (D) The total weight of AAR was determined between wild type and PHD2$^{-/-}$ mice. In total groups include 4 wild type and 5 PHD2$^{-/-}$ mice. Bars display mean ± SEM.

4. Discussion

Ischemic diseases such as peripheral artery disease or myocardial infarction trigger an inflammatory response, which can influence the extent of tissue damage. Major players in this sterile inflammation are macrophages and neutrophils which are recruited to the ischemic site and clear up necrotic tissue cells. The invasion of many oxygen-consuming cells however aggravates the hypoxic situation, to which both immune cells and tissue-resident cells have to adapt to. The adaptation to hypoxia is mediated by HIF-1 and HIF-2, which induce the expression of over 100 target genes identified so far. The regulation of HIF is mediated on protein level, via the prolyl-4-hydroxylation of conserved prolines within HIFα subunits, which leads to ubiquitination by pVHL and subsequent proteasomal degradation. The prolyl-4-hydroxylation is mediated via PHD 1-3, which need molecular O_2 as cofactor. Therefore, HIFα degradation can only take place when enough oxygen is present. In hypoxia, however, HIFα is stabilized. PHD1-3 thus act as the oxygen sensors of the cell. PHD1-3 have been described to have overlapping as well as distinct functions. Both PHD2 and PHD3 have been shown to regulate functions of myeloid cells. PHD3 deficiency *in vitro* protects macrophages from apoptosis. In the context of abdominal sepsis, PHD3 deficiency has been described to activate macrophages towards a pro-inflammatory phenotype. PHD2 deficiency in macrophages leads to a metabolic shift towards anaerobic glycolysis *in vitro*, which is linked to decreased migration and phagocytotic capacity.

Deficiency for the cellular oxygen sensors PHD2 and 3 in macrophages has not yet been studied in depth in the context of ischemic diseases. The aim of this thesis was therefore to elucidate the role of PHD2 and 3 in macrophages upon the induction of sterile inflammation in mouse models of ischemia.

4.1 Macrophage infiltration into the ischemic muscle is blunted in PHD3$^{-/-}$ mice

I studied macrophage and neutrophil infiltration and clearance in the ischemic muscle after hind limb ischemia via flow cytometry. Both populations have been shown to have an efficient PHD3 knock out in the applied mouse model.

In neutrophils, PHD3 deficiency did not affect the time course of infiltration and clearance compared to wild type. This result was surprising, because an earlier study identified PHD3 as potent regulator of neutrophil lifespan (Walmsley et al., 2011). Walmsley and colleagues found that PHD3$^{-/-}$ neutrophils died faster in hypoxia than wild type neutrophils. In an *in vivo* model of acute lung injury, this led to reduced neutrophil counts 18 hours after injury. Assuming that the inflamed site in the hind limb should also be hypoxic due to the surgical intervention of blood flow, one would expect the PHD3$^{-/-}$ neutrophils to have lower numbers

at day 1 and 3 after surgery. This was however not observed, which might be due to the different inflammatory triggers. Although the associated receptors and pathways in sterile and pathogen-associated inflammation can be overlapping, there are also pathways that are unique to each setting and could account for the observed differences. Moreover, in a model of abdominal sepsis, neutrophil infiltration into the lung was unchanged 8 hrs after LPS injection in a global PHD3 knock out (Kiss et al., 2012).

PHD3$^{-/-}$ macrophages showed a blunted inflammatory response after induction of hind limb ischemia. While initial recruitment until day 3 was still comparable to wild type macrophages, both at day 4 and 5 after surgery, PHD3$^{-/-}$ macrophages were present in significantly lower numbers compared to wild type macrophages. In a previous study, PHD3 deficiency was linked to higher inflammation and tissue infiltration of macrophages in a model of abdominal sepsis (Kiss et al., 2012). This finding was obtained in a global PHD3 knock out mouse, but transplantation of bone marrow from PHD3-deficient mice to wild type mice could mimic the effect, which suggests the involvement of a bone marrow-derived cell type. The reason for the striking difference in macrophage behavior observed by Kiss and colleagues compared to the data presented in this thesis could lie in the different trigger for inflammation. While the intraperitoneal injection with LPS presents a nonsterile inflammatory trigger, induction of hypoxia by ligation of an artery might trigger a different response. The versatility of the macrophage-response might allow for a differential role of PHD3, dependent on the stimulus. In human monocyte-derived macrophages and different human tissue samples, PHD3 seems to be a marker of pro-inflammatory macrophages (Escribese et al., 2012) which is in contrast to the findings by Kiss and colleagues in murine samples. However, the authors did not study to which extent the expression of PHD3 could regulate macrophage polarization into pro-inflammatory macrophages or whether PHD3 had an important role in mediating pro- or anti-inflammatory functions of macrophages.

In the present study, both at day 4 and 5 after surgery, macrophages displayed higher levels of the anti-inflammatory marker CD206 while a marker for pro-inflammatory macrophages (CD86) was not significantly changed. Anti-inflammatory macrophages are important for the resolution of inflammation and stimulate angiogenesis via secretion of VEGF. The upregulation of CD206 in PHD3$^{-/-}$ macrophages could be indicative of an earlier initiation of wound-healing processes. In cell culture, PHD3-deficient BMDM did not show a difference in polarization under basal conditions or after stimulation with IFN-ɣ and LPS or with IL-4 (Swain et al., 2014). Culturing of cells at 20% O_2 as well as the artificial stimulation can however not mimic the *in vivo* conditions of macrophages in the ischemic tissue, which could be a possible explanation for the divergent results obtained *in vivo* and *in vitro*.

In summary, the present study provides evidence for a so far not described anti-inflammatory effect of a myeloid-specific knock out of PHD3, which is mediated via a blunted macrophage response. The observed differences to already published work of other groups and our own group could be related to differences in the experimental setups that were used.

4.2 Reperfusion recovery and development of necrotic toes are unaffected in PHD3$^{-/-}$ mice

Macrophages can express pro-angiogenic factors such as VEGF to stimulate the formation of new blood vessels (Berse et al., 1992; Sunderkotter et al., 1994). Furthermore, a positive effect of macrophages on arteriogenesis has been shown (Arras et al., 1998; Takeda et al., 2011). Angiogenic and arteriogenic effects both contribute to the recovery of perfusion in models of hind limb ischemia. In order to evaluate the outcome of myeloid-specific PHD3-deficiency on reperfusion after hind limb ischemia surgery, laser Doppler images of paws were analyzed before and until 28 days after surgery. No difference could be observed at any of the time points between wild type and PHD3$^{-/-}$ mice.

In the context of hind limb ischemia, PHD3-deficiency has so far only been studied in global murine knock out or knock down models (Loinard et al., 2009; Rishi et al., 2015). While both studies observed a positive effect of decreased PHD3 levels for the angiogenic response, none could pinpoint this effect to a certain cell population or reveal the underlying mechanism. Loinard and colleagues observed an increased macrophage infiltration of the tissue in mice with a PHD3 knock down, which was linked to a better reperfusion and a higher capillary density. Whether the increased macrophage recruitment was an effect primarily mediated by the PHD3-deficient macrophages, or if other PHD3-deficient tissue-resident cells attracted more macrophages to the site of ischemia remains unclear.

My findings do not support the idea that PHD3-deficiency in myeloid cells has a positive effect on angiogenesis or arteriogenesis. The data obtained from laser Doppler images in this study was further secured by quantifying angiogenesis on tissue sections 3 and 28 days after surgery, which did not show any difference between wild type and PHD3-deficient mice. Also, the development of necrotic toes, which is an indicator for how well the hind paws are perfused, was unchanged between wild type and PHD3$^{-/-}$ mice.

4.3 Fibrosis is decreased in PHD3$^{-/-}$ mice which did not reflect in an improved motor function

Macrophages are key players in the restoration of organ homeostasis in the end phase of a sterile inflammation. In order to test, whether PHD3-deficiency in macrophages had any effect on fibrosis, mice underwent hind limb ischemia surgery. Gastrocnemicus muscles were excised 28 days after surgery and sections were stained for collagen-fibers using the dye picro-sirius red. In ligated legs of PHD3$^{-/-}$ mice, significantly less picro-sirius red-positive area

could be observed compared to wild type mice, indicating a better wound healing in PHD3$^{-/-}$ mice.

In a myeloid PHD3-knock out, no data on the development of fibrosis after induction of hind limb ischemia have been published yet. In a global PHD3 knock out, Rishi and colleagues observed less fibrosis 28 days after surgery, together with a better perfusion and higher capillary density in PHD3-deficient mice (Rishi et al., 2015). The decrease in fibrosis could be a secondary effect of the better perfusion recovery after hind limb ischemia. In my study however, perfusion was unchanged between wild type and PHD3$^{-/-}$ mice after hind limb ischemia surgery. The decreased fibrosis observed by me might have resulted from less damage in the early phase of inflammation due to less macrophage infiltration.

The ability to move the ischemic leg is an important clinical parameter which is affected by perfusion as well as fibrosis. I examined whether the myeloid-specific PHD3 knock out mice differed in their ability to move the ischemic leg both in resting conditions and by measuring the maximum speed they could run.

To study motor function in resting conditions, the motor score grading system used by Rishi and colleagues was applied (Rishi et al., 2015). No difference could be observed between wild type and PHD3$^{-/-}$ mice. Interestingly, motor function recovered to baseline within 7 days after surgery in my study, while Rishi and colleagues only saw complete recovery at day 14 for the PHD3 global knock out, and at day 28 for the wild type mice. This difference occurred, although mouse strain, sex, age and the general surgery technique were the same. This effect could have been caused by the inbreeding of the mice or by specific differences in the surgery technique which were not apparent from the brief description given by the authors in their publication.

The maximum running ability of mice was also tested using a RotaRod system. No difference could be observed between wild type and PHD3$^{-/-}$ mice. However, the drop in motor function after surgery was very mild, which indicates that mice of both genotypes could effectively compensate their impairment. Also, mouse behavior had a strong influence on the outcome of this experiment with “fast” and “slow learners” in both wild type and PHD3$^{-/-}$ groups which accounts for the high standard deviation.

My findings suggest that the myeloid-specific PHD3 knock out results in a decrease in fibrosis, which did however not reflect in an improved motor function in these mice. This might be caused by the in general rather small drop in motor function after surgery in wild type as well as PHD3$^{-/-}$ mice, which makes the detection of differences rather difficult.

4.4 Apoptosis and migration are unaltered in PHD3$^{-/-}$ macrophages

As described in a previous chapter, equal amounts of macrophages are present in the muscle tissue at day 3 after hind limb ischemia surgery when comparing wild type and PHD3$^{-/-}$ mice. At day 4 and 5, macrophage numbers are significantly lower in PHD3$^{-/-}$ compared to wild type mice. In order to find out by which mechanism this happened, apoptosis and migration of PHD3$^{-/-}$ macrophages were analyzed.

PHD3 has already been reported to be a potent regulator of apoptosis in various cell types (Lipscomb et al., 1999; Walmsley et al., 2011; Xie et al., 2015). In BMDM, PHD3-deficiency had an anti-apoptotic effect when cells were cultivated under stress conditions such as starvation or treatment with S-nitroso-N-acetyl penicillamine (SNAP) or stauroporine (Swain et al., 2014). In this thesis, apoptosis was analyzed both in wild type and PHD3$^{-/-}$ macrophages isolated from the gastrocnemicus muscle 4 days after hind limb ischemia surgery. No difference was observed between wild type and PHD3$^{-/-}$ macrophages in the abundance of apoptotic or dead cells. Swain and colleagues could only observe an anti-apoptotic phenotype in PHD3$^{-/-}$ BMDM after applying distinct triggers such as starvation or pro-apoptotic stimuli. These stimuli might not necessarily be present in the ischemic muscle, however, which might explain the difference to the findings of this thesis. Furthermore, the applied experimental setups of *in vitro* differentiated macrophages and macrophages isolated from an *in vivo* inflammatory reaction are not directly comparable.

PHD3 has been shown to mediate non-muscle actin hydroxylation and thereby impair the migration of HeLa cells (Luo et al., 2014). Furthermore, Kiss and colleagues could observe an enhanced migration in PHD3-deficient peritoneal macrophages (Kiss et al., 2012). I wanted to investigate whether a change in migration would be a possible explanation for the decreased macrophage numbers 4 and 5 days after surgery. I therefore performed single cell migration assays on wild type and PHD3$^{-/-}$ peritoneal macrophages and BMDM. No difference could be observed neither in basal conditions nor upon stimulation with MDA-MB231-conditioned medium. In contrast to Kiss and colleagues, the peritoneal macrophages I isolated were not elicited with thioglycollate, a substance which by itself already activates macrophages. The divergent migration results could therefore potentially be caused by this difference.

To conclude, my data do not suggest an involvement of an altered apoptosis rate or migratory capacity in the blunted PHD3$^{-/-}$ macrophage response after hind limb ischemia. The observed differences to the already published data might have resulted from the different experimental setups applied.

4.5 RNA sequencing of macrophages sorted from gastrocnemicus muscles 5 days after surgery revealed 10 differentially regulated genes

In order to characterize the PHD3-deficient macrophages present in the ischemic muscle even further, RNA expression was analyzed via RNA sequencing of macrophages sorted from the ischemic muscle 5 days after hind limb ischemia surgery. In total, 10 differentially regulated genes could be identified based on a p-value below 0.05 and a minimum log fold change of ±1.

The fact that only 10 genes were identified might be caused by a high variability due to several influencing parameters. The high variability in part derives from the surgery, which can never be reproduced exactly the same. Mice were age and sex-matched, but they originated from different litters. Another influencing factor is the digestion efficiency, which could have led to more variance, especially because the samples were isolated at 4 different days.

In total, 3 so far uncharacterized transcripts are significantly up- or downregulated in the RNA sequencing. Especially GM22567, which shows a -2.76 $\log_2$ fold downregulation and therefore the highest regulation of all 10 regulated genes, presents an interesting target for a future project to identify its function related to PHD3 in macrophages.

The PHD3-dependent regulation of miR-511, Cyp2s1 and Rbm4 in PHD3$^{-/-}$ cells has not yet been described before. All of these genes have previously been linked to inflammatory processes (Brudecki et al., 2013; Fromel et al., 2013; Puimege et al., 2015). A transcriptome screen performed by Swain and colleagues studying PHD3$^{-/-}$ and wild type BMDM could not identify these genes as differentially regulated (Swain et al., 2014). The screen described by Swain and colleagues applied different culturing conditions such as 48 hrs of normoxia or hypoxia as well as 48 hrs of starvation to the BMDMs. The differences between differentiating and culturing macrophages *in vitro* and the isolation of *in vivo* macrophages might account for the discrepancy between the findings of Swain and colleagues and the ones presented in this thesis. The genes Cyp2s1, miR-511 and Rbm4 were subsequently tested again for their differential regulation in an independent set of FACS-sorted macrophages via qRT-PCR, which could confirm the differential regulation for miR-511 and Cyp2s1, but not for Rbm4.

PHD3 was not significantly downregulated in PHD3$^{-/-}$ macrophages in the RNA sequencing. Although PHD3 levels were lower in PHD3$^{-/-}$ macrophages compared to wild type, PHD3 was in general expressed at very low levels. The expression level is characterized by the RPKM-value of each gene, which is calculated as the amount of transcripts which could be mapped to the respective gene in relation to the total amount of transcripts and the length of the respective gene. In this case, a cut-off of 1 was used. PHD3 showed a RPKM-value below 1

and was therefore not considered in the statistical analysis. A possible reason for the low expression of PHD3 could lie in the isolation process of the macrophages. PHD3 is expressed at low levels in normoxia, but heavily induced in hypoxia in BMDMs (Swain et al., 2014). During the isolation of macrophages from the ischemic hind limb muscle the reoxygenation of the cells upon exposure to the atmospheric pO_2 could not be prevented. This reoxygenation could have led to a rapid downregulation of PHD3 mRNA transcription.

The RNA sequencing did not reveal a differential expression of HIF-target genes in PHD3$^{-/-}$ macrophages compared to wild type. In line with this, HIF-1α and HIF-2α protein levels were not differentially regulated in PHD3$^{-/-}$ BMDM, nor was the expression of typical HIF-target genes such as phosphofructokinase (Pfk)-1, GLUT-1 or PDK-1 (Swain et al., 2014). The reason for the lack of HIF-1α stabilization in PHD3$^{-/-}$ BMDM could lie in the different importance of the three PHD isoforms for HIF degradation. Among the three PHDs, PHD2 has been demonstrated to be the main regulator of HIFα stability, at least in normoxia (Appelhoff et al., 2004; Berra et al., 2003). Silencing of PHD2 consequently leads to normoxic stabilization of HIFα and increased transcription of HIF-target genes (Berra et al., 2003). For PHD1 and 3 knock outs however, normoxic stabilization of HIFα and subsequent upregulation of its target genes is commonly not observed (Berra et al., 2003; Swain et al., 2014).

The RNA sequencing did not show any differential expression of typical pro- or anti-inflammatory cytokines such as TNF-α, IL-1β, IL-6 or IL-10. This is in line with studies performed in PHD3$^{-/-}$ BMDM, which could also not detect any differences in expression or secretion of pro-inflammatory cytokines (Swain et al., 2014). However, macrophages isolated from the hind limb showed a higher surface expression of the mannose receptor and M2-marker CD206 on day 4 and 5 after surgery. In the RNA sequencing, CD206, encoded by Mrc1, was slightly but not significantly upregulated. The higher surface expression of CD206 in PHD3$^{-/-}$ macrophages 4 and 5 days after hind limb ischemia surgery could be due to a regulation on protein level. CD206 is important for phagocytosis during which is gets internalized. A regulation of CD206 via protein degradation rates as well as via protein localization has been implicated (Fiani et al., 1998) which could possibly explain why no change in RNA expression was detected in the RNA sequencing though CD206 levels were higher on PHD3$^{-/-}$ macrophages.

4.6 miR-511 expression and TNF-R1 levels in PHD3$^{-/-}$ macrophages

TNF-R1, a receptor for TNF-α, is a target of miR-511 (Puimege et al., 2015). TNF-R1 downregulation caused by a 2-fold miR-511 upregulation led to less inflammation in a model of TNF-α-induced shock. The RNA sequencing identified miR-511 as upregulated in PHD3$^{-/-}$ macrophages. TNF-R1 expression on macrophages isolated from the gastrocnemicus

muscle 4 days after hind limb ischemia surgery was studied in order to see whether this could be a potential mechanism, by which the blunted inflammatory response of macrophages is mediated. However, only a mild and not significant downregulation of TNF-R1 was observed. TNF-R2, which has not been described to be targeted by miR-511 showed a similar mild downregulation. This could indicate a non-miR-511-related effect to be the cause for slightly decreased TNF-R1 levels. These data suggest that upregulation of miR-511 does not influence the anti-inflammatory macrophage behavior by regulating TNF-R1 levels.

To identify a different mechanism by which miR-511 influences macrophage behavior, mimicking the differential regulation of miR-511 in PHD3$^{-/-}$ macrophages *in vitro* would present a suitable model. However, even in different culture conditions such as hypoxia, normoxia, starvation as well as addition of glucocorticoids to stimulate miR-511 expression, no difference in mi-R511 expression could be observed between wild type and PHD3$^{-/-}$ macrophages. This impeded further studies on the effect of miR-511 in cell culture.

4.7 Cyp2s1 expression is downregulated in PHD3$^{-/-}$ BMDM which coincides with increased phagocytotic capacity and increased Prostaglandin E2 secretion

In line with the RNA sequencing results, the expression of Cyp2s1 was downregulated in PHD3$^{-/-}$ BMDM, at least in hypoxia combined with starvation. Cyp2s1 had not been described to be differentially regulated in a transcriptome screen performed on PHD3$^{-/-}$ BMDM (Swain et al., 2014). This might be caused by the fact that cells cultivated in hypoxia in starvation medium were not included in that screen.

Cyp2s1 has been described to identify pro-inflammatory macrophages both *in vitro* and *in vivo* (Fromel et al., 2013). *In vitro*, stimulation of human monocyte-derived macrophages with LPS and IFN-ɣ induced Cyp2s1 expression. In the present study, a set of 3 pro-inflammatory cytokines was tested to see if the decreased levels of Cyp2s1 in PHD3$^{-/-}$ macrophages correlated with the expression of these cytokines. No correlation between Cyp2s1 and cytokine expression patterns was observed, indicating that Cyp2s1 is rather a target of inflammatory regulation than an active part in its mediation.

Cyp2s1 is an epoxygenase which has been described to metabolize PGG2 and PGH2 to 12-HHT (Fromel et al., 2013). PGH2 is synthesized from arachidonic acids by the action of Cyclooxygenase-1 (COX-1) and 2 via the intermediate product PGG2. PGH2 also serves as a substrate for PGE2 synthesis via the PGE2 synthases (reviewed by (Kalinski, 2012)). PGE2 is a potent pro- and anti-inflammatory mediator, which in the early inflammatory phase mediates attraction and activation of neutrophils, but has also been described to enhance M2-polarization of macrophages and interfere with NLRP3 inflammasome activation in sterile inflammation (Sokolowska et al., 2015; Strassmann et al., 1994; Yu and Chadee, 1998).

These diverse roles are mediated by 4 different prostaglandin E2-receptors (EP) 1-4, which require different PGE2 concentrations for their activation (reviewed by (Kalinski, 2012)). The most commonly proposed regulation mechanism of PGE2 synthesis is via the expression of COX-1 and -2, which produce PGE2´s precursors PGH2 and G2. I here hypothesize that the accumulation of these precursors due to an attenuated metabolism to 12-HHT could also lead to an increased PGE2 synthesis. Given that the levels of Cyp2s1 are significantly lower in PHD3$^{-/-}$ macrophages compared to wild type, more PGG2 and PGH2 would be disposable as substrate for PGE2 synthesis. Indeed, increased levels of PGE2 were observed in PHD3$^{-/-}$ BMDM cultivated for 24 hrs in hypoxia in starvation medium. PGE2 has been shown to negatively affect phagocytosis in rat and murine alveolar macrophages and murine peritoneal macrophages (Aronoff et al., 2004; Hubbard et al., 2010; Konopski et al., 1993). However, IL-10 which is highly induced by PGE2 can also stimulate phagocytosis (Lingnau et al., 2007). Downregulation of Cyp2s1 by siRNA furthermore leads to increased phagocytosis in monocytes (Fromel et al., 2013). In this study, phagocytosis was increased in PHD3$^{-/-}$ BMDM upon starvation. Treating wild type cells with enough PGE2 to reach the levels secreted by PHD3$^{-/-}$ BMDM led to an increase in phagocytosis to the level of untreated PHD3$^{-/-}$ BMDM. This finding indicates that the differential PGE2 secretion might be responsible for the increased phagocytosis in PHD3$^{-/-}$ BMDM. This is in line with data suggesting that low doses of PGE2 can have stimulatory effects on phagocytosis while higher doses inhibit phagocytosis in macrophages (Razin et al., 1978; Razin and Globerson, 1979). The mechanism for this is so far unclear, but could involve the PGE2 receptors EP2 and EP3. While EP2 responds only to high doses of PGE2 and increases cAMP levels in the cell, EP3 is activated already with lower doses of PGE2 and decreases cAMP levels (reviewed by (Kalinski, 2012)). In line with this, cAMP has been shown to reduce phagocytosis (Rossi et al., 1998).

Further studies are needed to investigate whether increased PGE2 levels are responsible for the anti-inflammatory phenotype of PHD3$^{-/-}$ macrophages *in vivo*.

4.8 PHD2$^{-/-}$ macrophages show a delayed inflammatory response after induction of myocardial infarction as well as a worse heart function compared to wild type

PHD2-deficient macrophages have been shown to display a metabolic shift towards anaerobic glycolysis which is linked to a decreased migration and phagocytotic capacity (Guentsch et al., in revision). To evaluate whether this effect would influence macrophage behavior *in vivo*, myeloid-specific PHD2 knock out mice underwent myocardial infarction which induced an inflammatory response caused by ischemia. At day 3 after surgery, PHD2$^{-/-}$ macrophages were less abundant than wild type macrophages in isolated hearts. At day 7 after surgery, PHD2$^{-/-}$ macrophages were more abundant in isolated hearts than wild type

macrophages, which were already decreasing in number compared to day 3. This indicates a delayed response of the PHD2$^{-/-}$ macrophages, which could be caused by a delay of migration into the tissue combined with the incapability to phagocytose apoptotic neutrophils and thereby resolve the inflammation. In a model of angiotensin II-induced hypertension, myeloid-specific PHD2$^{-/-}$ mice displayed less macrophage infiltration into the heart which was linked to less fibrosis (Ikeda et al., 2013). *In vitro*, the authors observed a migration defect in peritoneal macrophages, which is in line with the migration data obtained from PHD2$^{-/-}$ BMDM (Guentsch et al., in revision).

Although a glycolytic metabolism has been linked to M1-polarization in macrophages, flow cytometric analysis of the M1-marker CD86 did not show differences neither at day 3 or 7 between wild type and PHD2$^{-/-}$ macrophages (Galvan-Pena and O'Neill, 2014). Also, no polarization into M2-macrophages could be observed, analyzed by the expression of CD206 on the cell surface of macrophages. This is in line with data from PHD2$^{-/-}$ BMDM, where no enhanced polarization into M1 or M2-macrophages was observed in basal conditions or upon stimulation with IL-4 or IFN-ɣ and LPS (Guentsch et al., in revision). Furthermore, two other reports did not observe a M2-polarization in PHD2$^{-/-}$ macrophages while M1-markers were slightly downregulated in myeloid-specific PHD2 knock out mice in models of hypertension and tumor formation (Ikeda et al., 2013; Mamlouk et al., 2014). In contrast to that, PHD2 haplodeficiency seems to be able to induce M2-like macrophages which exert a pro-arteriogenic effect on smooth muscle cells (Takeda et al., 2011). This effect seems to be strictly limited to heterozygous PHD2 knock out mice, as it could not be reproduced in homozygous PHD2 knock out mice (Takeda et al., 2011).

The heart function of wild type and PHD2$^{-/-}$ mice was significantly worse after induction of MI. This might have been caused by the delayed inflammation observed via flow cytometry. Further studies are needed to dissect whether the worse heart function was caused by a migration defect or by an impaired phagocytotic capacity. Interestingly, the migration defect, also observed in a model of increased afterload in myeloid-specific PHD2$^{-/-}$ where it had beneficial effects (Ikeda et al., 2013), seems to have a detrimental effect in the setting of myocardial infarction. This could be due to the different course of disease. While myocardial infarction induces a sudden injury which leads to cell necrosis and requires a prompt answer by the immune system, angiotensin II-treatment induces rather a chronic injury leading to cardiac remodeling. In the latter setting, macrophage infiltration might do more harm than good.

4.9 Therapeutic inhibition of PHDs - implications for myeloid cells

Lack of oxygen is not the only factor which can inhibit PHDs. PHDs can be inhibited by different substances which mostly interfere with the binding of its cofactors 2-OG or Fe(II) or

by inhibiting the enzyme´s catalytic site. Iron chelators such as Co_2Cl or desferrioxamine can decrease the availability of Fe(II) and thereby inhibit PHDs. The depletion of available Fe(II) by iron chelators is however unsuitable for clinical use due to systemic side effects. Furthermore, substances like DMOG, which is a 2-OG analogue, can inhibit PHD activity. DMOG is however rather unspecific and also inhibits other 2-OG-dependent dioxygenases, which makes it likewise unsuitable for clinical use.

In terms of specificity, advances have been made within the past decade. Substances such as Roxadustat (FG-4592, Fibrogen) or 2-(1-chloro-4-hydroxyisoquinoline-3-carboxamido) acetate (ICA) are 2-OG analogues which specifically target PHDs and do not interfere with other 2-OG-dependent dioxygenases. However, the differences between the 2-OG binding sites of PHD1, 2 and 3 isoforms are so little, that so far, no PHD isoform-specific inhibitor could be developed. Several of the PHD-specific inhibitors are in clinical trials at the moment. Roxadustat for example, is currently in a phase III clinical trial for the treatment of anemia in patients with chronic kidney disease (NTC01750190). A clinical trial with PAD patients using a similar compound called GSK1278863 could not show an amelioration in muscle performance, neither when administering a single dose nor small doses given over a period of 14 days (Olson et al., 2014). However, this might be due to dosage problems, as muscle biopsies could not show elevated HIF-stabilization. In myeloid cells, PHD inhibitors such as TM6008 exert anti-inflammatory effects in murine macrophages (Takeda et al., 2009). Clinical trials have not yet studied the effect of PHD-inhibitors in the setting of inflammation. The data presented in this thesis rather suggest that inhibition of PHD2 might have an unfavorable outcome due to decreased migration and phagocytosis capacity, which prolongs the course of inflammation. In contrast to that, PHD3-inhibition might present an advantage for wound healing. PHD-isoform specific inhibitors would be needed to dissect wanted from unwanted effects when treating patients undergoing a sterile inflammation caused by ischemia.

4.10 Conclusion and outlook

To conclude, this study presents novel findings regarding the function of PHD2 and 3 for macrophages in the setting of sterile inflammation.

In myeloid-specific PHD3 knock out mice, a blunted inflammatory response of the macrophages was observed upon the induction of hind limb ischemia. This finding was in contrast to earlier studies, which observed a more pronounced macrophage-infiltration in $PHD3^{-/-}$ mice upon induction of a non-sterile inflammation (Kiss et al., 2012). $PHD3^{-/-}$ macrophages however did not induce an angiogenic response, nor did myeloid PHD3-deficiency alter the reperfusion recovery after induction of hind limb ischemia by a different mechanism, for example arteriogenesis. In contrast, fibrosis was decreased in $PHD3^{-/-}$ mice,

indicating that the altered inflammatory response had a beneficial effect for the restoration of tissue homeostasis.

While differences in apoptosis or migration were apparently not the trigger for the decreased inflammatory response of PHD3$^{-/-}$ macrophages, a RNA sequencing of macrophages sorted from hind limb muscles 5 days after hind limb ischemia identified 10 differentially regulated genes. Out of those, Cyp2s1, which is downregulated in PHD3$^{-/-}$ macrophages, presents a putative mediator of the differential inflammatory response between wild type and PHD3$^{-/-}$ macrophages. As Cyp2s1 metabolizes the substrates for PGE2-production, I analyzed whether the decreased expression of Cyp2s1 in PHD3$^{-/-}$ BMDM correlated with increased PGE2 secretion. This was indeed the case. Since PGE2 can induce anti-inflammatory effects on macrophages, this is a putative mechanism for mediating the decreased levels of macrophages 4 and 5 days after surgery, which also showed an increased M2-marker expression.

PGE2 secretion was upregulated in PHD3$^{-/-}$ BMDM upon starvation in hypoxia. It is however unclear whether the increased PGE2 secretion is in fact due to Cyp2s1 downregulation. Transfection of wild type BMDMs with Cyp2s1 siRNA or its inhibition by CYP inhibitors liarozole or miconazole should be studied to see whether PGE2 secretion can be increased by these mechanisms. Furthermore, secretion of PGE2 by macrophages isolated from the ischemic muscle could be studied. This would include the sorting of macrophages and their subsequent culturing. If that was indeed the case, it would be interesting to study myeloid-specific Cyp2s1 knock out mice to see whether the reduced inflammatory response after hind limb ischemia is indeed due to Cyp2s1 levels. The role of 12-HHT, the product of Cyp2s1, should also be studied in further depth. In keratinocytes, 12-HHT stimulates migration via leukotriene B4 receptor type 2 (BLT2), which leads to enhanced wound healing in mouse models (Liu et al., 2014). In macrophages, no function has been described yet. Furthermore, it would be interesting to study miR-511 and its potential targets more in depth.

In a myeloid-specific PHD2-knock out, a delayed inflammatory response of the macrophages was observed in a model of myocardial infarction. This was linked to a worse heart function of PHD2$^{-/-}$ mice. These findings could be explained by *in vitro* data on PHD2$^{-/-}$ BMDM, which show a delayed migration as well as a decreased phagocytotic capacity. These effects were linked to a metabolic shift towards anaerobic glycolysis.

Further studies are needed to test whether the macrophages *in vivo* display a metabolic phenotype. For this, macrophages could be sorted from heart muscles after LAD surgery for RNA sequencing. In PHD2$^{-/-}$ BMDM, several metabolic enzymes such as PDK-1 are transcriptionally regulated. It would be interesting to see whether PHD2$^{-/-}$ macrophages isolated from the ischemic heart display a similar profile. In cell culture, treatment of PHD2$^{-/-}$

macrophages with dichloroacetate (DCA), which inhibits PDK-1 and thereby stimulates oxidative phosphorylation, could partly rescue their phenotype. It would be interesting to know if the *in vivo* phenotype could be rescued in a similar manner.

In addition, a direct comparison of the effects of myeloid-specific PHD2 and 3 knock outs would be desirable. For this, it would be interesting to study both in the same model of sterile inflammation. Preliminary data from $PHD2^{-/-}$ mice after hind limb ischemia did not show any striking phenotype in relation to perfusion recovery or in the inflammatory response compared to wild type mice. It would therefore be interesting to investigate the inflammatory response of $PHD3^{-/-}$ macrophages in a model of myocardial infarction. Therapeutic intervention is so far only possible by using Pan-PHD inhibitors. In a murine model of myocardial infarction, the administration of 2-(1-chloro-4-hydroxyisoquinoline-3-carboxamido) acetate (ICA) has already been tested. The application of ICA led to a robust HIF-1α and -2α stabilization for at least 24 hrs and to a decrease in infarction size and better heart function when administered 1 and 5 hrs after induction of MI (Vogler et al., 2015). If administered for longer, PHD-inhibitors might interfere with the inflammatory response mediated by macrophages. This would however, based on the divergent roles of the different PHDs observed in this thesis, not necessarily lead to a beneficial effect on the initial inflammatory response. As the inflammatory response is a determinant for tissue restoration and organ function on the long term, patients might not benefit from the administration of a pan-PHD inhibitor in the inflammatory phase. The presented data therefore suggests a helpful role for isoform-specific PHD inhibitors.

References

Appelhoff, R.J., Y.M. Tian, R.R. Raval, H. Turley, A.L. Harris, C.W. Pugh, P.J. Ratcliffe, and J.M. Gleadle. 2004. Differential function of the prolyl hydroxylases PHD1, PHD2, and PHD3 in the regulation of hypoxia-inducible factor. *J Biol Chem*. 279:38458-38465.

Aragones, J., M. Schneider, K. Van Geyte, P. Fraisl, T. Dresselaers, M. Mazzone, R. Dirkx, S. Zacchigna, H. Lemieux, N.H. Jeoung, D. Lambrechts, T. Bishop, P. Lafuste, A. Diez-Juan, S.K. Harten, P. Van Noten, K. De Bock, C. Willam, M. Tjwa, A. Grosfeld, R. Navet, L. Moons, T. Vandendriessche, C. Deroose, B. Wijeyekoon, J. Nuyts, B. Jordan, R. Silasi-Mansat, F. Lupu, M. Dewerchin, C. Pugh, P. Salmon, L. Mortelmans, B. Gallez, F. Gorus, J. Buyse, F. Sluse, R.A. Harris, E. Gnaiger, P. Hespel, P. Van Hecke, F. Schuit, P. Van Veldhoven, P. Ratcliffe, M. Baes, P. Maxwell, and P. Carmeliet. 2008. Deficiency or inhibition of oxygen sensor Phd1 induces hypoxia tolerance by reprogramming basal metabolism. *Nat Genet*. 40:170-180.

Aronoff, D.M., C. Canetti, and M. Peters-Golden. 2004. Prostaglandin E2 inhibits alveolar macrophage phagocytosis through an E-prostanoid 2 receptor-mediated increase in intracellular cyclic AMP. *J Immunol*. 173:559-565.

Arras, M., W.D. Ito, D. Scholz, B. Winkler, J. Schaper, and W. Schaper. 1998. Monocyte activation in angiogenesis and collateral growth in the rabbit hindlimb. *J Clin Invest*. 101:40-50.

Band, M., A. Joel, A. Hernandez, and A. Avivi. 2009. Hypoxia-induced BNIP3 expression and mitophagy: in vivo comparison of the rat and the hypoxia-tolerant mole rat, Spalax ehrenbergi. *Faseb J*. 23:2327-2335.

Berger, J.S., and W.R. Hiatt. 2012. Medical therapy in peripheral artery disease. *Circulation*. 126:491-500.

Berra, E., E. Benizri, A. Ginouves, V. Volmat, D. Roux, and J. Pouyssegur. 2003. HIF prolyl-hydroxylase 2 is the key oxygen sensor setting low steady-state levels of HIF-1alpha in normoxia. *Embo J*. 22:4082-4090.

Berra, E., A. Ginouves, and J. Pouyssegur. 2006. The hypoxia-inducible-factor hydroxylases bring fresh air into hypoxia signalling. *EMBO Rep*. 7:41-45.

Berse, B., L.F. Brown, L. Van de Water, H.F. Dvorak, and D.R. Senger. 1992. Vascular permeability factor (vascular endothelial growth factor) gene is expressed differentially in normal tissues, macrophages, and tumors. *Mol Biol Cell*. 3:211-220.

Bishop, T., D. Gallagher, A. Pascual, C.A. Lygate, J.P. de Bono, L.G. Nicholls, P. Ortega-Saenz, H. Oster, B. Wijeyekoon, A.I. Sutherland, A. Grosfeld, J. Aragones, M. Schneider, K. van Geyte, D. Teixeira, A. Diez-Juan, J. Lopez-Barneo, K.M. Channon, P.H. Maxwell, C.W. Pugh, A.M. Davies, P. Carmeliet, and P.J. Ratcliffe. 2008. Abnormal sympathoadrenal development and systemic hypotension in PHD3-/- mice. *Mol Cell Biol*. 28:3386-3400.

Bours, M.J., E.L. Swennen, F. Di Virgilio, B.N. Cronstein, and P.C. Dagnelie. 2006. Adenosine 5'-triphosphate and adenosine as endogenous signaling molecules in immunity and inflammation. *Pharmacol Ther*. 112:358-404.

Boxio, R., C. Bossenmeyer-Pourie, N. Steinckwich, C. Dournon, and O. Nusse. 2004. Mouse bone marrow contains large numbers of functionally competent neutrophils. *Journal of leukocyte biology*. 75:604-611.

Brevetti, G., G. Giugliano, L. Brevetti, and W.R. Hiatt. 2010. Inflammation in peripheral artery disease. *Circulation*. 122:1862-1875.

Brudecki, L., D.A. Ferguson, C.E. McCall, and M. El Gazzar. 2013. MicroRNA-146a and RBM4 form a negative feed-forward loop that disrupts cytokine mRNA translation following TLR4 responses in human THP-1 monocytes. *Immunol Cell Biol*. 91:532-540.

Cailleau, R., R. Young, M. Olive, and W.J. Reeves, Jr. 1974. Breast tumor cell lines from pleural effusions. *J Natl Cancer Inst*. 53:661-674.

Cavaillon, J.M. 2011. The historical milestones in the understanding of leukocyte biology initiated by Elie Metchnikoff. *J Leukoc Biol*. 90:413-424.

Chan, D.A., P.D. Sutphin, S.E. Yen, and A.J. Giaccia. 2005. Coordinate regulation of the oxygen-dependent degradation domains of hypoxia-inducible factor 1 alpha. *Mol Cell Biol*. 25:6415-6426.

Chen, C., N. Pore, A. Behrooz, F. Ismail-Beigi, and A. Maity. 2001. Regulation of glut1 mRNA by hypoxia-inducible factor-1. Interaction between H-ras and hypoxia. *J Biol Chem*. 276:9519-9525.

Chen, G.Y., and G. Nunez. 2010. Sterile inflammation: sensing and reacting to damage. *Nat Rev Immunol*. 10:826-837.

Chen, N., X. Chen, R. Huang, H. Zeng, J. Gong, W. Meng, Y. Lu, F. Zhao, L. Wang, and Q. Zhou. 2009. BCL-xL is a target gene regulated by hypoxia-inducible factor-1{alpha}. *J Biol Chem*. 284:10004-10012.

Chomczynski, P., and N. Sacchi. 1987. Single-step method of RNA isolation by acid guanidinium thiocyanate-phenol-chloroform extraction. *Analytical biochemistry*. 162:156-159.

Clausen, B.E., C. Burkhardt, W. Reith, R. Renkawitz, and I. Forster. 1999. Conditional gene targeting in macrophages and granulocytes using LysMcre mice. *Transgenic research*. 8:265-277.

Cohn, J.N., R. Ferrari, and N. Sharpe. 2000. Cardiac remodeling--concepts and clinical implications: a consensus paper from an international forum on cardiac remodeling. Behalf of an International Forum on Cardiac Remodeling. *J Am Coll Cardiol*. 35:569-582.

Connolly, D.T., D.M. Heuvelman, R. Nelson, J.V. Olander, B.L. Eppley, J.J. Delfino, N.R. Siegel, R.M. Leimgruber, and J. Feder. 1989. Tumor vascular permeability factor stimulates endothelial cell growth and angiogenesis. *J Clin Invest*. 84:1470-1478.

Cramer, T., Y. Yamanishi, B.E. Clausen, I. Forster, R. Pawlinski, N. Mackman, V.H. Haase, R. Jaenisch, M. Corr, V. Nizet, G.S. Firestein, H.P. Gerber, N. Ferrara, and R.S. Johnson. 2003. HIF-1alpha is essential for myeloid cell-mediated inflammation. *Cell*. 112:645-657.

Cummins, E.P., E. Berra, K.M. Comerford, A. Ginouves, K.T. Fitzgerald, F. Seeballuck, C. Godson, J.E. Nielsen, P. Moynagh, J. Pouyssegur, and C.T. Taylor. 2006. Prolyl hydroxylase-1 negatively regulates IkappaB kinase-beta, giving insight into hypoxia-induced NFkappaB activity. *Proc Natl Acad Sci U S A*. 103:18154-18159.

de Lemos, J.A., D.A. Morrow, M.A. Blazing, P. Jarolim, S.D. Wiviott, M.S. Sabatine, R.M. Califf, and E. Braunwald. 2007. Serial measurement of monocyte chemoattractant protein-1 after acute coronary syndromes: results from the A to Z trial. *J Am Coll Cardiol*. 50:2117-2124.

del Peso, L., M.C. Castellanos, E. Temes, S. Martin-Puig, Y. Cuevas, G. Olmos, and M.O. Landazuri. 2003. The von Hippel Lindau/hypoxia-inducible factor (HIF) pathway regulates the transcription of the HIF-proline hydroxylase genes in response to low oxygen. *J Biol Chem*. 278:48690-48695.

Demetri, G.D., and J.D. Griffin. 1991. Granulocyte colony-stimulating factor and its receptor. *Blood*. 78:2791-2808.

Eigenbrod, T., J.H. Park, J. Harder, Y. Iwakura, and G. Nunez. 2008. Cutting edge: critical role for mesothelial cells in necrosis-induced inflammation through the recognition of IL-1 alpha released from dying cells. *J Immunol*. 181:8194-8198.

Epelman, S., K.J. Lavine, and G.J. Randolph. 2014. Origin and functions of tissue macrophages. *Immunity*. 41:21-35.

Epstein, A.C., J.M. Gleadle, L.A. McNeill, K.S. Hewitson, J. O'Rourke, D.R. Mole, M. Mukherji, E. Metzen, M.I. Wilson, A. Dhanda, Y.M. Tian, N. Masson, D.L. Hamilton, P. Jaakkola, R. Barstead, J. Hodgkin, P.H. Maxwell, C.W. Pugh, C.J. Schofield, and P.J. Ratcliffe. 2001. C. elegans EGL-9 and mammalian homologs define a family of dioxygenases that regulate HIF by prolyl hydroxylation. *Cell*. 107:43-54.

Escribese, M.M., E. Sierra-Filardi, C. Nieto, R. Samaniego, C. Sanchez-Torres, T. Matsuyama, E. Calderon-Gomez, M.A. Vega, A. Salas, P. Sanchez-Mateos, and A.L.

Corbi. 2012. The prolyl hydroxylase PHD3 identifies proinflammatory macrophages and its expression is regulated by activin A. *J Immunol*. 189:1946-1954.

Fang, F.C. 1997. Perspectives series: host/pathogen interactions. Mechanisms of nitric oxide-related antimicrobial activity. *J Clin Invest*. 99:2818-2825.

Fiani, M.L., J. Beitz, D. Turvy, J.S. Blum, and P.D. Stahl. 1998. Regulation of mannose receptor synthesis and turnover in mouse J774 macrophages. *J Leukoc Biol*. 64:85-91.

Fowkes, F.G., D. Rudan, I. Rudan, V. Aboyans, J.O. Denenberg, M.M. McDermott, P.E. Norman, U.K. Sampson, L.J. Williams, G.A. Mensah, and M.H. Criqui. 2013. Comparison of global estimates of prevalence and risk factors for peripheral artery disease in 2000 and 2010: a systematic review and analysis. *Lancet*. 382:1329-1340.

Fromel, T., K. Kohlstedt, R. Popp, X. Yin, K. Awwad, E. Barbosa-Sicard, A.C. Thomas, R. Lieberz, M. Mayr, and I. Fleming. 2013. Cytochrome P4502S1: a novel monocyte/macrophage fatty acid epoxygenase in human atherosclerotic plaques. *Basic Res Cardiol*. 108:012-0319.

Fu, J., and M.B. Taubman. 2010. Prolyl hydroxylase EGLN3 regulates skeletal myoblast differentiation through an NF-kappaB-dependent pathway. *J Biol Chem*. 285:8927-8935.

Fujita, N., S.S. Gogate, K. Chiba, Y. Toyama, I.M. Shapiro, and M.V. Risbud. 2012. Prolyl hydroxylase 3 (PHD3) modulates catabolic effects of tumor necrosis factor-alpha (TNF-alpha) on cells of the nucleus pulposus through co-activation of nuclear factor kappaB (NF-kappaB)/p65 signaling. *J Biol Chem*. 287:39942-39953.

Furze, R.C., and S.M. Rankin. 2008. Neutrophil mobilization and clearance in the bone marrow. *Immunology*. 125:281-288.

Galvan-Pena, S., and L.A. O'Neill. 2014. Metabolic reprograming in macrophage polarization. *Front Immunol*. 5.

Geering, B., C. Stoeckle, S. Conus, and H.U. Simon. 2013. Living and dying for inflammation: neutrophils, eosinophils, basophils. *Trends Immunol*. 34:398-409.

Ginhoux, F., and S. Jung. 2014. Monocytes and macrophages: developmental pathways and tissue homeostasis. *Nat Rev Immunol*. 14:392-404.

Ginouves, A., K. Ilc, N. Macias, J. Pouyssegur, and E. Berra. 2008. PHDs overactivation during chronic hypoxia "desensitizes" HIFalpha and protects cells from necrosis. *Proc Natl Acad Sci U S A*. 105:4745-4750.

Gordon, S. 2007. The macrophage: past, present and future. *Eur J Immunol*. 37:S9-17.

Greenberg, J.I., A. Suliman, S. Barillas, and N. Angle. 2008. Chapter 7. Mouse models of ischemic angiogenesis and ischemia-reperfusion injury. *Methods in enzymology*. 444:159-174.

Gu, Y.Z., S.M. Moran, J.B. Hogenesch, L. Wartman, and C.A. Bradfield. 1998. Molecular characterization and chromosomal localization of a third alpha-class hypoxia inducible factor subunit, HIF3alpha. *Gene Expr*. 7:205-213.

Hamm, A., L. Veschini, Y. Takeda, S. Costa, E. Delamarre, M.L. Squadrito, A.T. Henze, M. Wenes, J. Serneels, F. Pucci, C. Roncal, A. Anisimov, K. Alitalo, M. De Palma, and M. Mazzone. 2013. PHD2 regulates arteriogenic macrophages through TIE2 signalling. *EMBO Mol Med*. 5:843-857.

Hirsila, M., P. Koivunen, V. Gunzler, K.I. Kivirikko, and J. Myllyharju. 2003. Characterization of the human prolyl 4-hydroxylases that modify the hypoxia-inducible factor. *J Biol Chem*. 278:30772-30780.

Hoff, J. 2000. Methods of Blood Collection in the Mouse. *In* Lab animal, Vol. 29, No. 10. 47-53.

Hoffman, E.C., H. Reyes, F.F. Chu, F. Sander, L.H. Conley, B.A. Brooks, and O. Hankinson. 1991. Cloning of a factor required for activity of the Ah (dioxin) receptor. *Science*. 252:954-958.

Hofmann, M.A., S. Drury, C. Fu, W. Qu, A. Taguchi, Y. Lu, C. Avila, N. Kambham, A. Bierhaus, P. Nawroth, M.F. Neurath, T. Slattery, D. Beach, J. McClary, M. Nagashima, J. Morser, D. Stern, and A.M. Schmidt. 1999. RAGE mediates a novel

proinflammatory axis: a central cell surface receptor for S100/calgranulin polypeptides. *Cell*. 97:889-901.

Holmquist-Mengelbier, L., E. Fredlund, T. Lofstedt, R. Noguera, S. Navarro, H. Nilsson, A. Pietras, J. Vallon-Christersson, A. Borg, K. Gradin, L. Poellinger, and S. Pahlman. 2006. Recruitment of HIF-1alpha and HIF-2alpha to common target genes is differentially regulated in neuroblastoma: HIF-2alpha promotes an aggressive phenotype. *Cancer Cell*. 10:413-423.

Huang, J., Q. Zhao, S.M. Mooney, and F.S. Lee. 2002. Sequence determinants in hypoxia-inducible factor-1alpha for hydroxylation by the prolyl hydroxylases PHD1, PHD2, and PHD3. *J Biol Chem*. 277:39792-39800.

Huang, L.E., J. Gu, M. Schau, and H.F. Bunn. 1998. Regulation of hypoxia-inducible factor 1alpha is mediated by an O2-dependent degradation domain via the ubiquitin-proteasome pathway. *Proc Natl Acad Sci U S A*. 95:7987-7992.

Hubbard, L.L., M.N. Ballinger, P.E. Thomas, C.A. Wilke, T.J. Standiford, K.S. Kobayashi, R.A. Flavell, and B.B. Moore. 2010. A role for IL-1 receptor-associated kinase-M in prostaglandin E2-induced immunosuppression post-bone marrow transplantation. *J Immunol*. 184:6299-6308.

Hutton, J.J., Jr., A.L. Trappel, and S. Udenfriend. 1966. Requirements for alpha-ketoglutarate, ferrous ion and ascorbate by collagen proline hydroxylase. *Biochem Biophys Res Commun*. 24:179-184.

Hyvarinen, J., M. Parikka, R. Sormunen, M. Ramet, K. Tryggvason, K.I. Kivirikko, J. Myllyharju, and P. Koivunen. 2010. Deficiency of a transmembrane prolyl 4-hydroxylase in the zebrafish leads to basement membrane defects and compromised kidney function. *J Biol Chem*. 285:42023-42032.

Ichikawa, Y., D.H. Pluznik, and L. Sachs. 1966. In vitro control of the development of macrophage and granulocyte colonies. *Proc Natl Acad Sci U S A*. 56:488-495.

Ikeda, J., T. Ichiki, H. Matsuura, E. Inoue, J. Kishimoto, A. Watanabe, C. Sankoda, S. Kitamoto, T. Tokunou, K. Takeda, G.H. Fong, and K. Sunagawa. 2013. Deletion of phd2 in myeloid lineage attenuates hypertensive cardiovascular remodeling. *J Am Heart Assoc*. 2:000178.

Imaeda, A.B., A. Watanabe, M.A. Sohail, S. Mahmood, M. Mohamadnejad, F.S. Sutterwala, R.A. Flavell, and W.Z. Mehal. 2009. Acetaminophen-induced hepatotoxicity in mice is dependent on Tlr9 and the Nalp3 inflammasome. *J Clin Invest*. 119:305-314.

Ivan, M., K. Kondo, H. Yang, W. Kim, J. Valiando, M. Ohh, A. Salic, J.M. Asara, W.S. Lane, and W.G. Kaelin, Jr. 2001. HIFalpha targeted for VHL-mediated destruction by proline hydroxylation: implications for O2 sensing. *Science*. 292:464-468.

Jaakkola, P., D.R. Mole, Y.M. Tian, M.I. Wilson, J. Gielbert, S.J. Gaskell, A. von Kriegsheim, H.F. Hebestreit, M. Mukherji, C.J. Schofield, P.H. Maxwell, C.W. Pugh, and P.J. Ratcliffe. 2001. Targeting of HIF-alpha to the von Hippel-Lindau ubiquitylation complex by O2-regulated prolyl hydroxylation. *Science*. 292:468-472.

Jakobsson, A., and G.E. Nilsson. 1993. Prediction of sampling depth and photon pathlength in laser Doppler flowmetry. *Medical & biological engineering & computing*. 31:301-307.

Jiang, B.H., J.Z. Zheng, S.W. Leung, R. Roe, and G.L. Semenza. 1997. Transactivation and inhibitory domains of hypoxia-inducible factor 1alpha. Modulation of transcriptional activity by oxygen tension. *J Biol Chem*. 272:19253-19260.

Jiang, D., J. Liang, J. Fan, S. Yu, S. Chen, Y. Luo, G.D. Prestwich, M.M. Mascarenhas, H.G. Garg, D.A. Quinn, R.J. Homer, D.R. Goldstein, R. Bucala, P.J. Lee, R. Medzhitov, and P.W. Noble. 2005. Regulation of lung injury and repair by Toll-like receptors and hyaluronan. *Nat Med*. 11:1173-1179.

Kalinski, P. 2012. Regulation of immune responses by prostaglandin E2. *J Immunol*. 188:21-28.

Kallio, P.J., K. Okamoto, S. O'Brien, P. Carrero, Y. Makino, H. Tanaka, and L. Poellinger. 1998. Signal transduction in hypoxic cells: inducible nuclear translocation and recruitment of the CBP/p300 coactivator by the hypoxia-inducible factor-1alpha. *Embo J*. 17:6573-6586.

Kim, J.W., I. Tchernyshyov, G.L. Semenza, and C.V. Dang. 2006. HIF-1-mediated expression of pyruvate dehydrogenase kinase: a metabolic switch required for cellular adaptation to hypoxia. *Cell Metab*. 3:177-185.

Kiss, J., M. Mollenhauer, S.R. Walmsley, J. Kirchberg, P. Radhakrishnan, T. Niemietz, J. Dudda, G. Steinert, M.K. Whyte, P. Carmeliet, M. Mazzone, J. Weitz, and M. Schneider. 2012. Loss of the oxygen sensor PHD3 enhances the innate immune response to abdominal sepsis. *J Immunol*. 189:1955-1965.

Kochi, T., Y. Imai, A. Takeda, Y. Watanabe, S. Mori, M. Tachi, and T. Kodama. 2013. Characterization of the arterial anatomy of the murine hindlimb: functional role in the design and understanding of ischemia models. *PloS one*. 8:e84047.

Koditz, J., J. Nesper, M. Wottawa, D.P. Stiehl, G. Camenisch, C. Franke, J. Myllyharju, R.H. Wenger, and D.M. Katschinski. 2007. Oxygen-dependent ATF-4 stability is mediated by the PHD3 oxygen sensor. *Blood*. 110:3610-3617.

Koivunen, P., P. Tiainen, J. Hyvarinen, K.E. Williams, R. Sormunen, S.J. Klaus, K.I. Kivirikko, and J. Myllyharju. 2007. An endoplasmic reticulum transmembrane prolyl 4-hydroxylase is induced by hypoxia and acts on hypoxia-inducible factor alpha. *J Biol Chem*. 282:30544-30552.

Kong, X., B. Alvarez-Castelao, Z. Lin, J.G. Castano, and J. Caro. 2007. Constitutive/hypoxic degradation of HIF-alpha proteins by the proteasome is independent of von Hippel Lindau protein ubiquitylation and the transactivation activity of the protein. *J Biol Chem*. 282:15498-15505.

Kono, H., C.J. Chen, F. Ontiveros, and K.L. Rock. 2010. Uric acid promotes an acute inflammatory response to sterile cell death in mice. *J Clin Invest*. 120:1939-1949.

Konopski, Z., R. Seljelid, and T. Eskeland. 1993. Cytokines and PGE2 modulate the phagocytic function of the beta-glucan receptor in macrophages. *Scand J Immunol*. 37:587-592.

Laitala, A., E. Aro, G. Walkinshaw, J.M. Maki, M. Rossi, M. Heikkila, E.R. Savolainen, M. Arend, K.I. Kivirikko, P. Koivunen, and J. Myllyharju. 2012. Transmembrane prolyl 4-hydroxylase is a fourth prolyl 4-hydroxylase regulating EPO production and erythropoiesis. *Blood*. 120:3336-3344.

Lando, D., D.J. Peet, J.J. Gorman, D.A. Whelan, M.L. Whitelaw, and R.K. Bruick. 2002a. FIH-1 is an asparaginyl hydroxylase enzyme that regulates the transcriptional activity of hypoxia-inducible factor. *Genes Dev*. 16:1466-1471.

Lando, D., D.J. Peet, D.A. Whelan, J.J. Gorman, and M.L. Whitelaw. 2002b. Asparagine hydroxylation of the HIF transactivation domain a hypoxic switch. *Science*. 295:858-861.

Lech, M., and H.-J. Anders. 2013. Macrophages and fibrosis: How resident and infiltrating mononuclear phagocytes orchestrate all phases of tissue injury and repair. *Biochimica et Biophysica Acta (BBA) - Molecular Basis of Disease*. 1832:989-997.

Li, D., M. Hirsila, P. Koivunen, M.C. Brenner, L. Xu, C. Yang, K.I. Kivirikko, and J. Myllyharju. 2004. Many amino acid substitutions in a hypoxia-inducible transcription factor (HIF)-1alpha-like peptide cause only minor changes in its hydroxylation by the HIF prolyl 4-hydroxylases: substitution of 3,4-dehydroproline or azetidine-2-carboxylic acid for the proline leads to a high rate of uncoupled 2-oxoglutarate decarboxylation. *J Biol Chem*. 279:55051-55059.

Lieb, M.E., K. Menzies, M.C. Moschella, R. Ni, and M.B. Taubman. 2002. Mammalian EGLN genes have distinct patterns of mRNA expression and regulation. *Biochem Cell Biol*. 80:421-426.

Limbourg, A., T. Korff, L.C. Napp, W. Schaper, H. Drexler, and F.P. Limbourg. 2009. Evaluation of postnatal arteriogenesis and angiogenesis in a mouse model of hind-limb ischemia. *Nature protocols*. 4:1737-1746.

Lingnau, M., C. Hoflich, H.D. Volk, R. Sabat, and W.D. Docke. 2007. Interleukin-10 enhances the CD14-dependent phagocytosis of bacteria and apoptotic cells by human monocytes. *Hum Immunol*. 68:730-738.

Lipscomb, E.A., P.D. Sarmiere, R.J. Crowder, and R.S. Freeman. 1999. Expression of the SM-20 gene promotes death in nerve growth factor-dependent sympathetic neurons. *J Neurochem*. 73:429-432.

Liu, M., K. Saeki, T. Matsunobu, T. Okuno, T. Koga, Y. Sugimoto, C. Yokoyama, S. Nakamizo, K. Kabashima, S. Narumiya, T. Shimizu, and T. Yokomizo. 2014. 12-Hydroxyheptadecatrienoic acid promotes epidermal wound healing by accelerating keratinocyte migration via the BLT2 receptor. *J Exp Med*. 211:1063-1078.

Loinard, C., A. Ginouves, J. Vilar, C. Cochain, Y. Zouggari, A. Recalde, M. Duriez, B.I. Levy, J. Pouyssegur, E. Berra, and J.S. Silvestre. 2009. Inhibition of prolyl hydroxylase domain proteins promotes therapeutic revascularization. *Circulation*. 120:50-59.

Luo, W., H. Hu, R. Chang, J. Zhong, M. Knabel, R. O'Meally, R.N. Cole, A. Pandey, and G.L. Semenza. 2011. Pyruvate kinase M2 is a PHD3-stimulated coactivator for hypoxia-inducible factor 1. *Cell*. 145:732-744.

Luo, W., B. Lin, Y. Wang, J. Zhong, R. O'Meally, R.N. Cole, A. Pandey, A. Levchenko, and G.L. Semenza. 2014. PHD3-mediated prolyl hydroxylation of nonmuscle actin impairs polymerization and cell motility. *Mol Biol Cell*. 25:2788-2796.

Mahon, P.C., K. Hirota, and G.L. Semenza. 2001. FIH-1: a novel protein that interacts with HIF-1alpha and VHL to mediate repression of HIF-1 transcriptional activity. *Genes Dev*. 15:2675-2686.

Makino, Y., A. Kanopka, W.J. Wilson, H. Tanaka, and L. Poellinger. 2002. Inhibitory PAS domain protein (IPAS) is a hypoxia-inducible splicing variant of the hypoxia-inducible factor-3alpha locus. *J Biol Chem*. 277:32405-32408.

Mamlouk, S., J. Kalucka, R.P. Singh, K. Franke, A. Muschter, A. Langer, C. Jakob, M. Gassmann, G.B. Baretton, and B. Wielockx. 2014. Loss of prolyl hydroxylase-2 in myeloid cells and T-lymphocytes impairs tumor development. *Int J Cancer*. 134:849-858.

Mariathasan, S., D.S. Weiss, K. Newton, J. McBride, K. O'Rourke, M. Roose-Girma, W.P. Lee, Y. Weinrauch, D.M. Monack, and V.M. Dixit. 2006. Cryopyrin activates the inflammasome in response to toxins and ATP. *Nature*. 440:228-232.

Martinon, F., V. Petrilli, A. Mayor, A. Tardivel, and J. Tschopp. 2006. Gout-associated uric acid crystals activate the NALP3 inflammasome. *Nature*. 440:237-241.

Maxwell, P.H., M.S. Wiesener, G.-W. Chang, S.C. Clifford, E.C. Vaux, M.E. Cockman, C.C. Wykoff, C.W. Pugh, E.R. Maher, and P.J. Ratcliffe. 1999. The tumour suppressor protein VHL targets hypoxia-inducible factors for oxygen-dependent proteolysis. *Nature*. 399:271-275.

Mazzone, M., D. Dettori, R. Leite de Oliveira, S. Loges, T. Schmidt, B. Jonckx, Y.M. Tian, A.A. Lanahan, P. Pollard, C. Ruiz de Almodovar, F. De Smet, S. Vinckier, J. Aragones, K. Debackere, A. Luttun, S. Wyns, B. Jordan, A. Pisacane, B. Gallez, M.G. Lampugnani, E. Dejana, M. Simons, P. Ratcliffe, P. Maxwell, and P. Carmeliet. 2009. Heterozygous deficiency of PHD2 restores tumor oxygenation and inhibits metastasis via endothelial normalization. *Cell*. 136:839-851.

Melillo, G., T. Musso, A. Sica, L.S. Taylor, G.W. Cox, and L. Varesio. 1995. A hypoxia-responsive element mediates a novel pathway of activation of the inducible nitric oxide synthase promoter. *J Exp Med*. 182:1683-1693.

Melillo, G., L.S. Taylor, A. Brooks, T. Musso, G.W. Cox, and L. Varesio. 1997. Functional requirement of the hypoxia-responsive element in the activation of the inducible nitric oxide synthase promoter by the iron chelator desferrioxamine. *J Biol Chem*. 272:12236-12243.

Metzen, E., U. Berchner-Pfannschmidt, P. Stengel, J.H. Marxsen, I. Stolze, M. Klinger, W.Q. Huang, C. Wotzlaw, T. Hellwig-Burgel, W. Jelkmann, H. Acker, and J. Fandrey. 2003. Intracellular localisation of human HIF-1 alpha hydroxylases: implications for oxygen sensing. *J Cell Sci*. 116:1319-1326.

Metzen, E., D.P. Stiehl, K. Doege, J.H. Marxsen, T. Hellwig-Burgel, and W. Jelkmann. 2005. Regulation of the prolyl hydroxylase domain protein 2 (phd2/egln-1) gene: identification of a functional hypoxia-responsive element. *Biochem J*. 387:711-717.

Minamishima, Y.A., J. Moslehi, N. Bardeesy, D. Cullen, R.T. Bronson, and W.G. Kaelin, Jr. 2008. Somatic inactivation of the PHD2 prolyl hydroxylase causes polycythemia and congestive heart failure. *Blood*. 111:3236-3244.

Moroz, E., S. Carlin, K. Dyomina, S. Burke, H.T. Thaler, R. Blasberg, and I. Serganova. 2009. Real-time imaging of HIF-1alpha stabilization and degradation. *PLoS One*. 4:4.

Moussion, C., N. Ortega, and J.P. Girard. 2008. The IL-1-like cytokine IL-33 is constitutively expressed in the nucleus of endothelial cells and epithelial cells in vivo: a novel 'alarmin'? *PLoS One*. 3:0003331.

Murray, P.J., J.E. Allen, S.K. Biswas, E.A. Fisher, D.W. Gilroy, S. Goerdt, S. Gordon, J.A. Hamilton, L.B. Ivashkiv, T. Lawrence, M. Locati, A. Mantovani, F.O. Martinez, J.L. Mege, D.M. Mosser, G. Natoli, J.P. Saeij, J.L. Schultze, K.A. Shirey, A. Sica, J. Suttles, I. Udalova, J.A. van Ginderachter, S.N. Vogel, and T.A. Wynn. 2014. Macrophage activation and polarization: nomenclature and experimental guidelines. *Immunity*. 41:14-20.

Murray, P.J., and T.A. Wynn. 2011. Protective and pathogenic functions of macrophage subsets. *Nat Rev Immunol*. 11:723-737.

Niiyama, H., N.F. Huang, M.D. Rollins, and J.P. Cooke. 2009. Murine model of hindlimb ischemia. *Journal of visualized experiments : JoVE*.

Obacz, J., S. Pastorekova, B. Vojtesek, and R. Hrstka. 2013. Cross-talk between HIF and p53 as mediators of molecular responses to physiological and genotoxic stresses. *Mol Cancer*. 12:1476-4598.

Oehme, F., P. Ellinghaus, P. Kolkhof, T.J. Smith, S. Ramakrishnan, J. Hutter, M. Schramm, and I. Flamme. 2002. Overexpression of PH-4, a novel putative proline 4-hydroxylase, modulates activity of hypoxia-inducible transcription factors. *Biochem Biophys Res Commun*. 296:343-349.

Olson, E., L. Demopoulos, T.F. Haws, E. Hu, Z. Fang, K.M. Mahar, P. Qin, J. Lepore, T.A. Bauer, and W.R. Hiatt. 2014. Short-term treatment with a novel HIF-prolyl hydroxylase inhibitor (GSK1278863) failed to improve measures of performance in subjects with claudication-limited peripheral artery disease. *Vasc Med*. 19:473-482.

Papandreou, I., R.A. Cairns, L. Fontana, A.L. Lim, and N.C. Denko. 2006. HIF-1 mediates adaptation to hypoxia by actively downregulating mitochondrial oxygen consumption. *Cell Metab*. 3:187-197.

Peach, G., M. Griffin, K.G. Jones, M.M. Thompson, and R.J. Hinchliffe. 2012. Diagnosis and management of peripheral arterial disease. *Bmj*. 14.

Percy, M.J., P.W. Furlow, P.A. Beer, T.R. Lappin, M.F. McMullin, and F.S. Lee. 2007. A novel erythrocytosis-associated PHD2 mutation suggests the location of a HIF binding groove. *Blood*. 110:2193-2196.

Percy, M.J., Q. Zhao, A. Flores, C. Harrison, T.R. Lappin, P.H. Maxwell, M.F. McMullin, and F.S. Lee. 2006. A family with erythrocytosis establishes a role for prolyl hydroxylase domain protein 2 in oxygen homeostasis. *Proc Natl Acad Sci U S A*. 103:654-659.

Pescador, N., Y. Cuevas, S. Naranjo, M. Alcaide, D. Villar, M.O. Landazuri, and L. Del Peso. 2005. Identification of a functional hypoxia-responsive element that regulates the expression of the egl nine homologue 3 (egln3/phd3) gene. *Biochem J*. 390:189-197.

Pillay, J., I. den Braber, N. Vrisekoop, L.M. Kwast, R.J. de Boer, J.A. Borghans, K. Tesselaar, and L. Koenderman. 2010. In vivo labeling with 2H2O reveals a human neutrophil lifespan of 5.4 days. *Blood*. 116:625-627.

Pugh, C.W., J.F. O'Rourke, M. Nagao, J.M. Gleadle, and P.J. Ratcliffe. 1997. Activation of hypoxia-inducible factor-1; definition of regulatory domains within the alpha subunit. *J Biol Chem*. 272:11205-11214.

Puimege, L., F. Van Hauwermeiren, S. Steeland, S. Van Ryckeghem, J. Vandewalle, S. Lodens, L. Dejager, S. Vandevyver, J. Staelens, S. Timmermans, R.E. Vandenbroucke, and C. Libert. 2015. Glucocorticoid-induced microRNA-511 protects against TNF by down-regulating TNFR1. *EMBO Mol Med*. 7:1004-1017.

Quaegebeur, A., I. Segura, R. Schmieder, D. Verdegem, I. Decimo, F. Bifari, T. Dresselaers, G. Eelen, D. Ghosh, S.M. Davidson, S. Schoors, D. Broekaert, B. Cruys, K. Govaerts, C. De Legher, A. Bouche, L. Schoonjans, M.S. Ramer, G. Hung, G. Bossaert, D.W.

Cleveland, U. Himmelreich, T. Voets, R. Lemmens, C.F. Bennett, W. Robberecht, K. De Bock, M. Dewerchin, B. Ghesquiere, S.M. Fendt, and P. Carmeliet. 2016. Deletion or Inhibition of the Oxygen Sensor PHD1 Protects against Ischemic Stroke via Reprogramming of Neuronal Metabolism. *Cell Metab*. 23:280-291.

Quintana, F.J., and I.R. Cohen. 2005. Heat shock proteins as endogenous adjuvants in sterile and septic inflammation. *J Immunol*. 175:2777-2782.

Ravichandran, K.S. 2010. Find-me and eat-me signals in apoptotic cell clearance: progress and conundrums. *J Exp Med*. 207:1807-1817.

Razin, E., S. Bauminger, and A. Globerson. 1978. Effect of prostaglandins on phagocytosis of sheep erythrocytes by mouse peritoneal macrophages. *J Reticuloendothel Soc*. 23:237-242.

Razin, E., and A. Globerson. 1979. The effect of various prostaglandins on plasma membrane receptors and function of mouse macrophages. *Adv Exp Med Biol*. 114:415-419.

Rishi, M.T., V. Selvaraju, M. Thirunavukkarasu, I.A. Shaikh, K. Takeda, G.H. Fong, J.A. Palesty, J.A. Sanchez, and N. Maulik. 2015. Deletion of prolyl hydroxylase domain proteins (PHD1, PHD3) stabilizes hypoxia inducible factor-1 alpha, promotes neovascularization, and improves perfusion in a murine model of hind-limb ischemia. *Microvasc Res*. 97:181-188.

Robbins, C.S., I. Hilgendorf, G.F. Weber, I. Theurl, Y. Iwamoto, J.L. Figueiredo, R. Gorbatov, G.K. Sukhova, L.M. Gerhardt, D. Smyth, C.C. Zavitz, E.A. Shikatani, M. Parsons, N. van Rooijen, H.Y. Lin, M. Husain, P. Libby, M. Nahrendorf, R. Weissleder, and F.K. Swirski. 2013. Local proliferation dominates lesional macrophage accumulation in atherosclerosis. *Nat Med*. 19:1166-1172.

Roche, P.A., and K. Furuta. 2015. The ins and outs of MHC class II-mediated antigen processing and presentation. *Nat Rev Immunol*. 15:203-216.

Rodriguez, J., R. Pilkington, A. Garcia Munoz, L.K. Nguyen, N. Rauch, S. Kennedy, N. Monsefi, A. Herrero, C.T. Taylor, and A. von Kriegsheim. 2016. Substrate-Trapped Interactors of PHD3 and FIH Cluster in Distinct Signaling Pathways. *Cell Rep*. 14:2745-2760.

Rossi, A.G., J.C. McCutcheon, N. Roy, E.R. Chilvers, C. Haslett, and I. Dransfield. 1998. Regulation of macrophage phagocytosis of apoptotic cells by cAMP. *J Immunol*. 160:3562-3568.

Roszer, T. 2015. Understanding the Mysterious M2 Macrophage through Activation Markers and Effector Mechanisms. *Mediators Inflamm*. 816460:18.

Ruas, J.L., U. Berchner-Pfannschmidt, S. Malik, K. Gradin, J. Fandrey, R.G. Roeder, T. Pereira, and L. Poellinger. 2010. Complex regulation of the transactivation function of hypoxia-inducible factor-1 alpha by direct interaction with two distinct domains of the CREB-binding protein/p300. *J Biol Chem*. 285:2601-2609.

Sanford, K.K., W.R. Earle, and G.D. Likely. 1948. The growth in vitro of single isolated tissue cells. *J Natl Cancer Inst*. 9:229-246.

Scaffidi, P., T. Misteli, and M.E. Bianchi. 2002. Release of chromatin protein HMGB1 by necrotic cells triggers inflammation. *Nature*. 418:191-195.

Schneider, M., K. Van Geyte, P. Fraisl, J. Kiss, J. Aragones, M. Mazzone, H. Mairbaurl, K. De Bock, N.H. Jeoung, M. Mollenhauer, M. Georgiadou, T. Bishop, C. Roncal, A. Sutherland, B. Jordan, B. Gallez, J. Weitz, R.A. Harris, P. Maxwell, M. Baes, P. Ratcliffe, and P. Carmeliet. 2010. Loss or silencing of the PHD1 prolyl hydroxylase protects livers of mice against ischemia/reperfusion injury. *Gastroenterology*. 138:1143-1154.

Semenza, G.L., and G.L. Wang. 1992. A nuclear factor induced by hypoxia via de novo protein synthesis binds to the human erythropoietin gene enhancer at a site required for transcriptional activation. *Mol Cell Biol*. 12:5447-5454.

Seth, P., I. Krop, D. Porter, and K. Polyak. 2002. Novel estrogen and tamoxifen induced genes identified by SAGE (Serial Analysis of Gene Expression). *Oncogene*. 21:836-843.

Shi, C., and E.G. Pamer. 2011. Monocyte recruitment during infection and inflammation. *Nat Rev Immunol*. 11:762-774.

Shweiki, D., A. Itin, D. Soffer, and E. Keshet. 1992. Vascular endothelial growth factor induced by hypoxia may mediate hypoxia-initiated angiogenesis. *Nature*. 359:843-845.

Sica, A., and A. Mantovani. 2012. Macrophage plasticity and polarization: in vivo veritas. *J Clin Invest*. 122:787-795.

Silva, M.T. 2010. When two is better than one: macrophages and neutrophils work in concert in innate immunity as complementary and cooperative partners of a myeloid phagocyte system. *J Leukoc Biol*. 87:93-106.

Simon, M.C., and B. Keith. 2008. The role of oxygen availability in embryonic development and stem cell function. *Nat Rev Mol Cell Biol*. 9:285-296.

Singh, R.P., K. Franke, J. Kalucka, S. Mamlouk, A. Muschter, A. Gembarska, T. Grinenko, C. Willam, R. Naumann, K. Anastassiadis, A.F. Stewart, S. Bornstein, T. Chavakis, G. Breier, C. Waskow, and B. Wielockx. 2013. HIF prolyl hydroxylase 2 (PHD2) is a critical regulator of hematopoietic stem cell maintenance during steady-state and stress. *Blood*. 121:5158-5166.

Smirnova, N.A., D.M. Hushpulian, R.E. Speer, I.N. Gaisina, R.R. Ratan, and I.G. Gazaryan. 2012. Catalytic mechanism and substrate specificity of HIF prolyl hydroxylases. *Biochemistry*. 77:1108-1119.

Soehnlein, O., and L. Lindbom. 2010. Phagocyte partnership during the onset and resolution of inflammation. *Nat Rev Immunol*. 10:427-439.

Sokolowska, M., L.Y. Chen, Y. Liu, A. Martinez-Anton, H.Y. Qi, C. Logun, S. Alsaaty, Y.H. Park, D.L. Kastner, J.J. Chae, and J.H. Shelhamer. 2015. Prostaglandin E2 Inhibits NLRP3 Inflammasome Activation through EP4 Receptor and Intracellular Cyclic AMP in Human Macrophages. *J Immunol*. 194:5472-5487.

Steg, P.G., S.K. James, D. Atar, L.P. Badano, C.B. Lundqvist, M.A. Borger, C. Di Mario, K. Dickstein, G. Ducrocq, F. Fernandez-Aviles, A.H. Gershlick, P. Giannuzzi, S. Halvorsen, K. Huber, P. Juni, A. Kastrati, J. Knuuti, M.J. Lenzen, K.W. Mahaffey, M. Valgimigli, A. van't Hof, P. Widimsky, D. Zahger, J.J. Bax, H. Baumgartner, C. Ceconi, V. Dean, C. Deaton, R. Fagard, C. Funck-Brentano, D. Hasdai, A. Hoes, P. Kirchhof, P. Kolh, T. McDonagh, C. Moulin, B.A. Popescu, Ž. Reiner, U. Sechtem, P.A. Sirnes, M. Tendera, A. Torbicki, A. Vahanian, S. Windecker, F. Astin, K. Åström-Olsson, A. Budaj, P. Clemmensen, J.-P. Collet, K.A. Fox, A. Fuat, O. Gustiene, C.W. Hamm, P. Kala, P. Lancellotti, A.P. Maggioni, B. Merkely, F.-J. Neumann, M.F. Piepoli, F. Van de Werf, F. Verheugt, and L. Wallentin. 2012. ESC Guidelines for the management of acute myocardial infarction in patients presenting with ST-segment elevation. *The Task Force on the management of ST-segment elevation acute myocardial infarction of the European Society of Cardiology (ESC)*. 33:2569-2619.

Steinhoff, A., F.K. Pientka, S. Möckel, A. Kettelhake, E. Hartmann, M. Köhler, and R. Depping. 2009. Cellular oxygen sensing: Importins and exportins are mediators of intracellular localisation of prolyl-4-hydroxylases PHD1 and PHD2. *Biochemical and Biophysical Research Communications*. 387:705-711.

Strassmann, G., V. Patil-Koota, F. Finkelman, M. Fong, and T. Kambayashi. 1994. Evidence for the involvement of interleukin 10 in the differential deactivation of murine peritoneal macrophages by prostaglandin E2. *J Exp Med*. 180:2365-2370.

Sunderkotter, C., K. Steinbrink, M. Goebeler, R. Bhardwaj, and C. Sorg. 1994. Macrophages and angiogenesis. *J Leukoc Biol*. 55:410-422.

Swain, L., M. Wottawa, A. Hillemann, A. Beneke, H. Odagiri, K. Terada, M. Endo, Y. Oike, K. Farhat, and D.M. Katschinski. 2014. Prolyl-4-hydroxylase domain 3 (PHD3) is a critical terminator for cell survival of macrophages under stress conditions. *Journal of leukocyte biology*. 96:365-375.

Takeda, K., and G.H. Fong. 2007. Prolyl hydroxylase domain 2 protein suppresses hypoxia-induced endothelial cell proliferation. *Hypertension*. 49:178-184.

Takeda, K., V.C. Ho, H. Takeda, L.J. Duan, A. Nagy, and G.H. Fong. 2006. Placental but not heart defects are associated with elevated hypoxia-inducible factor alpha levels in mice lacking prolyl hydroxylase domain protein 2. *Mol Cell Biol*. 26:8336-8346.

Takeda, K., T. Ichiki, E. Narabayashi, K. Inanaga, R. Miyazaki, T. Hashimoto, H. Matsuura, J. Ikeda, T. Miyata, and K. Sunagawa. 2009. Inhibition of prolyl hydroxylase domain-containing protein suppressed lipopolysaccharide-induced TNF-alpha expression. *Arterioscler Thromb Vasc Biol*. 29:2132-2137.

Takeda, N., E.L. O'Dea, A. Doedens, J.W. Kim, A. Weidemann, C. Stockmann, M. Asagiri, M.C. Simon, A. Hoffmann, and R.S. Johnson. 2010. Differential activation and antagonistic function of HIF-{alpha} isoforms in macrophages are essential for NO homeostasis. *Genes Dev*. 24:491-501.

Takeda, Y., S. Costa, E. Delamarre, C. Roncal, R. Leite de Oliveira, M.L. Squadrito, V. Finisguerra, S. Deschoemaeker, F. Bruyere, M. Wenes, A. Hamm, J. Serneels, J. Magat, T. Bhattacharyya, A. Anisimov, B.F. Jordan, K. Alitalo, P. Maxwell, B. Gallez, Z.W. Zhuang, Y. Saito, M. Simons, M. De Palma, and M. Mazzone. 2011. Macrophage skewing by Phd2 haplodeficiency prevents ischaemia by inducing arteriogenesis. *Nature*. 479:122-126.

Tambuwala, M.M., E.P. Cummins, C.R. Lenihan, J. Kiss, M. Stauch, C.C. Scholz, P. Fraisl, F. Lasitschka, M. Mollenhauer, S.P. Saunders, P.H. Maxwell, P. Carmeliet, P.G. Fallon, M. Schneider, and C.T. Taylor. 2010. Loss of prolyl hydroxylase-1 protects against colitis through reduced epithelial cell apoptosis and increased barrier function. *Gastroenterology*. 139:2093-2101.

Thygesen, K., J.S. Alpert, A.S. Jaffe, M.L. Simoons, B.R. Chaitman, and H.D. White. 2012. Third universal definition of myocardial infarction. *Glob Heart*. 7:275-295.

Tracy, K., B.C. Dibling, B.T. Spike, J.R. Knabb, P. Schumacker, and K.F. Macleod. 2007. BNIP3 is an RB/E2F target gene required for hypoxia-induced autophagy. *Mol Cell Biol*. 27:6229-6242.

Tuckerman, J.R., Y. Zhao, K.S. Hewitson, Y.M. Tian, C.W. Pugh, P.J. Ratcliffe, and D.R. Mole. 2004. Determination and comparison of specific activity of the HIF-prolyl hydroxylases. *FEBS Lett*. 576:145-150.

Vabulas, R.M., P. Ahmad-Nejad, C. da Costa, T. Miethke, C.J. Kirschning, H. Hacker, and H. Wagner. 2001. Endocytosed HSP60s use toll-like receptor 2 (TLR2) and TLR4 to activate the toll/interleukin-1 receptor signaling pathway in innate immune cells. *J Biol Chem*. 276:31332-31339.

Van Welden, S., D. Laukens, L. Ferdinande, M. De Vos, and P. Hindryckx. 2013. Differential expression of prolyl hydroxylase 1 in patients with ulcerative colitis versus patients with Crohn's disease/infectious colitis and healthy controls. *J Inflamm*. 10:1476-9255.

Vaupel, P., F. Kallinowski, and P. Okunieff. 1989. Blood flow, oxygen and nutrient supply, and metabolic microenvironment of human tumors: a review. *Cancer Res*. 49:6449-6465.

Vogler, M., A. Zieseniss, A.R. Hesse, E. Levent, M. Tiburcy, E. Heinze, N. Burzlaff, G. Schley, K.U. Eckardt, C. Willam, and D.M. Katschinski. 2015. Pre- and post-conditional inhibition of prolyl-4-hydroxylase domain enzymes protects the heart from an ischemic insult. *Pflugers Arch*. 467:2141-2149.

Walmsley, S.R., E.R. Chilvers, A.A. Thompson, K. Vaughan, H.M. Marriott, L.C. Parker, G. Shaw, S. Parmar, M. Schneider, I. Sabroe, D.H. Dockrell, M. Milo, C.T. Taylor, R.S. Johnson, C.W. Pugh, P.J. Ratcliffe, P.H. Maxwell, P. Carmeliet, and M.K. Whyte. 2011. Prolyl hydroxylase 3 (PHD3) is essential for hypoxic regulation of neutrophilic inflammation in humans and mice. *J Clin Invest*. 121:1053-1063.

Walmsley, S.R., C. Print, N. Farahi, C. Peyssonnaux, R.S. Johnson, T. Cramer, A. Sobolewski, A.M. Condliffe, A.S. Cowburn, N. Johnson, and E.R. Chilvers. 2005. Hypoxia-induced neutrophil survival is mediated by HIF-1alpha-dependent NF-kappaB activity. *J Exp Med*. 201:105-115.

Wang, G.L., B.H. Jiang, E.A. Rue, and G.L. Semenza. 1995. Hypoxia-inducible factor 1 is a basic-helix-loop-helix-PAS heterodimer regulated by cellular O2 tension. *Proc Natl Acad Sci U S A*. 92:5510-5514.

Wang, G.L., and G.L. Semenza. 1995. Purification and characterization of hypoxia-inducible factor 1. *J Biol Chem*. 270:1230-1237.

Weischenfeldt, J., and B. Porse. 2008. Bone Marrow-Derived Macrophages (BMM): Isolation and Applications. *CSH Protoc*. 1.

Wenger, R.H., D.P. Stiehl, and G. Camenisch. 2005. Integration of oxygen signaling at the consensus HRE. *Sci STKE*. 18.

Xie, L., X. Pi, Z. Wang, J. He, M.S. Willis, and C. Patterson. 2015. Depletion of PHD3 protects heart from ischemia/reperfusion injury by inhibiting cardiomyocyte apoptosis. *J Mol Cell Cardiol*. 80:156-165.

Xie, L., K. Xiao, E.J. Whalen, M.T. Forrester, R.S. Freeman, G. Fong, S.P. Gygi, R.J. Lefkowitz, and J.S. Stamler. 2009. Oxygen-regulated beta(2)-adrenergic receptor hydroxylation by EGLN3 and ubiquitylation by pVHL. *Sci Signal*. 2:2000444.

Xue, J., X. Li, S. Jiao, Y. Wei, G. Wu, and J. Fang. 2010. Prolyl hydroxylase-3 is down-regulated in colorectal cancer cells and inhibits IKKbeta independent of hydroxylase activity. *Gastroenterology*. 138:606-615.

Yu, M., H. Wang, A. Ding, D.T. Golenbock, E. Latz, C.J. Czura, M.J. Fenton, K.J. Tracey, and H. Yang. 2006. HMGB1 signals through toll-like receptor (TLR) 4 and TLR2. *Shock*. 26:174-179.

Yu, Y., and K. Chadee. 1998. Prostaglandin E2 stimulates IL-8 gene expression in human colonic epithelial cells by a posttranscriptional mechanism. *J Immunol*. 161:3746-3752.

Zhang, Q., M. Raoof, Y. Chen, Y. Sumi, T. Sursal, W. Junger, K. Brohi, K. Itagaki, and C.J. Hauser. 2010. Circulating mitochondrial DAMPs cause inflammatory responses to injury. *Nature*. 464:104-107.

Zhang, X., R. Goncalves, and D.M. Mosser. 2008. The isolation and characterization of murine macrophages. *Curr Protoc Immunol*. 14.

Danksagung

Ganz herzlich möchte ich mich bei Prof. Dörthe Katschinski bedanken, die es mir ermöglicht hat, in ihrer Arbeitsgruppe zu promovieren. Das mir entgegengebrachte Vertrauen weiß ich sehr zu schätzen. Vielen Dank für eine exzellente Betreuung, viele gute Ratschläge und für ihre aufbauenden Worte an den richtigen Stellen. Vielen Dank auch für die Förderung und das besondere Interesse an meinem weiteren beruflichen Werdegang.

Des Weiteren möchte ich mich bei den Mitgliedern meines Thesis Committees, Prof. Holger Reichardt und Prof. Thomas Meyer für das stete Interesse an meiner Arbeit sowie für die fachliche Unterstützung und für die guten Ratschläge bedanken.

Außerdem möchte ich Prof. Heidi Hahn, Prof. Thomas Dresbach und Prof. Michael Müller danken, die sich freundlicherweise bereit erklärt haben meiner Prüfungskommission beizutreten.

Ich möchte mich ganz herzlich bei Liza Swain bedanken, die mir am Anfang meiner Doktorarbeit viele Techniken beigebracht hat und mir somit einen guten Einstieg in das Projekt ermöglicht hat. Ihr, Annette Hillemann und Annemarie Güntsch möchte ich außerdem für die enge Zusammenarbeit und für ihre technische Unterstützung in meinem Projekt danken, das oftmals mehr als zwei Hände erforderte und ohne sie so nicht möglich gewesen wäre. Ebenso möchte ich mich bei Aline Jatho und Anke Zieseniss bedanken, die wichtige Versuche für mein Projekt durchgeführt haben.

Sehr dankbar bin ich auch meiner ehemaligen Büronachbarin Marieke Wottawa, die mich gerade in den Durststrecken meiner Doktorarbeit mental unterstützt hat. Anke Zieseniss, Annemarie Güntsch und Gijsbert van Belle möchte ich außerdem für die schnelle Korrektur dieser Arbeit und für wichtige Anmerkungen danken. Amke Hesse möchte ich dafür danken, dass sie mich am Anfang bei Tierversuchen und den dazugehörigen Formalitäten unterstützt hat. Außerdem möchte ich mich bei allen Mitgliedern der Arbeitgruppe ganz herzlich für die tolle und produktive Arbeitsatmosphäre und für die große Hilfsbereitschaft bedanken.

Ich möchte außerdem meinen Eltern danken, die mich in jeder Lebenslage uneingeschränkt unterstützt und mich immer gefördert haben. Fernando Rozenblit danke ich ebenso für seine große Unterstützung, insbesondere während der letzten anstrengenden Monate. Des Weiteren möchte ich Annemarie Güntsch, Liza Swain und Marieke Wottawa danken, mit denen ich auch außerhalb des Labors eine wunderbare Zeit in Göttingen verbracht habe.